Aix*Marseille université
Socialement engagée

UASLP
Universidad Autónoma de San Luis Potosí

NNT/NL : 2022AIXM0353/039ED352

THÈSE DE DOCTORAT

Soutenue à Universidad Autónoma de San Luis Potosí
dans le cadre d'une cotutelle avec Aix-Marseille Université
le 04 novembre 2022 par

Andrea Arlette ESPAÑA

Complexité définie comme une mesure des chemins conduisant à une certaine notion de régularité.

Discipline
Physique et Sciences de la Matière

Spécialité
Physique Théorique et Mathématique

École doctorale
ED 352 : Physique et Sciences de la Matière

Laboratoire/Partenaires de recherche
Centre de Physique Théorique

Composition du jury

Stefanella BOATTO Universidade Federal de Rio de Janeiro	Rapporteure
Bastien FERNÁNDEZ CNRS - Univ. Paris Cité - Sorbonne Univ.	Rapporteur
Olivier AGULLO Aix-Marseille Université	Examinateur
Leticia RAMÍREZ Universidad Autónoma de Zacatecas	Examinatrice
Gabriela ARAUJO Universidad Nacional Autónoma de México	Examinatrice
Gelasio SALAZAR Universidad Autónoma de San Luis Potosí	Président du jury
Xavier LEONCINI Aix-Marseille Université	Directeur de thèse
Edgardo UGALDE Universidad Autónoma de San Luis Potosí	Co-Directeur de thèse

Affidavit

Je soussigné, Andrea Arlette España, déclare par la présente que le travail présenté dans ce manuscrit est mon propre travail, réalisé sous la direction scientifique de Xavier Leoncini et Edgardo Ugalde, dans le respect des principes d'honnêteté, d'intégrité et de responsabilité inhérents à la mission de recherche. Les travaux de recherche et la rédaction de ce manuscrit ont été réalisés dans le respect à la fois de la charte nationale de déontologie des métiers de la recherche et de la charte d'Aix-Marseille Université relative à la lutte contre le plagiat.

Ce travail n'a pas été précédemment soumis en France ou à l'étranger dans une version identique ou similaire à un organisme examinateur.

Fait à San Luis Potosí, Mexique, le 26 août 2022

List of publications and participation in conferences

List of publications produced as part of the thesis project :

1. A. España, X. Leoncini, E. Ugalde (2022). **Combinatorics of the paths towards synchronization**, *Physica D*.
2. A. España (2022). **Another way to see the synchronization**, *jIAPS* (Accepted).

Participation in conferences and summer schools during the thesis period :

1. International Conference of Physics Students 2022.
2. Canadian – Cuban – American – Mexican Graduate Student Conference.
3. EPS Forum.
4. XIII Conference on Dynamical Systems Applied to Biology and Natural Sciences.
5. Conferencia de Mujeres Estudiantes de Física CUWIP MX 2022.
6. II Encuentro para la Divulgación e Investigación en el Estudio de Sistemas Complejos y sus Aplicaciones.
7. TalentLand Latinoamerica.
8. V Meeting of Mexican Mathematicians in the World.
9. III Franco-Mexican Forum on Science, Technology and Innovation.
10. I Simposio Virtual Iberoamericano de Sociología Computacional.
11. Semana del Instituto de Física UASLP.
12. International Conference of Physics Students 2021.
13. International Congress for Young Professionals in Physics and Technology.
14. XXIV Rencontre de non-linéarité.
15. Congreso Nacional Virtual de la Sociedad Matemática Mexicana.
16. VII Congreso Internacional de Ciencia No Lineal y Complejidad.
17. II Encuentro de Dinámica Nacional.
18. II Encuentro de Mujeres Matemáticas Mexicanas
19. III Taller de Matemáticas en las Ciencias de la Vida “Dr. Valentin Afraimovich”.

20. II School in Dynamic Systems IF-UASLP.
21. XIX School of Probability and Statistics CIMAT.
22. I School in Dynamic Systems IF-UASLP.

Résumé

Les systèmes complexes peuvent être considérés comme des systèmes composés d'un grande quantité d'individus, ayant le plus souvent des interactions non linéaires définies par un réseau. Lorsque la dynamique est introduite, suivant les conditions initiales et le système considéré, le système peut finir par atterrir dans un attracteur final donné, qui dans le cas le plus simple n'est qu'un point fixe du système dynamique. Un des phénomènes marquants dans le domaine des systèmes complexes est celui étudié dans cette thèse : le phénomène de synchronisation.

Nous pouvons trouver de nombreux phénomènes dans la nature dans lesquels la synchronisation est clairement observé, par exemple des groupes d'oiseaux qui volent en créant des motifs dans le ciel, ou des groupes de poissons qui nagent très près les uns des autres de manière fluide dans l'océan. On peut même retrouver ce phénomène dans certains comportements humains, lorsqu'à la fin d'un concert, les applaudissements commencent et, après quelques instants, il semble que tout le monde applaudisse en même temps. C'est ainsi que la synchronisation des événements semble se faire naturellement, comme s'ils étaient programmés de telle manière que l'interaction entre eux, même si elle est très faible, se traduirait par un ajustement de leurs rythmes.

Dans cette thèse, j'introduis une nouvelle approche afin de quantifier la synchronisation de ce type de systèmes. Ensuite, via une codification des chemins vers la synchronisation j'étudie le comportement transitoire des flux de synchronisation définis sur un réseau. Plus précisément, je me concentre sur le système Laplacien et le modèle de Kuramoto agissant sur trois types de graphes.

Pour commencer, fixons un graphe $G = (V, E)$ où V est l'ensemble des sommets et E est l'ensemble des arêtes, et considérons un système d'équations différentielles couplées sur $I^{|V|}$, où I est soit l'ensemble des nombres réels $\mathbb{R}$ soit le cercle, que j'écrive sous la forme S^1. Le flux est généré par un système d'équations différentielles ordinaires couplées selon les interactions définies par E. Alors, pour le premier cas, le *flux Laplacien discret* ou simplement *flux Laplacien* sur le graphe G, est le système linéaire défini par

$$\begin{aligned} \frac{dx_v}{dt} &= (Lx)_v, \\ &= \sum_{u \in V : (u,v) \in E} (x_u - x_v). \end{aligned}$$

Avec $x_v \in \mathbb{R}$ pour chaque $v \in V$. Aussi, dans cette équation $L = L(M_G)$ est la matrice Laplacienne de la matrice d'adjacence M_G. En utilisant ce concept mathématique, il a été possible d'étudier la vibration d'une membrane discrète et certaines propriétés chimiques des substances.

D'autre part, pour le système non linéaire considéré dans cette thèse, nous avons que selon Kuramoto, asymptotiquement, la dynamique de certains systèmes est presque identique, et il a proposé que les N oscillateurs couplés soient décrits par le système d'équations couplées suivant

$$\frac{dx_i}{dt} = \omega_i + \sum_{j=1}^{N} \Gamma_{i,j}(x_j - x_i),$$

pour $i = 1,..,N$, où la fonction d'interaction $\Gamma_{i,j}$ détermine la forme du couplage entre chaque oscillateur i et j, aussi, ω_i est la fréquence naturelle, et x_i est l'angle de phase de chaque oscillateur.

En raison du caractère général de l'équation précédente et de la complexité de la fonction d'interaction introduite $\Gamma_{i,j}$, qui autorise tout type de couplage, l'analyse théorique reste extrêmement difficile. Afin de réduire considérablement la difficulté de l'étude, considérons dans un premier temps que Γ est égal à la fonction identité, alors nous avons une traduction du système Laplacien qui dépend de ω_i. Ainsi, il semble qu'à chaque fois que nous modifions la fonction Γ, elle peut faire l'objet d'un vaste domaine d'étude.

Pour relever ce défi de taille, Kuramoto considère une interaction de « couplage global » i.e. chaque oscillateur affecte l'ensemble des autres oscillateurs. Dans le même temps, il a supposé que les interactions entre les oscillateurs soient égales et ne dépendent que de manière sinusoïdale de la différence de phase, donnée par la fonction suivante

$$\Gamma_{i,j}(x_j - x_i) = \frac{K}{N}\sin\big(x_j - x_i\big).$$

Où le paramètre K détermine la force de couplage.

En introduisant ce couplage dans les équations ci-dessus, nous obtenons le célèbre *Modèle de Kuramoto*. C'est un modèle simple de N oscillateurs mutuellement couplés ayant différentes fréquences naturelles ω_i distribuées suivant une certaine densité de probabilité $\omega \mapsto g(\omega)$, avec des phases x_i, comme dans l'équation suivante

$$\frac{dx_i}{dt} = \omega_i + \frac{K}{N}\sum_{j=1}^{N} \sin\big(x_j - x_i\big).$$

Ce système a été largement étudié, il a été prouvé qu'il est nécessaire de fixer des conditions initiales et des paramètres particuliers pour observer l'état de synchronisa-

tion global. De plus, il a été démontré que le type de graphe sur lequel agit cet état est connexe. Je me concentre uniquement sur les cas pour lesquels nous pouvons trouver une synchronisation globale.

De l'observation précédente, il n'est pas difficile de prouver que dans les deux systèmes, la diagonale

$$\mathscr{D} = \{x \in I^{|V|} : x_u = x_v \ \forall \ u, v \in V\}.$$

Est un attracteur global, c'est-à-dire qu'il que pour toutes conditions initiales, $\lim_{t\to\infty} dist(x(t), \mathscr{D}) = 0$. Remarquons que, spécialement pour le flux de Kuramoto, la diagonale est un attracteur pour les conditions initiales qui sont dans un petit voisinage de la diagonale.

Je suis intéressé à mesurer la synchronisation du système, à un instant donné t, avant d'atteindre l'attracteur. Pour cela, avec une précision $\epsilon > 0$ et dire que deux voisins sont ϵ-synchronisés, si la distance entre eux n'est pas supérieure à ϵ.

Ainsi, à chaque seuil fixe $\epsilon > 0$, graphe $G = (V, E)$ et à chaque configuration $x \in \mathbb{R}^{|V|}$, j'associe un *sous-réseau ϵ-synchronisé* $G_x = (V, E_x)$, où $E_x \subset E$ est l'ensemble des arêtes

$$E_x = \{(u, v) \in E : |x_u - x_v| \leq \epsilon\}.$$

Le graphe G a $2^{|E|}$ sous-graphes, alors pour chaque condition initiale appropriée $x \in \mathbb{R}^{|V|}$ il existe une suite finie de temps de commutation $t_0 = 0 < t_1 < t_2 < \cdots < t_\ell$ et une séquence correspondante de sous-réseaux ϵ-synchronisés $(G_x, G_{x(t_1)}, \ldots, G_{x(t_\ell)})$ tel que

$$G_{x(t_\tau)} \neq G_{x(t_{\tau+1})},$$

pour chaque $0 \leq \tau < N$, et

$$G_{x(t)} = G_{x(t_\tau)},$$

avec $\tau = \max\{0 \leq j \leq \ell : \ t \geq t_j\}$. En d'autres termes, dans la séquence de sous-réseaux, aucun sous-réseau consécutif répété n'est trouvé.

Il est important de souligner que l'objectif principal de ce travail est de déterminer et de décrire l'évolution de ces sous-réseaux.

En raison des hypothèses sur la synchronisation que j'effectue dans cette thèse, les systèmes considérés possèdent la propriété suivante : $G_{x(t)} \to G$ lorsque $t \to +\infty$ dans tout son espace si la condition initiale est suffisamment proche à la diagonale $\mathscr{D}$.

Clairement, les séquences ϵ-synchronisée son fini, donc, ils peuvent être réalisée par un nombre infini de conditions initiales. Ce qui pourrait très probablement permettre de réaliser une partition de l'espace initial, c'est-à-dire le bassin d'attraction de l'état synchronisé final. L'ensemble des chemins vers la synchronisation définit une

structure combinatoire, que s'appellent : le diagramme de transition.

Ensuite, je restreins l'étude aux familles de réseaux suivant le graphe complet K_N, le graphe biparti complet $K_{N,N}$ et le famille de graphes cycliques $C(N,k)$.

En considérant ces familles, j'aborde les questions suivantes :

1. Étant donné le réseau sous-jacent, quels sous-graphes sont réalisables comme sous-réseaux ϵ-synchronisants, quelle est la taille de cet ensemble et comment croît-il avec la taille N du graphe sous-jacent ?
2. Étant donné un réseau sous-jacent, quelle est la structure du diagramme de transition ? En particulier, quel est le chemin le plus long dans ce digraphe et quelle est la distribution des longueurs de chemin ?

Afin de répondre à ces questions, je vais définir le diagramme de transition non pas sur les sous-réseaux ϵ-synchronisés mais sur un autre objet combinatoire qui encode à la fois les sous-réseaux ϵ-synchronisés, et en même temps, qui reconnaît l'ordre des coordonnées. Ce faisant, nous faciliterons la description des diagrammes de transition puisque le codage que j'utilise permet de déterminer facilement l'ordre d'apparition des nouvelles arêtes dans la séquence synchronisée. C'est pour cette raison que ce codage est non seulement pratique mais nécessaire, si l'on veut garder une trace de l'ordre des coordonnées afin de construire de nouvelles arêtes.

Dans le cas du flux Laplacien appliqué sur le graphe complet K_N, je code le sous-réseau ϵ-synchronisé G_x, déterminé par la configuration ordonnée $x_1 \leq x_2 \leq \cdots \leq x_N$ par la fonction croissante $\phi_x : \{1,2,\ldots,N\} \to \{1,2,\ldots,N\}$ donné par

$$\phi_x(m) = \max\{n \geq m : x_n \leq x_m + \epsilon\}.$$

La fonction ϕ_x est clairement croissante et telle que $\phi_x(n) \geq n$ pour chaque $1 \leq n \leq N$. Autrement dit, cette fonction passe au-dessus de la diagonale $\phi_x \geq \mathrm{Id}$. Ici, Id désigne la fonction d'identité dans $\{1,2,\ldots,N\}$.

De plus, je prouve que la collection suivante

$$\Phi_N := \{\phi : \{1,\ldots,N\} \to \{1,\ldots,N\} \text{ croissante et telle que } \phi \geq \mathrm{Id}\}.$$

Est en correspondance un à un avec l'ensemble de tous les sous-réseaux ϵ-synchronisés de K_N définis par des conditions initiales ordonnées, i.e. $x_1 \leq x_2 \leq \cdots \leq x_N$. Cette correspondance est donnée par

$$\phi \mapsto (\{1,2,\ldots,N\}, E_\phi) \text{ où } E_\phi = \{\{m,n\} : \min(m,n) \leq \phi(\max(n,m))\}.$$

Grâce à ce résultat nous pouvons observer que la collection ϕ_N est équivalente à un ensemble combinatoire bien connu : L'ensemble des chemins de Dyck d'ordre N. Ces chemins aussi nommés chemins de Dyck d'ordre N est une marche en escalier de $(0,0)$

à (N,N) de longueur $2N$ et qui est inférieure ou égale à la diagonale. Cet ensemble combinatoire a une cardinalité donnée par les nombres Catalan :

$$\begin{aligned} |\Phi_N| = & \quad C_N \\ = & \quad \tfrac{1}{N+1}\binom{2N}{N}. \end{aligned}$$

Compte tenu de cette équivalence établie au paragraphe précédent, chaque séquence de sous-réseaux ϵ-synchronisés $(G_x, G_{x(t_1)}, \dots, G_{x(t_\ell)})$ générée par une condition initiale ordonnée $x \in \mathbb{R}$, est fidèlement codifiée par les suites correspondantes de fonctions croissantes $(\phi_x, \phi_{x(t_1)}, \dots, \phi_{x(t_\ell)}) \in \Phi_N$. Il est clair que la fonction $t \mapsto \phi_{x(t)}(n)$ augmente avec t pour chaque n fixé, et converge vers $\phi_{x(t)} = N$ au temps $t_{1,N} = \big(\log(x_N - x_1) - \log(\epsilon)\big)/N$. En raison de cette monotonie, la longueur ℓ d'une séquence ϵ-synchronisée est majorée par le nombre d'arêtes dans K_N, c'est-à-dire

$$\ell \leq \frac{N(N-1)}{2}.$$

Ensuite, je présente et décrive les diagrammes de transition de dimension 3 et 4, qui sont ceux qui apparaissent ci-dessous.

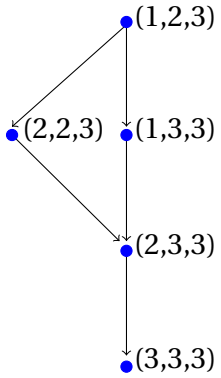

FIGURE 0.1 – Le diagramme de transition de $L(M_{K_3})$ avec les étiquettes attribuées par les fonctions croissantes correspondantes est affiché. Celui-ci est composé de 5 sommets et 5 arêtes. En haut, on peut voir le sommet $(1,2,3)$ qui correspond au graphe totalement déconnecté de dimension 3, et en bas, on peut voir le sommet $(3,3,3)$ qui correspond au graphe complet de dimension 3. Ce diagramme de transition correspond aux conditions initiales ordonnées $x = (x_1, x_2, x_3) \in \mathbb{R}^3$ telles que $x_1 < x_2 < x_3$, donc les autres symétries n'apparaissent plus .

En revanche, dans le cas du graphe biparti complet $K_{N,N}$, considérant le flux Laplacien, je code le sous-réseau ϵ-synchronisé G_x défini par $x_1 \leq x_2 \leq \cdots \leq x_N$, $x_{N+1} \leq x_{N+2} \leq \cdots \leq x_{2N}$, par le couple de fonctions $\alpha_x, \omega_x : \{1,2,\dots,N\} \to \{0,1,2,\dots,N+1\}$

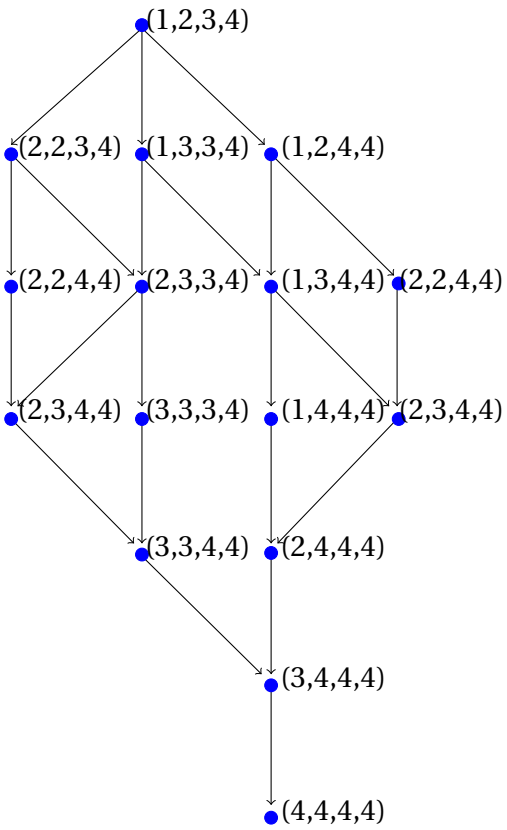

FIGURE 0.2 – Le diagramme de transition de $L(M_{K_4})$ avec les étiquettes attribuées par les fonctions croissantes correspondantes est affiché. Celui-ci est composé de 16 sommets et 22 arêtes. En haut, on peut voir le sommet $(1,2,3,4)$ qui correspond au graphe totalement déconnecté de dimension 4, et en bas, on peut voir le sommet $(4,4,4,4)$ qui correspond au graphe complet de dimension 4 K_4. Ce diagramme de transition correspond aux conditions initiales ordonnées $x = (x_1, x_2, x_3, x_4) \in \mathbb{R}^4$ telles que $x_1 < x_2 < x_3 < x_4$, donc les autres symétries n'apparaissent plus.

donné par

$$\alpha_x(n) = \begin{cases} \min\{\ell \leq N : x_n - \epsilon \leq x_{N+\ell}\} & \text{si } x_{2N} \geq x_n - \epsilon, \\ N+1 & \text{si } x_{2N} < x_n - \epsilon, \end{cases}$$

$$\omega_x(n) = \begin{cases} \max\{\ell \leq N : x_n + \epsilon \geq x_{N+\ell}\} & \text{si } x_{N+1} \leq x_n + \epsilon, \\ 0 & \text{si } x_{N+1} > x_n + \epsilon. \end{cases}$$

Il convient de noter que $\operatorname{im}(\alpha_x) \subset [1, N+1]$ tandis que $\operatorname{im}(\omega_x) \subset [0, N]$. Les deux fonctions sont croissantes et telles que $\alpha_x(n) \leq \omega_x(n) + 1$ pour chaque $1 \leq n \leq N$.

De plus, j'ai prouvé que la collection suivante de paires de fonctions croissantes

$$\begin{aligned}\Phi_{N,N} \quad := \quad & \{(\alpha,\omega) \in I_N \times I_N : \ \mathrm{im}(\alpha) \subset [1, N+1], \\ & \mathrm{im}(\omega) \subset [0, N] \text{ et } \alpha \leq \omega + 1\},\end{aligned}$$

Où

$$I_N := \{\phi : \{1,\dots,N\} \to \{0,\dots,N+1\} : \phi(n+1) \geq \phi(n) \text{ pour tous } 1 \leq n < N\},$$

Codifiant tous les sous-réseaux ϵ-synchronisés de $K_{N,N}$ compatibles avec une condition initiale ordonnée $x_1 \leq x_2 \leq \cdots \leq x_N$, $x_{N+1} \leq x_{N+2} \leq \cdots \leq x_{2N}$. La correspondance est donnée comme suit. À $(\alpha,\omega) \in \Phi_{N,N}$ je associe le sous-réseau $G_{(\alpha,\omega)} \subset K_{N,N}$ aux arêtes de l'ensemble

$$E_{(\alpha,\omega)} = \{(n, N+m) : 1 \leq n, m \leq N, \text{ et } \alpha(n) \leq m \leq \omega(n)\},$$

ce qui est cohérent avec le fait que $(\alpha,\omega) = (\alpha_x, \omega_x)$ si et seulement si $G_{(\alpha,\omega)} = G_x$.

Les paires de fonctions croissantes dans $\Phi_{N,N}$ peuvent être reliées à des objets combinatoires, les parallélo-polyminos inscrits dans un rectangle.

Formellement, le nombre de parallélo-polyminos dans le réseau de taille $p \times q$ est donné par le nombre de Narayanan et la dépendance est donnée par l'expression suivante

$$T_q^{p+q-1} = \frac{1}{p+q-1}\binom{p+q-1}{q}\binom{p+q-1}{q-1}.$$

Alors, à chaque couple de fonctions croissantes $(\alpha,\omega) \in \Phi_{N,N}$ je associe un parallélo-polyminoe (un parallélo-polyminoe dans le réseau rectangulaire de taille $p \times q$ est une union connexe de carrés délimités par deux fonctions frontières croissantes $L, U : \{1,2,\dots,p\} \to \{0,1,\dots,q\}$ telles que $L(1) = 0$, $U(p) = q$, et $L(n) < U(n-1)$ pour chaque $2 \leq n \leq p$) dans $\{0,1,\dots,N+1\} \times \{0,1,\dots,N+1\}$ avec les fonctions de bordure $L, U : \{1,\dots,N+1\} \to \{0,1,\dots,N+1\}$, tel que

$$L(n) = \begin{cases} 0 & \text{pour } n = 1, \\ \alpha(n-1) - 1 & \text{pour } 2 \leq n \leq N+1, \end{cases}$$

et

$$U(n) = \begin{cases} \omega(n) + 1 & \text{pour } 1 \leq n \leq N, \\ N+1 & \text{pour } n = N+1. \end{cases}$$

Je peux ainsi établir une correspondance injective entre les parallélo-polyminos et les couples de fonctions croissantes dans $\Phi_{N,N}$, et vous obtenez

$$|\Phi_{N,N}| = T_{N+1}^{2N+1} = \frac{1}{2N+1}\binom{2N+1}{N+1}\binom{2N+1}{N}.$$

Du fait de l'équivalence précédente, chaque suite de sous-réseaux ϵ-synchronisés définis par une condition initiale ordonnée et équilibrée est fidèlement codifiée par les suites correspondantes de couples de fonctions croissantes. De plus, je présente et explique les diagrammes de transition de dimension $N = 2$, qui apparaissent ci-dessous.

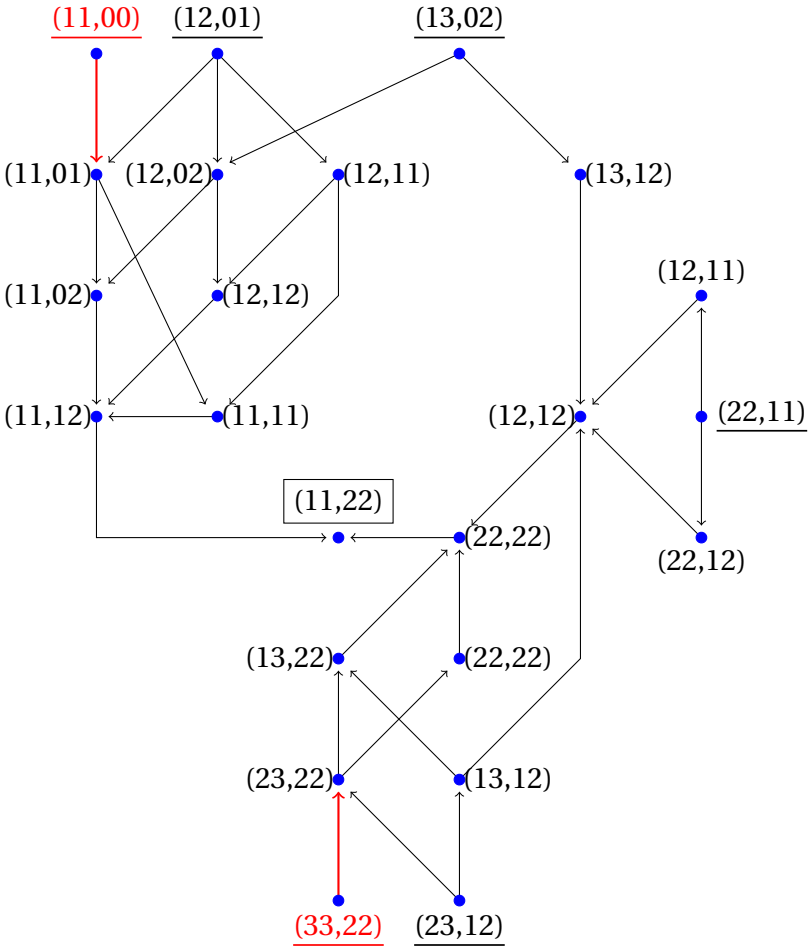

FIGURE 0.3 – Le diagramme de transition de $L(M_{K_{2,2}})$ avec les étiquettes attribuées par les fonctions croissantes correspondantes est affiché. Celui-ci est composé de 23 sommets et 31 arêtes. Les sommets où un chemin peut commencer (pour qu'il soit aussi long que possible), sont soulignés et sont $(22,11),(12,01),(13,02),(23,12),(11,00),(33,22)$. Les sommets en rouge sont ceux qui correspondent à des conditions initiales non équilibrées. Et au milieu, on voit le sommet $(1,1,2,2)$ qui correspond au graphe biparti complet $K_{2,2}$. Ce diagramme de transition correspond aux conditions initiales ordonnées $x = (x_1, x_2, x_3, x_4) \in \mathbb{R}^4$ telles que $x_1 < x_2$ et $x_3 < x_4$, qui sont celles qui gardez la monotonie.

Les deux codages présentés ci-dessus, l'un pour coder le comportement des conditions initiales ordonnées lorsqu'on leur applique le flux Laplacien dans le graphe complet K_N et le second, le graphe complet bipartite $K_{N,N}$, nous permettent d'utiliser les stratégies déjà existantes en combinatoire pour étudier les diagrammes de transition que je génère, avec lesquelles je peux fournir des formules fermées, et des bornes pour différentes caractéristiques de ces digraphes.

J'analyse ensuite la dynamique sous flux Laplacien du graphe cyclique C_N. Contrairement aux deux autres systèmes présentés précédemment, celui-ci possède un comportement non monotone ce qui accroît grandement la difficulté de l'étude. Afin d'avoir une vision claire de la dynamique, je réalise des simulations numériques. En effet, un comportement non monotone, implique par exemple que, une fois que nous descendons d'un niveau dans le diagramme de transition, à l'étape suivane, nous pouvons remonter ce niveau. En particulier, je constate que les conditions initiales diminuent et augmentent aux premiers niveaux $(N-1)/2$. Malgré cela, certains calculs exacts pourraient être fournis sans qu'il soit nécessaire de passer par un quelconque codage.

L'une des notes les plus importantes liées à la dynamique du graphe cyclique est que tous ses sous-graphes sont réalisables pour une condition initiale donnée. Ainsi :

$$\sharp\text{Sommets dans le diagramme de transition de } L(M_{C_N}) = 2^{N-1}.$$

Dans ce cas précis, du fait que les arrêtes peuvent être connectées et déconnectées, le chemin le plus long dépasse le nombre total d'arrêtes du graphe cyclique C_N qui est $N-1$. Dans le cas plus général (dimension N), mes calculs suggèrent que le chemin le plus long fait environ $3N$ de long.

Avant de continuer, j'observe que dans le cas du flux Laplacien appliqué sur le graphe cyclique, comme le comportement de son spectre change en fonction de la parité de la dimension alors la dynamique transitoire du système change également en fonction de la parité. Autrement dit, le système de dimension paire se comporte différemment du système de dimension impaire. Ainsi, ils doivent être traités comme deux cas différents pour la dynamique du graphe cyclique C_N.

Une caractéristique importante à étudier dans le cas des systèmes de synchronisation analysés dans cette thèse est le nombre de chemins de synchronisation qui peuvent être générés à partir de cette méthodologie dans les différents types de graphes prit en compte. Cette mesure des chemins de synchronisation peut être vue comme une mesure de complexité, au sens de croissance par rapport à leur dimension.

De plus, je présente et décrive le diagramme de transition de C_6, qui apparaît ci-dessous.

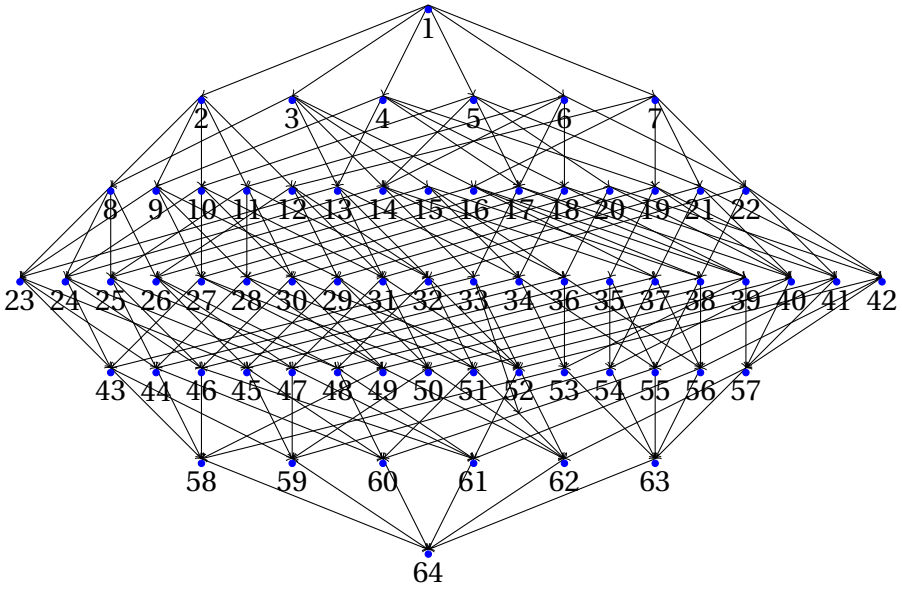

FIGURE 0.4 – Diagramme de transition de $L(M_{C_6})$ avec des étiquettes attribuées par le numéro du sous-graphe qui lui correspond lexicographiquement. Celui-ci est composé de 64 sommets et arêtes. En haut, on peut voir le sommet 1 qui correspond au graphe totalement déconnecté de dimension 6, et en bas, on peut voir le sommet 64 qui correspond au graphe cyclique de dimension 6, C_6.

Dans le cas des deux systèmes dans lesquels je fournis un codage pour décrire leur comportement, je rencontre un problème qui semble NP-difficile, à savoir, compter le nombre de chemins de synchronisation dans le graphe complet K_N est équivalent à trouver des règles de Golomb combinatoirement distinctes. Malgré cela, je peux fournir une borne non triviale pour la croissance des chemins vers la synchronisation par rapport à la dimension, donnée par l'expression suivante

$$(N-1)! < \sharp\text{Chemins vers la sync de } L(M_{K_N}) \leq \left(\frac{N(N+1)}{2}\right)! \frac{\prod_{i=1}^{N-1} i!}{\prod_{i=1}^{N}(2i-1)!}.$$

Dans le cas du graphe biparti complet $K_{N,N}$, le nombre de chemins vers la synchronisation est majoré par l'expression suivante

$$(2N-1)! < \sharp\text{Chemins vers la sync de } L(M_{K_{N,N}}) \leq \left(\binom{2N}{N} - 2\right)\text{Golomb}(2N).$$

Et encore une fois, la croissance du nombre de chemins vers la synchronisation par rapport à N définit une fonction de complexité analogue à la complexité topologique FARBER 2003 en fonction du temps.

Pour le nombre de chemins vers la synchronisation dans le cas du graphe cyclique C_N, d'après mes calculs numériques, j'observe que lorsque la dimension augmente, l'ordre de grandeur des chemins augmente également, un à la fois. Dans ce cas, comme dans les précédents, le nombre de chemins augmente trop vite et je n'ai pas assez de ressources de calcul pour donner une estimation précise.

Les résultats obtenus pour le comportement du flux Laplacien appliqué au graphe complet K_N et au graphe complet bipartite $K_{N,N}$ sont appliqués au flux de Kuramoto sur le même graphe lorsque des conditions initiales proches de la diagonale sont considérées, et de plus, ils se généralisent aux flux qui sont monotones, qui maintiennent l'ordre des coordonnées, et dont les différences maintiennent également l'ordre.

En résumé, grâce au comportement monotone du flux Laplacien dans le graphe complet K_N, il a été possible de décrire complètement le comportement de leur dynamique transitoire en utilisant une codification des sous-réseaux ϵ-synchronisés par des fonctions croissantes, qui sont bien connues et étudiées. En revanche, dans le cas du comportement du graphe biparti complet $K_{N,N}$, une codification similaire a été présentée, mais elle se limite uniquement aux chemins de synchronisation qui commencent à un type particulier de conditions initiales : les équilibrés i.e., celles pour lesquels un comportement monotone est obtenu. En ce qui concerne le régime transitoire du modèle de Kuramoto appliqué sur le graphe complet K_N, j'ai montré que nous pouvons utiliser la méthodologie déjà définie pour décrire le système Laplacien sur le même graphe dans un voisinage autour de la diagonal. Grâce à cette remarque, nous savons que nous pouvons étudier de manière complète leur dynamique dans cette région.

Mots clés : Non linéarité, Synchronisation, Laplacien, Modèle de Kuramoto

Abstract

In this thesis, a way to quantify the synchronization of a system is introduced. It is made from a codification of the paths towards synchronization for synchronizing flows defined over a network. The collection of paths toward synchronization defines a combinatorial structure, called *the transition diagram*, the main object of study. The cardinality of this collection defines a measure of complexity which depends on the dimension of the system.

The transition diagram corresponding to the Laplacian flow over the complete graph K_N and the complete bipartite graph $K_{N,N}$ is described, through a coding: the feasible states by increasing functions, and the transitions between them by consecutive functions that follow certain rules. These results are applied to the Kuramoto flow (over the same graph) when a neighborhood close to the diagonal is considered. Furthermore, it generalizes to flows that are monotonic (that is, its coordinates and the differences of the coordinates maintain the order).

It is presented as well some numerical and analytical results concerning the Laplacian and Kuramoto flows over the cycle graph C_N, and the ring lattice family $C(N,k)$. In this case there are a different perspective, due to their no-monotonic behavior.

Keywords: Non-linearity, Synchronization, Laplacian, Kuramoto model

Acknowledgments

I am very grateful to my advisors, Dr. Ugalde and Dr. Leoncini, for accompanying me in this process of becoming a doctor. I thank you for the training and life lessons you gave me, for caring about my well-being, and for having been great scientists whom I admire and who are an example for me to follow.

I thank the members of my tutoring committee in Mexico, Dr. Espinosa-Soto and Dr. Salazar, and the members of my tutoring committee in France, Dr. Barrat, Dr. Martin, and Dr. Verga, for giving me feedback on my research in each evaluation period.

I thank the members of my Mexico-France jury, Dr. Agullo, Dr. Ramírez-Hernández, Dr. Araujo, Dr. Salazar, and the reporters Dr. Boatto and Dr. Fernández, for having agreed to be part of my jury and for having granted their time for the evaluation of this thesis, as well as all their valuable comments, through which a better version of this work could be presented.

I greatly appreciate the guidance of Dr. García-Ramos and Dr. Molés. I also appreciate all the administrative help in my co-tutelage process to Cristina Cázares. I am very grateful to my colleagues MSc. Posadas, MSc. Tovar, MSc. Corona, MSc. Ramírez-Medrano for having accompanied me through my doctorate.

Finally, I am grateful for the financial support received throughout my doctorate to carry out stays and attend conferences, offered by

— ECOS-CONACyT-ANUIES through Grant M16M01.
— National Scholarship No. 722957 offered by CONACyT-México.
— Fundación Sofia Kovalevskaia.
— Sociedad Matemática Mexicana.
— European Mathematical Society.
— International Association of Physics Students.
— Group 3 - Centre de Physique Théorique AMU.

Agradecimientos especiales

El trabajo que aquí presento, no se podría haber llevado acabo sin el apoyo de muchas personas. Quiero tomarme el tiempo para agradecerles a cada uno de ellos por sus aportaciones (intelectuales, afectivas, económicas y espirituales).

Primero, le agradezco a Dios por haberme concedido cuatro años de salud física, los que aproveché para trabajar en este proyecto. Le agradezco que también mantuvo con salud a mi familia y de esa forma privilegiada me pude concentrar tranquilamente en mi trabajo.

Le agradezco enormemente a mi esposo MSc. Santino Ramírez, el haber puesto todas y cada una de sus virtudes al servicio de nuestra relación, que han sido un periodo de ocho años de felicidad, retos y aventuras.

Les agradezco eternamente a mis papás Jorge y Marychuy, por todo su apoyo afectivo. Por desvelarse escuchando mis eternas llamadas telefónicas donde les contaba mis anécdotas semanales. Por toda la sabiduría que compartieron conmigo: sus consejos, palabras de apoyo, su perspectiva que me mantuvo cuerda.

A mis hermanos Jorge, Jessica y Jesús, les agradezco todos los ánimos que me dieron, el haberme llenado de energía con sus chistes, risas y anécdotas. Por estar al pendiente de mi cuando sabían que estaba en un momento importante. Gracias por la ayuda cuando me sentía atorada en mi proyecto.

Mis dos grandes apoyos a lo largo del doctorado, morales, éticos, intelectuales, entre otros, son MSc. Yuridia Posadas y MSc. Angélica Tovar, a las cuales les agradezco todo su tiempo, escucha, consejos y el formar parte de mi red más importante de apoyo.

Por último, me agradezco a mi misma, por no haberme dado por vencida, incluso cuando parecía todo estar en mi contra. Por ser valiente al haber ido hasta el otro lado del mundo sola. Por haber aprendido a defender mis ideales. Por reconocerme humana y aceptar mis limitaciones. Por ser matemática, científica y por ser mujer.

Contents

List of Figures

List of Tables

Introduction

A complex system can be defined as systems composed of many components whose interactions form a complex network. The study of complex systems, currently in full expansion (Deutsch, Fatès, and Makowiec 2022), deals with phenomena encountered in physics, biology, social sciences, economics and finance, amongst others. When the time evolution is considered, the system may end-up on a given attractor, which in the most simple cases is a fixed point or a one-dimensional invariant manifold. This is precisely the case in one of the most outstanding phenomena in complex systems, which is the subject of study of the present work, the synchronization phenomena.

The synchronization of a composite system seems to happen naturally, as if the system's components were programmed in such a way that the interactions between them, even if it is very small, would result in an adjustment of their rhythms. One familiar example of this is the following. Imagine that we are in an auditorium, listening to an orchestra concert. The venue is full, and the musicians are doing a really great job. The minutes pass and we hear the final note of the melody. We are so excited that we begin to applaud. Next, the person by our side also applauds and, in a few seconds, the whole audience is doing so. It turns out that the initial irregular sound synchronized as the time passed, resulting in what would seem as if a single pair of enormous hands was applauding at a higher volume. This phenomenon occurs agreeing on how often they would applaud, but just by listening to the way the others do, thus leading to a spontaneous synchronization. Another example, probably one of the most famous one, is an observation by the Dutch astronomer, physicist, and mathematician, Christiaan Huygens (1629-1695). He was sick and resting in a room, when he realized that there were two perfectly synchronized pendulum clocks hanging on the wall. He analysed the phenomenon and concluded that both clocks were interacting, and they did so because of the only link that existed between them, the wall on which they were hang, which he later analyzed mathematically (Yoder 2005). There are many other examples that we can find in the literature, in particular in the already classical Pikovsky's treatise (Pikovsky, Rosenblum, and Jürgen Kurths 2001), which presents and illustrates several physical and biological models where the synchronization phenomenon occurs.

Different models and tools have been developed to understand the synchronization phenomena. These tools have been applied in a variety of fields ranging from mechanics to neuroscience. In this respect, of particular interest is the study of the phenomenon of self-organization observed in the birds flocking or fishes schooling. The classical model was introduced in (Vicsek, Czirók, Ben-Jacob, et al. 1995), and

since then, it has been further studied and developed (see for instance (Grégoire and Chaté 2004)). Another related phenomenon is the synchronization of chaotic systems in interaction, first studied in the seminal work by Pecora and Carrol (Pecora and Carroll 1990) and for which Pikovsky's book presents a comprehensive account. In both instances, the self-organization of self-propelled agents and the chaotic synchronization, the relevant feature is the emergence of a more regular behavior, as some parameters governing the dynamics change. This transition was being studied using the tools coming from statistical mechanics and dynamical systems theory. The study of this kind of phenomena, where a more regular regime emerges after a transition driven by a change in the parameters, has followed an intense development in recent decades. In this respect I would like to mention some studies concerning the characterization of the emerging regular regime, by Valentin Afraimovich and coauthors in (Afraimovich, Chazottes, and Cordonet 2001) and Bastien Fernandez (Fernandez 2012), where the so-called synchronization function is rigorously studied.

In the above mentioned examples, when a system undergoes a transition towards a more regular regime, the resulting behavior is generally a complex one. In contrast, in this work I focus on the case when the system asymptotically achieves a very simple regime known in the literature as global synchronization. It occurs in systems of many coupled components, as it is the paradigmatic example, by Kuramoto (Kuramoto 1975). We will assume all the components of the systems are equivalent and that their asymptotic states coalesce. Even though the asymptotic behavior is uninteresting, the are in principle many distinguishable ways in which the system attains such a state. When characterizing distinguishable behaviors of a chaotic system, a finite coding is usually employed to represent distinguishable behaviors by different codes. A code being a sequence of levels taken from a finite set (the letters of a finite alphabet in symbolic dynamics). The complexity of the system is then quantified by means of the growth rate of different sequences representing distinguishable behaviors, as the time or the dimension of the system increases. For a chaotic system, when the number of admissible sequences grows exponentially, the exponential rate is a lower bound for the so-called topological entropy (Collet and Eckmann 2006). In our case, after codification, the sequences representing the possible paths towards the complete synchronization are all of finite length, therefore their number ceases to increase with time after a finite transient period. Nevertheless, the number of these sequences suffers a very rapid increase as the dimension of the system increases. It is the rigorous analysis of this combinatorial explosion, which constitutes the main contribution of the present work. In this aim, I have restricted the discussion to systems of coupled differential equations for which the coupling structure defines a regular network. The system being invariant under the symmetries of the resulting network. My more detailed results concern the fully connected network on N nodes and the complete bipartite network on $2N$ nodes. In all cases I will consider either a dissipative linear dynamics defined by the Laplacian matrix of the network, or the Kuramoto model with uniform natural frequencies.

Among the many studies considering homogeneously coupled systems (fully connected, randomly coupled or coupled according to a network) we may cite the following (Acebrón, Bonilla, Pérez Vicente, et al. 2005; Delabays, Jacquod, and Dörfler 2019; Fonseca and Abud 2018; DeVille and B. Ermentrout 2016; van Hemmen and Wreszinski 1993; Medvedev and Tang 2017; Moreno and Pacheco 2004; Sokolov and G. B. Ermentrout 2019; Strogatz 2000). Those works study the conditions under which global or partial synchronization can be observed, with partial synchronization consisting on phase locking and different degrees of incoherence. The determination of sufficient conditions for synchronization, depending on the structure of the underlying network and the particularities of the dynamics, has been one of the main subjects of research in this area. On the contrary, the behavior of the system in its path towards synchronization, once the conditions of full synchronization are fulfilled, largely remains an open problem. How this behavior depends on the structure of the underlying network is the aim of the present work. To my knowledge, there is only a handful of works concerning this topic, among them (Gómez-Gardeñes, Moreno, and Arenas 2007) is found, where a related notion of the path towards synchronization is studied. The authors of that work study the evolution of the asymptotic partial synchronization patterns towards an asymptotic complete synchronization, as a function of the coupling strength. They characterize the degree of synchronization by looking at the structure of the subnetwork defined by the nodes whose states have already coalesced, which they name synchronized subnetwork.

As noticed by Arenas in (Arenas, Diaz-Guilera, Jurgen Kurths, et al. 2008), the way in which the connectivity of the synchronized subnetwork increases in time, can be related to the spectrum of the linearized dynamics. Indeed, the authors show how the number of synchronized subnetworks decrease in qualitatively the same way as the Laplacian cumulative spectral density increases. This relationship between the spectrum of the Laplacian and the structure of the paths towards synchronization, which in the above mentioned reference is numerically explored in the case of random complex networks, is this thesis explored in a rigorous way. In this thesis, I study the structure of the paths towards synchronization for the Laplacian dynamics in first place, then I investigate in which extend the structure appearing in the lineal case extends to the corresponding Kuramoto model. There are obvious differences between the linear and the non-linear dynamics. On the other side, it is well known that the non-linear dynamics is not always fully synchronizing, contrary to the Laplacian case. On the other hand, the local basin of attraction for the synchronizing non-linear dynamics, depends on the structure of the underlying network. I showed that, despite these differences, some features of the synchronizing dynamics around the local basin of attraction are preserved. It is worth mentioning that a linear reformulation of the Kuramoto system (Roberts 2008), in complex variable, exhibits a transition from non-synchronized to a synchronized asymptotic state, in the same way as the original Kuramoto model. Nevertheless, this linear version of Kuramoto is not equivalent to the non-linear classical model and the behavior it deploys does not correspond to the Laplacian dynamics of the same network.

As mentioned above, in this work I assume the systems are fully synchronized and, through a novel approach, I describe the transitory state; that is, the sequence of distinguishable events that occur while the system reaches synchronization. The description of the different ways in which the asymptotic synchronizing state is reached is what I refer to as paths towards synchronization. This notion, related to the one introduced by Gómez-Gardeñes and coauthors (Gómez-Gardeñes, Moreno, and Arenas 2007), refers to the precise combinatorial description of all possible transient states and mine constitutes the first such precise description. By doing so, I am able to count the number of these paths in the simple case, which allows to quantify the complexity of the transient dynamics. It is worth noticing that the characterization the complexity of the system by measuring the diversity of paths is a classical approach that has been employed in (Afraimovich and Zaslavsky 2003; Zaslavsky and Afraimovich 2005; X. Leoncini and Zaslavsky 2002) among many other works.

The main objective of this thesis is to describe the transient behavior of a system defined in a network that fully synchronizes. This description is achieved through a well-defined coding that allows to globally describe all the distinguishable states of the system, states associated with classes of initial conditions. Then, by using this coding, the aim is to quantify the complexity of the transient dynamics of the synchronized system. In addition, this coding must allow describing the properties and characteristics of the transient state of the system.

The particular objectives of this work are:

- To give a precise description of the combinatorial structures defined by the paths to synchronization.
- To study how these combinatorial structures depend on:
  - The network.
  - The linearity or non-linearity of the system.
  - The precision of the description.
  - The time scale.
- To study the complexity of resulting combinatorial structures.

To achieve these objectives, I start by introducing the concept of synchronization sequences, which can be related to the evolution of the connectivity matrix, defined in (Arenas, Díaz-Guilera, and Pérez-Vicente 2006). In the case of a fully synchronizing system, the set of all synchronizing sequences form a transition diagram, encoding the full transient dynamics towards synchronization. To be more precise, this thesis is devoted to the study of this combinatorial structure for synchronizing dynamical systems defined on the fully connected network on K_N, and the complete bipartite network $K_{N,N}$. I start by considering the Laplacian dynamics on those networks, and then study the in which extend the resulting structure describes the corresponding Kuramoto dynamics.

The thesis is organized as follows. After establishing the basic concepts in graph theory, linear algebra, and combinatorics in Chapter 1, the Laplacian system and the Kuramoto model are defined. Then, I present the formal construction of the paths to synchronization, through successions of subgraphs. This is the main object of study in this thesis. In Chapter 2, the formal and rigorous results of this work are presented, organized in three important sections, each one of them focusing on the study of the resulting combinatorial object.

— Firstly, the transition diagram of synchronization paths for the fully connected network K_N is presented and studied in full detail. For this I use a coding of the synchronizing subnetworks by increasing functions.

— Secondly, I study the structure of the transition diagram for the complete bipartite graph $K_{N,N}$ when considering for balanced initial conditions. This formulation allows a formal, but not complete, description of all the paths towards synchronization. For this I use a coding by pairs of increasing functions.

— Thirdly, I discuss the behavior of the Laplacian dynamics on the cycle graph C_N.

I close this chapter with an important discussion concerning the behavior of the transition diagram of the Kuramoto model on the complete graph and of the complete bipartite graph, where I analyse the extent in which the results obtained for the Laplacian flow, apply to the corresponding Kuramoto model.

A preliminar numerical exploration of networks is presented in Chapter 3. Their rigorous complete description is out of the scope of the present study, though remains as perspective work. There I consider the Laplacian system and the Kuramoto model on the cycle graph and the family of ring lattices. This exploration is carried out by considering the behavior of a set of random initial conditions in different dimensions, for which I evaluate:

— The depth of the transition graph.
— The number of possible states in the transition graph.
— The distribution of path lengths.
— The number of different paths towards synchronization.

This chapter includes as well a discussion concerning the behavior of these quantities when varying the topology of the graph.

Finally, in Chapter 3.2.1 the conclusions and perspectives of this work are presented, where several possible directions for further research are disclosed.

1 Theoretical and methodological frameworks

Contents

1.1 Basic concepts

This section presents the definitions that will be used throughout the thesis. The classic definitions of mathematical concepts in graph theory, linear algebra, and combinatorics will be recalled, and the new concepts that were proposed to study the transient state of synchronizing systems will be highlighted. In addition, examples of the definitions are displayed for a better understanding. The content of this section has as main topics: graph theory, linear algebra, the Laplacian system, the Kuramoto model and it is finalized with a section about combinatorics.

1.1.1 Graph theory

Throughout this thesis, it will be considered a system of coupled differential equations that acts on an initial condition, in which each of its components interacts with the others according to an interaction rule. For example, consider a fixed system, for which an initial condition has 4 components. The interaction rule in this case is as follows: component number 1 interacts with component 2 and 3 (and vice versa) and component 4 interacts with component 3 (and vice versa). This interaction rule can be seen in the following Figure 1.1.

This representation of the interaction rules between the components of an initial condition is called *graph* or *network*, and it will be defined formally below.

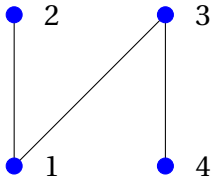

Figure 1.1 – Example of interaction rules between the components of a four-dimensional initial condition, in which it indicates that vertex 1 interacts with vertices 2 and 3 and vice versa, in addition, vertex 3 interacts with vertex 4 and vice versa.

On the one hand, a *graph* or *network* refers to an undirected graph $G = (V, E)$, with vertices in V and edges in E. On the other hand, a *directed graph* is a couple $D = (V, A)$ of vertices in V and arrows in A. An *edge* is a set of two vertices (one at the start, one at the end), while an *arrow* is an ordered pair of vertices (the first indicates the start and the second indicates the end). It is denoted by $|V|$ the number of vertices that a graph has.

In this thesis I focus mainly on the study of three graphs: the complete graph, the bipartite complete graph, and the cycle graph (with their respective family called ring lattice), each of which is defined below. First, in the *complete graph* $K_N = (V, E)$ such that $|V| = N$, each of its vertices has an edge with all the others, that is $(v_i, v_j) \in E$ for all $v_i \in V$ where $1 \leq i, j \leq N$ and $i \neq j$. In Figure 1.2 (a), an example of the complete graph is shown where $N = 4$, that is, K_4. Continuing with the concept of the *complete bipartite graph* denoted by $K_{N,N} = (V, E)$, in this case $|V| = 2N$ and it is defined as follows, it is defined two disjoint subsets of V, let's say $V_1, V_2 \subset V$ such that $|V_1| = |V_2| = N$, and for each vertex in V_1 and each vertex in V_2, there exists an edge between the two vertices, that is, $(v_1, v_2) \in E$, for all $v_1 \in V_1$ and all $v_2 \in V_2$. In Figure 1.2 (b), an example of the complete bipartite graph is shown where $N = 2$, that is, $K_{2,2}$. Finally, the *cycle graph* denoted by $C_N = (V, E)$ such that $|V| = N$, each vertex is connected to its consecutive, also the first vertex is connected to the last one. In other words $(v_i, v_{i+1}) \in E$ for all $v_i \in V$ with $1 \leq i < N$ and $(v_1, v_N) \in E$. In Figure 1.2 (c), an example of the cycle graph is shown where $N = 4$, that is, C_4.

There is a type of graph called *ring lattice*, that is a graph which is obtained by taking a cycle graph and connecting each vertex to its neighbors two "hops" away, which is written as $C(N, 2)$ giving as a result a 4-regular graph (that is, all its vertices have degree 4), as it can be seen in Figure 1.3, an example of the ring lattice $C(6, 2)$ is shown, where each of its vertices has degree 4. The definition can be generalized to other even numbers greater than 4 (connecting each vertex to its neighbors three hops away, that is $C(N, 3)$ giving a 6-regular graph, and so on: $C(N, k)$, the particular case when $k = 1$ is exactly the cycle graph C_N).

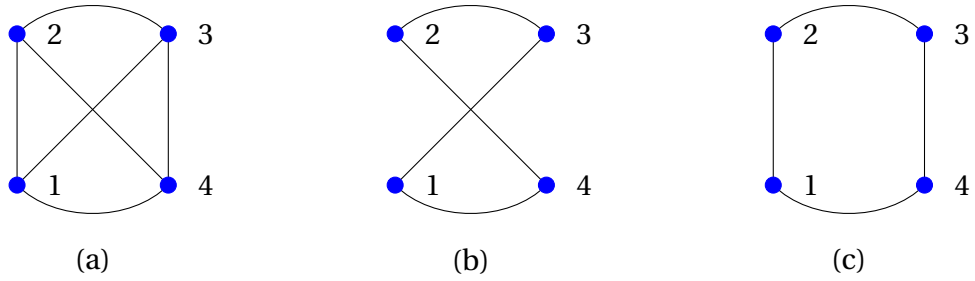

Figure 1.2 – Example of a complete graph, a bipartite complete graph and a cycle graph. In (a) the complete graph of dimension 4 is presented, denoted by K_4, in (b) the complete bipartite graph is shown with two sets of dimension two, which is denoted as $K_{2,2}$ and finally, in (c) the cycle graph of dimension 4 is shown, which is written as C_4.

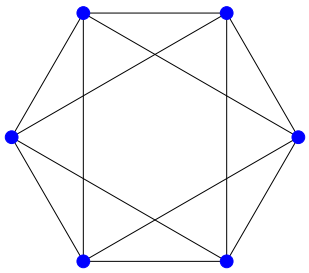

Figure 1.3 – Ring lattice example $C(6,2)$, which is made based on a cycle graph C_6 and each vertex is joined with its first two neighbors to the left and to the right.

From the graphs, it can be defined their subsets to study each of their parts. A *subgraph* of G (or *subnetwork*) is also a graph, written $G' = (V', E')$ such that $V' \subset V$ and all the edges in $E' \subset E$ have end vertices in V'. As it is easy to infer, in general, each subgraph has multiple subgraphs, Figure 1.4 shows in (a) an example of a graph with 4 vertices and 4 edges, and in (b) one of its subgraphs composed of 3 vertices and 2 edges which are included in the sets of vertices and edges of the original graph (a). The set of vertices with which a fixed vertex v is connected, it is called *neighborhood*, and each one of them is called *neighbor*. For example, in Figure 1.4 (a), vertices 2 and 3 are neighbors of vertex 1. In addition, the number of neighbors that a vertex v has can be called the *degree* of v. In Figure 1.4 (a), all the vertices have degree 2, while in (b) the vertex 1 has degree 2 and vertices 2 and 3 have degree 1.

From the subgraphs, other types of graphs can be defined that preserve certain properties. For instance, an *induced subgraph* $G' = (V', E')$ of a graph $G = (V, E)$ is one subgraph such that for the vertices subset $V' \subset V$ all of the edges $E' \subset E$ connecting

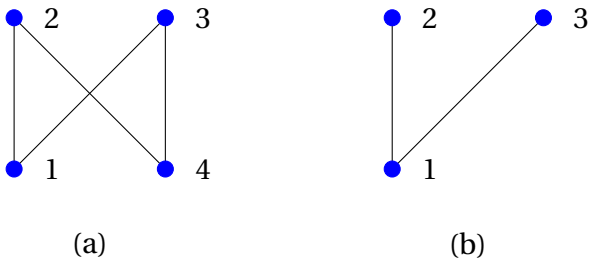

(a) (b)

Figure 1.4 – Example of a graph and one of its subgraphs. In (a) a graph is shown, which is the cycle graph of dimension 4 C_4 and in (b) a subgraph of it is shown. All the vertices that appear in (b) are in (a) and this happens analogously for the edges.

pairs of vertices in V'. In Figure 1.5, an example of a graph, an induced subgraph and a subgraph that is not induced is shown. For the same set of vertices. In (a) a graph is shown. In (b), an induced subgraph of it is shown, because all the edges connecting to the vertices in (a) appear in (b). In (c), a subgraph is shown that is not induced by (a), because not all the edges connecting the vertices in (a) appear in (c).

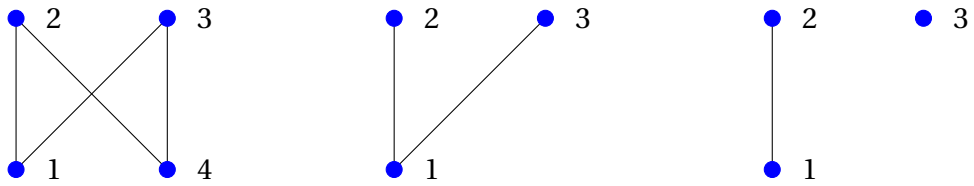

(a) (b) (c)

Figure 1.5 – Example of a graph, an induced subgraph and a not induced subgraph. In (a), a graph is shown. In (b), an induced subgraph of (a) is shown, because all the edges connecting to the vertices in (a) appear in (b). In (c), a subgraph of (a) is shown, but it is not induced by (a), because not all the edges connecting the vertices in (a) appear in (c).

Now, I am interested in exploring the type of connections that exist in the graph beyond the first neighbors. That is, if one vertex can be reached to another by following a succession of vertices in such a way that they are connected by an edge. This concept is called *path*, and more formally, it is a sequence of vertices in an undirected graph G such that each couple of consecutive vertices form an edge. On the other hand, a path in a directed graph D is an ordered sequence of vertices:

$$v_1 \to v_2 \to \cdots \to v_{n-1} \to v_n$$

such that, each couple of consecutive vertices form an arrow. In this case it is said that v_1 is the *starting* vertex of the path and v_n the *ending* one. Furthermore, if the number of arrows in the sequence is counted, that is $n-1$, this amount is called *length of the path*. In Figure 1.6 it is shown an example of different paths that are in the same graph. They are two different paths to get from vertex 1 to vertex 3 highlighted in red. Explaining them in detail. In (a), the path $v_1 \to v_2 \to v_3$ is shown. In (b), the path $v_1 \to v_3$ is shown as well. The first path has length 2 and the second path has length 1. This is a very important concept for later definitions. Also, a path is said to be *maximal* if it cannot be added any new vertex to make it longer.

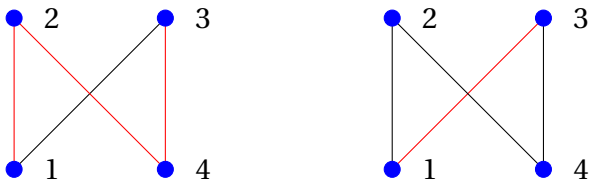

(a) (b)

Figure 1.6 – Example of two paths between two vertices in the same graph. Both in (a) and in (b) the same graph is shown, the difference between them is the red highlighted lines that denote different paths through which one can get from vertex 1 to vertex 3. In (a), there is a path of length 3, passing through vertices 1, 2, 4, and 3. In (b), a path of length 1 is shown, passing directly from vertex 1 to vertex 3.

From the definition of a path of a graph, it can be defined properties of it. In this case, it is said that a graph is *connected* if each couple of vertices belong to a path. If for a given graph there is a path through all its vertices, then the graph is connected. As can be seen in Figure 1.6, both graphs are connected. On the other hand, any graph G can be decomposed in a unique manner as a disjoint union of connected subgraphs $G_1, ..., G_n$, called *connected components*. As is depicted in Figure 1.7, a graph of 5 vertices and 4 edges, which has two connected components is shown. The first subgraph is composed of vertices 1 and 2 and the edge that joins them. The second subgraph is composed of vertices 3, 4 and 5 and the edges that go from vertices 3 to 4, 4 to 5 and 5 to 3. These subgraphs are disjoint, connected and they are the only ones that the graph is composed of, that is, they are its connected components.

Each of the directed or undirected graphs can be written as a square matrix with entries in the real numbers, in which each row and column represents a vertex, coded

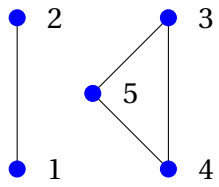

Figure 1.7 – Example of a graph with two connected components. This figure shows a graph with five vertices and 4 edges, in this case there are two connected components, the first is the one composed of vertices 1 and 2 and the edge that joins them, and the second is formed by the vertices 3,4 and 5 and the edges that join this set of vertices.

0 if there are no edges or arrows between them, and 1 if there are some connection type. This object is called the *adjacency matrix* associated with the graph G. It can be written each of its entries as $a_{i,j}$ where i represents the row number and j represents the column number. The set of square matrices with N rows and N columns with entries in the real numbers is written as $\mathscr{M}_{N\times N}(\mathbb{R})$. In Figure 1.8 (a), an example of an undirected graph is shown, and in (b), the adjacency matrix associated with this graph is shown as well. In blue, the numbering of the rows and columns are shown, with they each entry can be written if there is an edge between the associated vertices (with a 1) or not (with a 0).

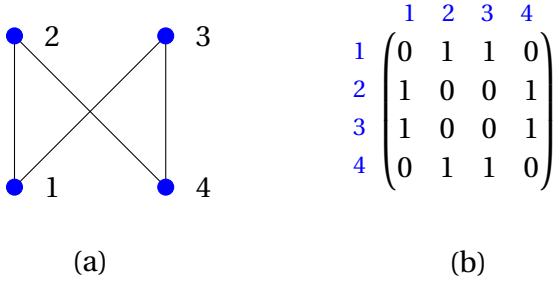

(a) (b)

Figure 1.8 – Example of an adjacency matrix associated to a graph. In (a) a cycle graph of dimension 4 is shown, and in (b) the adjacency matrix associated with this graph is shown. In blue, the numbering of the rows and columns of the matrix is shown, which serves to guide us in the construction of the matrix, which represents the vertices in the graph shown in (a), this construction is done as follows: at position i, j of the matrix a 1 is written when there is an edge connecting vertex i with vertex j and a 0 when there is no edge between them.

There are many types of matrices, and in this case, there are presented two types

that will be useful later to define the system. First of all, it is the *diagonal matrix* that is denoted by $Diag(\{x_1, x_2, ..., x_N\})$ where $x_1, x_2, ..., x_N \in \mathbb{R}$, and is defined as follows $a_{i,j} = x_i$, if $i = j$ where $1 \leq i, j \leq N$, and 0 otherwise. Here is an example of a diagonal matrix.

$$Diag(\{1,2,3,4\}) = \begin{pmatrix} 1 & 0 & 0 & 0 \\ 0 & 2 & 0 & 0 \\ 0 & 0 & 3 & 0 \\ 0 & 0 & 0 & 4 \end{pmatrix}.$$

Second, the *degree matrix* associated with an adjacency matrix M_G that is denoted $Deg(M_G)$ is a diagonal matrix defined as follows, each entry $a_{i,j} \neq 0$ corresponds to the degree of the vertex v_i of G. As it can be seen in the example depicted in Figure 1.9. In (a), it is shown one graph, and in (b), is its degree matrix associated.

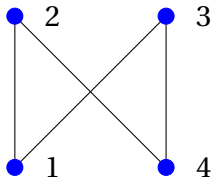

(a)

$$Deg(M_G) = \begin{pmatrix} 2 & 0 & 0 & 0 \\ 0 & 2 & 0 & 0 \\ 0 & 0 & 2 & 0 \\ 0 & 0 & 0 & 2 \end{pmatrix}$$

(b)

Figure 1.9 – Example of a degree matrix associated with a graph. In (a), an example of the cycle graph of dimension 4 C_4 is shown, and in (b), the degree matrix associated with its adjacency matrix (which can be seen in the Figure 1.8) is shown. In this case, all the vertices of the graph shown in (a) they have degree 2, then, in (b), there are only twos on the diagonal of the matrix.

From these definitions, the function called *Laplacian matrix* $L : \mathscr{M}_{N\times N}(\mathbb{R}) \to \mathscr{M}_{N\times N}(\mathbb{R})$ is presented. It is applied to the adjacency matrix M_G associated with a graph G and is defined as follows:

$$L(M_G) = M_G - Deg(M_G). \tag{1.1}$$

This is the finite matrix-analogue of the classical Laplacian operator in physics Cvetkovic, Doob, and Sachs 1995 that describe multiple phenomena such as heat conduction or wave propagation. In Figure 1.10 is shown in (a) a fixed graph and in (b) the computation of the Laplacian matrix associated with the adjacency matrix of (a), which in this case is nothing more than using the previous examples shown in Figures 1.8 and 1.9. Also, $L(M_G)$ is a *symmetric matrix*, that is, $a_{i,j} = a_{j,i}$ for all $1 \leq i, j \leq N$, this happens as long as G is undirected. Using this mathematical concept, it has been possible to study the vibration of a discrete membrane Cvetkovic, Doob, and Sachs

1995 and some chemical properties of substances Merris 1994. In addition, its spectrum has been widely studied when applied to different types of graphs, for example, in K. Das 2004; K. C. Das 2004; Liu, Dolgushev, Qi, et al. 2015, whose definitions are in the next section.

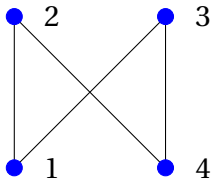

(a)

$$L(M_G) = \begin{pmatrix} -2 & 1 & 1 & 0 \\ 1 & -2 & 0 & 1 \\ 1 & 0 & -2 & 1 \\ 0 & 1 & 1 & -2 \end{pmatrix}$$

(b)

Figure 1.10 – Example of Laplacian matrix associated with a graph. In (a) an example of the cycle graph of dimension 4 C_4 is shown and in (b) shows the Laplacian matrix associated with its adjacency matrix, which is defined as the subtraction of the adjacency matrix (calculated in the Figure 1.8) and the degree matrix (calculated in the Figure 1.9), resulting in the matrix that is shown in (b).

As it is mentioned before, in this thesis there is an interest in the behavior of three graphs in particular, then it proceeds to write the Laplacian matrix of the complete graph K_N, the complete bipartite graph $K_{N,N}$ and the cycle graph C_N in a generalized manner for future reference.

It is recalled that in the Equation (1.1), the calculation of the Laplacian matrix depends on the adjacency matrix and the degree matrix. In the case of the complete graph K_N, its adjacency matrix M_{K_N} is formed by ones in all the entries except the diagonal (which is formed only by zeros), furthermore, each one of the vertices is connected to all the others, that is why the degree of each vertex is $N-1$, then:

$$\left(L(M_{K_N})\right)_{i,j} = \begin{cases} -(N-1) & \text{if } i = j, \\ 1 & \text{otherwise.} \end{cases} \tag{1.2}$$

The matrix form of the Equation (1.2) is as follows.

$$L(M_{K_N}) = \begin{pmatrix} -(N-1) & 1 & \cdots & 1 & 1 \\ 1 & -(N-1) & \cdots & 1 & 1 \\ \vdots & & \ddots & & \vdots \\ 1 & 1 & \cdots & -(N-1) & 1 \\ 1 & 1 & \cdots & 1 & -(N-1) \end{pmatrix}.$$

Now, for the calculation of the Laplacian matrix in the case of the complete bipartite

graph $K_{N,N}$, it is remembered that each vertex of V_i is joined with the N vertices of the other subset V_j where $i, j \in \{1,2\}$ with $i \neq j$. In addition, its adjacency matrix $M_{K_{N,N}}$ is composed of 2 blocks of zeros and 2 blocks of ones, then:

$$\left(L(M_{K_{N,N}})\right)_{i,j} = \begin{cases} -N & \text{if } i = j, \\ 1 & \text{if } N < i \leq 2N \text{ and } 0 < j \leq N \\ & \text{or } N < j \leq 2N \text{ and } 0 < i \leq N, \\ 0 & \text{otherwise.} \end{cases} \tag{1.3}$$

The matrix form of the Equation (1.3) is as follows.

$$L(M_{K_{N,N}}) = \begin{pmatrix} -N & 0 & \cdots & 0 & 1 & \cdots & 1 & 1 \\ 0 & -N & & 0 & 1 & \cdots & 1 & 1 \\ \vdots & & \ddots & & \vdots & & \vdots & \vdots \\ 0 & 0 & & -N & 1 & \cdots & 1 & 1 \\ 1 & 1 & \cdots & 1 & -N & & 0 & 0 \\ \vdots & \vdots & & \vdots & & \ddots & & \vdots \\ 1 & 1 & \cdots & 1 & 0 & & -N & 0 \\ 1 & 1 & \cdots & 1 & 0 & \cdots & 0 & -N \end{pmatrix}.$$

In the case of the cycle graph C_N, it is remembered that each vertex is joined to its two adjacent vertices, so each one has degree 2. In addition, the adjacency matrix M_{C_N} is made up of two ones in each row and the other entries are zero. This is repeated cyclically and symmetrically in each of the rows, that is why there is the following Laplacian matrix:

$$\left(L(M_{C_N})\right)_{i,j} = \begin{cases} -2 & \text{if } i = j, \\ 1 & \text{if } i = j+1 \text{ and } 0 < j \leq N-1 \\ & \text{or } i = j-1 \text{ and } 1 < j \leq N, \\ & \text{or } i = 1 \text{ and } j = N, \\ & \text{or } i = N \text{ and } j = 1, \\ 0 & \text{otherwise.} \end{cases} \tag{1.4}$$

The matrix form of the Equation (1.4) is as follows.

$$L(M_{C_N}) = \begin{pmatrix} -2 & 1 & 0 & 0 & \cdots & 0 & 0 & 0 & 1 \\ 1 & -2 & 1 & 0 & \cdots & 0 & 0 & 0 & 0 \\ 0 & 1 & -2 & 1 & & 0 & 0 & 0 & 0 \\ & \ddots & & & \ddots & & & \ddots & \\ 0 & 0 & 0 & 0 & & 1 & -2 & 1 & 0 \\ 0 & 0 & 0 & 0 & \cdots & 0 & 1 & -2 & 1 \\ 1 & 0 & 0 & 0 & \cdots & 0 & 0 & 1 & -2 \end{pmatrix}.$$

Finally, in the case of the family of ring lattices $C(N,k)$, specifically when two neigh-

bors to the left and two neighbors to the right are considered, that is, $C(N,2)$, the Laplacian matrix associated with its adjacency matrix $M_{C(N,2)}$ is written as follows:

$$\left(L(M_{C(N,2)})\right)_{i,j} = \begin{cases} -4 & \text{if } i = j, \\ 1 & \text{if } i = j+1 \text{ and } 0 < j \leq N-1 \\ & \text{or } i = j-1 \text{ and } 1 < j \leq N, \\ & \text{or } i = j+2 \text{ and } 0 < j \leq N-2 \\ & \text{or } i = j-2 \text{ and } 2 < j \leq N, \\ & \text{or } i = 1 \text{ and } N-1 \leq j \leq N, \\ & \text{or } i = 2 \text{ and } j = N, \\ & \text{or } i = N-1 \text{ and } j = 1, \\ & \text{or } i = N \text{ and } 1 \leq j \leq 2, \\ 0 & \text{otherwise.} \end{cases} \tag{1.5}$$

The matrix form of the Equation (1.5) is as follows.

$$L(M_{C(N,2)}) = \begin{pmatrix} -4 & 1 & 1 & 0 & \cdots & 0 & 0 & 1 & 1 \\ 1 & -4 & 1 & 1 & \cdots & 0 & 0 & 0 & 1 \\ 1 & 1 & -4 & 1 & & 0 & 0 & 0 & 0 \\ & \ddots & & & \ddots & & & \ddots & \\ 0 & 0 & 0 & 0 & & 1 & -4 & 1 & 1 \\ 1 & 0 & 0 & 0 & \cdots & 1 & 1 & -4 & 1 \\ 1 & 1 & 0 & 0 & \cdots & 0 & 1 & 1 & -4 \end{pmatrix}.$$

From the matrices described in this section, which represent the Laplacian system applied to the complete graph, the complete bipartite graph, the cycle graph, and the ring lattice family, it is then possible to define the system of coupled differential equations that corresponds to each type of matrix, as will be seen in later sections.

1.1.2 Linear algebra

A matrix $M \in \mathscr{M}_{N\times N}(\mathbb{R})$, can be interpreted as a linear transformation (because this set is a vector space), such that $M : \mathbb{R}^N \to \mathbb{R}^N$ such that for certain $v, w \in \mathbb{R}^N$, $M(v) = w$.

In the case where $v \neq 0$ and $w = \lambda v$, for some $\lambda \in \mathbb{R}$, that is, w is a multiple of v, so it is called λ *eigenvalue* of M and v is its corresponding *eigenvector* (of M). The set of all eigenvalues and eigenvectors of a given matrix M is called the *eigensystem* of M.

On the other hand, a square matrix M is called *diagonalizable*, if there exist $P, D \in \mathscr{M}_{N\times N}(\mathbb{R})$ such that P is *invertible* (that means, there is a $P^{-1} \in \mathscr{M}_{N\times N}(\mathbb{R})$ such that $P^{-1}P = \mathbb{I} = PP^{-1}$, where $\mathbb{I} = Diag(\{1,...,1\})$ and $D = Diag(\{\lambda_1,...,\lambda_N\})$ such that:

$$M = PDP^{-1}.$$

It should be noted that not all square matrices can be diagonalized, but there are certain subsets that always have this characteristics, an example are the symmetric matrices.

It is important to know that all the elements that appear on the diagonal of D are eigenvalues of M and this set is called the *spectrum* of M denoted as $Spec(M)$. The largest value in the spectrum of M is called the *maximal eigenvalue*. When an eigenvalue does not repeat, it is called a *simple eigenvalue*. On the other hand, the number of times an eigenvalue λ is repeated is called the *algebraic multiplicity* of λ.

Each of the columns of P forms a *eigenbasis* or just *basis* $\mathscr{B}$ of $\mathscr{M}_{N\times N}(\mathbb{R})$, that is, all the elements of $\mathscr{M}_{N\times N}(\mathbb{R})$ can be written as a *linear combination* of the elements of $\mathscr{B}$ (that means, for all $M \in \mathscr{M}_{N\times N}(\mathbb{R})$ there exist $a_1, ..., a_N \in \mathbb{R}$ such that $M = \sum_{i=1}^{N} a_i b_i$, where $b_i \in \mathscr{B}$), in other words we can say that the elements of $\mathscr{B}$ *generate* the space and furthermore, all its elements are *linearly independent* (which means that none of the elements of $\mathscr{B}$ is a linear combination of the other elements of $\mathscr{B}$).

There are several types of bases, in this case will be discussed about the three most used. First of all, the *canonical basis*, in $\mathbb{R}^N$ is formed as the following set, where each of the N vectors has N components (1 equals one and $N-1$ equals zero). It is denoted the i-th element as e^i.

$$\left\{ \begin{pmatrix} 1 \\ 0 \\ \vdots \\ 0 \\ 0 \end{pmatrix}, \begin{pmatrix} 0 \\ 1 \\ \vdots \\ 0 \\ 0 \end{pmatrix}, \cdots, \begin{pmatrix} 0 \\ 0 \\ \vdots \\ 1 \\ 0 \end{pmatrix}, \begin{pmatrix} 0 \\ 0 \\ \vdots \\ 0 \\ 1 \end{pmatrix} \right\}.$$

Secondly, the *orthogonal basis*, is a basis in which each pair of its elements has a scalar product equal to zero. For example, the canonical basis for $\mathbb{R}^2$, $\mathscr{B}^* = \{\binom{1}{0}, \binom{0}{1}\}$ also is an orthogonal basis. Finally, the *orthonormal basis*, which is an orthogonal basis and its elements have *norm* (in this case, if $v = (v_1, .., v_N)$, then $||v|| = \sqrt{\sum_{i=1}^{N} v_i^2}$) equal to one, $\mathscr{B}^*$ is also an example of an orthonormal basis. Now it is taken the opportunity to define the *dominant eigenvector* of a basis, it refers to the eigenvector with the largest norm.

An important property that will be used throughout this thesis is the fact that any symmetric matrix is diagonalizable. As already described, the Laplacian matrix is always symmetric, so it can always be diagonalized. Next it is described the eigensystems of the Laplacian matrices of the three graphs that are the object of study of this thesis, the complete graph K_N, the complete bipartite graph $K_{N,N}$ and the cycle graph C_N, which were calculated in the previous Section 1.1.2.

First, for the Laplacian matrix of the complete graph $L(M_{K_N})$ shown in Equation (1.2),

and:

$$Spec(L(M_{K_N})) = \{0, -N\}. \tag{1.6}$$

Where 0 has algebraic multiplicity 1 and $-N$ has algebraic multiplicity $N-1$. On the other hand, the eigenvectors are of the following form:

$$(v_i)_j = \begin{cases} 1 & \text{if } i = N, \text{ for all } 1 \leq j \leq N, \\ & \text{or } i = N+1-j \text{ and } 0 < j \leq N, \\ -1 & \text{if } j = 1, \text{ for all } 1 \leq i < N, \\ 0 & \text{otherwise.} \end{cases} \tag{1.7}$$

Where v_N is the eigenvector corresponding to the eigenvalue 0 and v_i where $1 \leq i < N$ are the eigenvectors corresponding to the eigenvalue $-N$.

In vector form, the vectors of the Equation (1.7) can be written as follows.

$$\left\{ \begin{pmatrix} -1 \\ 0 \\ 0 \\ \vdots \\ 0 \\ 0 \\ 1 \end{pmatrix}, \begin{pmatrix} -1 \\ 0 \\ 0 \\ \vdots \\ 0 \\ 1 \\ 0 \end{pmatrix}, \begin{pmatrix} -1 \\ 0 \\ 0 \\ \\ 1 \\ 0 \\ 0 \end{pmatrix}, \cdots, \begin{pmatrix} -1 \\ 0 \\ 1 \\ \\ 0 \\ 0 \\ 0 \end{pmatrix}, \begin{pmatrix} -1 \\ 1 \\ 0 \\ \vdots \\ 0 \\ 0 \\ 0 \end{pmatrix}, \begin{pmatrix} 1 \\ 1 \\ 1 \\ \vdots \\ 1 \\ 1 \\ 1 \end{pmatrix} \right\}.$$

The norm of these vectors is:

$$\|v_i\| = \begin{cases} \sqrt{2} & \text{if } 1 \leq i < N, \\ \sqrt{N} & \text{if } i = N. \end{cases} \tag{1.8}$$

that means that, when $N > 2$, v_N is the dominant eigenvector of $L(M_{K_n})$.

Secondly, the eigensystem for the Laplacian matrix of the complete bipartite graph $L(M_{K_{N,N}})$ shown in Equation (1.3):

$$Spec(L(M_{K_{N,N}})) = \{0, -N, -2N\}. \tag{1.9}$$

For this spectrum, 0 and $-2N$ have algebraic multiplicity equal to 1 and $-N$ has algebraic multiplicity $2(N-1)$. Now, the respective eigenvectors are defined in the following way:

$$(v_i)_j = \begin{cases} 1 & \text{if } i = 2N, \text{ for all } 1 \leq j \leq 2N, \\ & \text{or } i = 1 \text{ and } N < j \leq 2N, \\ & \text{or } i = N+1-j \text{ and } 0 < j \leq N, \\ & \text{or } i = N+2-j \text{ and } N+1 < j \leq 2N, \\ -1 & \text{if } i = 1, \text{ for all } 1 \leq j \leq N, \\ & \text{or } j = 1 \text{ and } N \leq i < 2N, \\ & \text{or } j = N \text{ and } 1 < i \leq N, \\ 0 & \text{otherwise.} \end{cases} \tag{1.10}$$

Where v_{2N} is the eigenvector corresponding to the eigenvalue 0, v_1 is the eigenvector corresponding to the eigenvalue $-2N$ and v_i where $1 < i < 2N$ are the eigenvectors corresponding to the eigenvalue $-N$.

In vector form, the vectors of the Equation (1.10) can be written as follows.

$$\left\{ \begin{pmatrix} -1 \\ -1 \\ \vdots \\ -1 \\ -1 \\ 1 \\ \vdots \\ 1 \\ 1 \end{pmatrix}, \begin{pmatrix} 0 \\ 0 \\ \vdots \\ 0 \\ -1 \\ 0 \\ \vdots \\ 0 \\ 1 \end{pmatrix}, \begin{pmatrix} 0 \\ 0 \\ \vdots \\ 0 \\ -1 \\ 0 \\ \\ 1 \\ 0 \end{pmatrix}, \cdots, \begin{pmatrix} 0 \\ 0 \\ \vdots \\ 0 \\ -1 \\ 1 \\ \\ 0 \\ 0 \end{pmatrix}, \begin{pmatrix} -1 \\ 0 \\ \\ 1 \\ 0 \\ 0 \\ \vdots \\ 0 \\ 0 \end{pmatrix}, \cdots, \begin{pmatrix} -1 \\ 1 \\ \\ 0 \\ 0 \\ 0 \\ \vdots \\ 0 \\ 0 \end{pmatrix}, \begin{pmatrix} 1 \\ 1 \\ 1 \\ 1 \\ \vdots \\ 1 \\ 1 \\ 1 \\ 1 \end{pmatrix} \right\}.$$

The norm of these vectors is:

$$\|v_i\| = \begin{cases} \sqrt{2N} & \text{if } i = 1, \\ & \text{or } i = 2N, \\ \sqrt{2} & \text{if } 1 < i < 2N. \end{cases} \tag{1.11}$$

In this case there are two eigenvectors corresponding to two different eigenvalues that have the same largest norm.

Then, the eigensystem for the Laplacian matrix of the cycle graph $L(M_{C_N})$ shown in Equation (1.4):

$$Spec\left(L(M_{C_N})\right) = \left\{ 2\left(\cos\left(\frac{2\pi i}{N}\right) - 1\right) : 1 \leq i \leq N \right\}. \tag{1.12}$$

For eachλ_i, by the symmetry of the function $\cos(x)$ and the considered interval $(0, 2\pi)$, $\lambda_i = \lambda_{N-i}$ for $1 \leq i \leq \left\lfloor \frac{N-1}{2} \right\rfloor$, that is, all eigenvalues have algebraic multiplicity equal to 2, except when λ_N, it has algebraic multiplicity equal to 1 and when N is even,

$\lambda_{\frac{N}{2}}$ also has algebraic multiplicity equal to 1.

On the other hand, the eigenvectors of $L(M_{C_n})$ are:

$$(v_i)_j = \cos\left(\frac{2\pi ij}{N}\right), \text{ for } 1 \leq i, j \leq N. \tag{1.13}$$

Where each v_i is the corresponding eigenvector to the eigenvalue λ_i.

In vector form, the vectors of the Equation (1.13) can be written as follows.

$$\left\{ \begin{pmatrix} \cos\left(\frac{2\pi}{N}\right) \\ \cos\left(\frac{4\pi}{N}\right) \\ \vdots \\ \cos\left(\frac{2\pi(N-1)}{N}\right) \\ 1 \end{pmatrix}, \begin{pmatrix} \cos\left(\frac{4\pi}{N}\right) \\ \cos\left(\frac{8\pi}{N}\right) \\ \vdots \\ \cos\left(\frac{2\pi(N-1)}{N}\right) \\ 1 \end{pmatrix}, \cdots, \begin{pmatrix} \cos\left(\frac{2\pi(N-1)}{N}\right) \\ \cos\left(\frac{4\pi(N-1)}{N}\right) \\ \vdots \\ \cos\left(\frac{2\pi(N-1)^2}{N}\right) \\ 1 \end{pmatrix}, \begin{pmatrix} 1 \\ 1 \\ \vdots \\ 1 \\ 1 \end{pmatrix} \right\}.$$

Since $|\cos(x)| \leq 1$ for all $x \in \mathbb{R}$:

$$\|v_i\| \leq \sqrt{N} \tag{1.14}$$

Furthermore, $\|v_i\| = \sqrt{N}$ when each $\cos\left(\frac{2\pi ij}{N}\right) = 1$, it occurs when $i = N$ for all $1 \leq j \leq N$, and when N is even, also if $i = \frac{N}{2}$ which means that v_N is the dominant eigenvector when N is odd, and also $v_{\frac{N}{2}}$ when N is even. This different behavior in the eigensystem depending on the parity of N has repercussions on the dynamic behavior of this matrix as discussed below in Section 3.1.1 where the behavior of the ring lattice family, which is mentioned below, will also be discussed.

The spectrum of the Laplacian matrix associated to the ring lattice family $C(N,k)$ having N vertices and $2k$ neighbors is also known, which is given by:

$$Spec(L(M_{C(N,k)})) = \left\{ 2k - \left(\frac{\sin\left(\frac{\pi}{N}(i-1)(2k+1)\right)}{\sin\left(\frac{\pi}{N}(i-1)\right)} - 1 \right), \quad i = 1, 2, ..., N \right\}.$$

Knowing the behavior of the eigensystems associated with these types of graphs, allows to analytically find the solutions to the associated system of differential equations, which is discussed in the next section.

1.1.3 The Laplacian system

Once the way in which the components of an initial condition will interact and the functions that can be applied to the adjacency matrices associated to the graphs have been defined, it proceeds to define the systems that are considered in this thesis. A graph $G = (V, E)$ is fixed and it is considered a system of coupled differential

equations on $I^{|V|}$, where I is either the set of real numbers $\mathbb{R}$ or the circle, written as S^1. The flow is generated by a system of ordinary differential equations (hereinafter, this phrase is abbreviated as ODEs) coupled according to the interactions defined by E.

As has been anticipated, in this thesis I will focus on the *discrete Laplacian flow* or just *Laplacian flow* on the graph G, which is the linear system defined by:

$$\frac{dx_v}{dt} = (Lx)_v = \sum_{u \in V:(u,v)\in E} (x_u - x_v), \tag{1.15}$$

with $x_v \in \mathbb{R}$ for each $v \in V$. Also, in this equation $L = L(M_G)$ is the Laplacian matrix of the adjacency matrix M_G. In this case, the set that is formed by vectors $x \in I^{|V|}$, such that all its components have the same value, called the *diagonal*:

$$\mathscr{D} = \{x \in I^{|V|} : x_u = x_v \ \forall \ u, v \in V\}, \tag{1.16}$$

is a *global attractor*, i.e., it is such that $\lim_{t\to\infty} dist(x(t), \mathscr{D}) = 0$, for all initial conditions.

For example, in $\mathbb{R}^2$ the set $\mathscr{D}$, is the identity function shown in Figure 1.11, since it is formed by the points whose coordinates (x_1, x_2) are equal, that is $x_1 = x_2$.

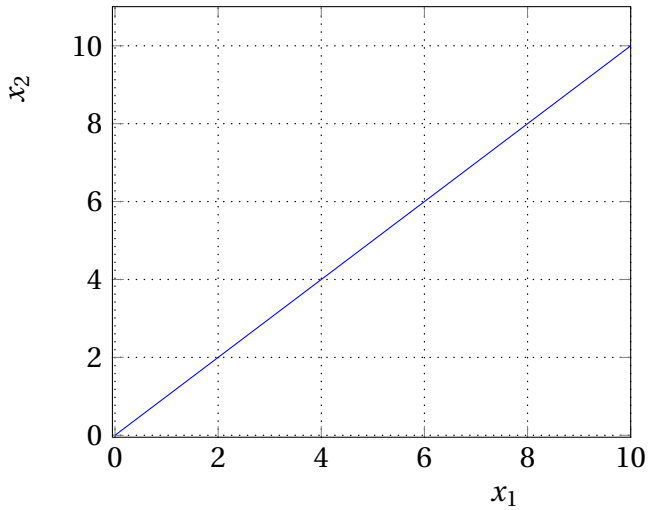

Figure 1.11 – In blue line, the set of the diagonal in dimension 2 is shown for the case of $\mathbb{R}^2$, this particular set has all the points $x = (x_1, x_2)$ whose coordinates are equal $x_1 = x_2$, this is the global attractor of the Laplacian system in dimension 2, analogously it is built for larger dimensions.

The Equation (1.15), is a linear equation with solution $x(t) = e^{tL}x(0)$. Since the Laplacian matrix M_G is symmetric, it can be diagonalized over an orthonormal basis:

$$\mathscr{B}_L := \{v_1, v_2, \ldots, v_N\} \subset \mathbb{R}^N, \tag{1.17}$$

so that:

$$x(t) = \sum_{i=1}^{N} \langle v_i | x(0) \rangle e^{t\lambda_i} v_i, \tag{1.18}$$

where, for each $1 \leq i \leq N$, $\lambda_i \in \mathbb{R}$ is the eigenvalue corresponding to the eigenvector v_i. It is well known, and not so difficult to deduce (see Cvetkovic, Doob, and Sachs 1995 for instance) that, L has a simple maximal eigenvalue $\lambda_N = 0$, and $\lambda_i < 0$ for each $1 \leq i \leq N-1$, that can be verified from the Equations (1.6), (1.9) and (1.12). The dominant eigenvector, v_N is the same as in Equations (1.7), (1.10) and (1.13) but normalized, is precisely the generator of the diagonal, that is $v_N = \frac{1}{\sqrt{N}}(1, ..., 1)$, and in this case:

$$x(t) \to \langle v_N | x(0) \rangle v_N \equiv \left(\frac{1}{N} \sum_{i=1}^{N} x_i(0) \right) v_N \text{ when } t \to \infty.$$

In fact, $dist(x(t), \mathscr{D}) = \sqrt{\sum_{i=2}^{N} |\langle v_i | x(0) \rangle|^2 e^{2\lambda_i t}}$ for each $t \in \mathbb{R}$, as $\lambda_i < 0$, then

$$\lim_{t \to \infty} dist(x(t), \mathscr{D}) = 0.$$

This is the sense in which in this thesis it is considered that the Laplacian system synchronizes, because when time passes, all the coordinates to which the system was applied have the same value.

Consider the complete graph K_N, then, each of its coordinates has a monotonous behavior. Let's consider $L(M_{K_N})$ and either $x \in \mathbb{R}^N$, by Equations (1.6) and (1.7):

$$x(t) = e^{-Nt} \sum_{i=1}^{N-1} x_i v_i + x_N v_N,$$

then, for each coordinate:

$$x_j(t) = e^{-Nt}(x_{N+1-j} - x_1) + x_N,$$

therefore $x_j(t)$ is monotonous. This behavior will be used in Section 2.1 to perform the formal and rigorous analysis of its paths towards synchronization.

1.1.4 The Kuramoto model

Now, the synchronization phenomenon is seen specifically in the case of coupled oscillators. Let's imagine that we have several metronomes, these are artefacts used by beginning musicians that when they are well seated on a table, they can mark the time correctly so that they can trust them to mark the beat, this is done by means

of the sound of a needle that moves from left to right at equal time intervals. This behavior changes when one metronome is influenced by another. This happens when, for example, we put them next to each other on a swing, in this way their mechanical movement flows through the board and thus, that movement is "felt" by the other metronome. We let them interact for a few moments and after time passes, it turns out that, despite the fact that the two metronomes have begun to oscillate at different times with different frequencies, we could see one of the following cases, first, that the influence between them has been so much that they are *synchronized*, that is, that both mark the same beat, when one goes to the right or to the left, the other also, as it is shown in Figure 1.12 (a) represents metronome 1 and (b) represents metronome 2. Secondly, it may be that they both mark the same beat, but when one goes to the left, the other goes to the right and vice versa, which causes some compensation in the oscillation, in other words they are in a *phase locking* state as it is shown in Figure 1.13 (a) represents metronome 1 and (b) represents metronome 2. Finally, if the influence they exerted on each other is too weak, what can happen is that they never get to synchronize and each one marks different and independent beats, that is, they remain in a state of *incoherence* as it is shown in Figure 1.14 (a) represents metronome 1 and (b), represents metronome 2.

Mathematically, according to Kuramoto, asymptotically the dynamics of some systems are almost identical, and he proposed that N coupled oscillators are described by the following coupled system of equations:

$$\frac{dx_i}{dt} = \omega_i + \sum_{j=1}^{N} \Gamma_{i,j}(x_j - x_i), \tag{1.19}$$

for $i = 1,..,N$, where the *interaction function* $\Gamma_{i,j}$ determines the form of coupling between each oscillator i and j, also, ω_i is the *natural frequency*, and x_i is the *phase angle* of each oscillator.

The Equation (1.19) is very general, allowing any type of coupling $\Gamma_{i,j}$, however, this interaction function is very complicated to analyze, which makes the theoretical analysis considerably more difficult. The first and clearest example, is when Γ is equal to the identity function, then, there is a translation of the Laplacian system that depends on the ω_i. This can give an idea that every time that the function Γ is modified, it can be the subject of a large area of study.

Due to this great challenge, Kuramoto assumed that each oscillator affects all other oscillators by calling this kind of interaction *global coupling*. At the same time, he assumed that the interactions between the oscillators are equal and depend only sinusoidally on the phase difference, given by the following function:

$$\Gamma_{i,j}(x_j - x_i) = \frac{K}{N}\sin\big(x_j - x_i\big), \tag{1.20}$$

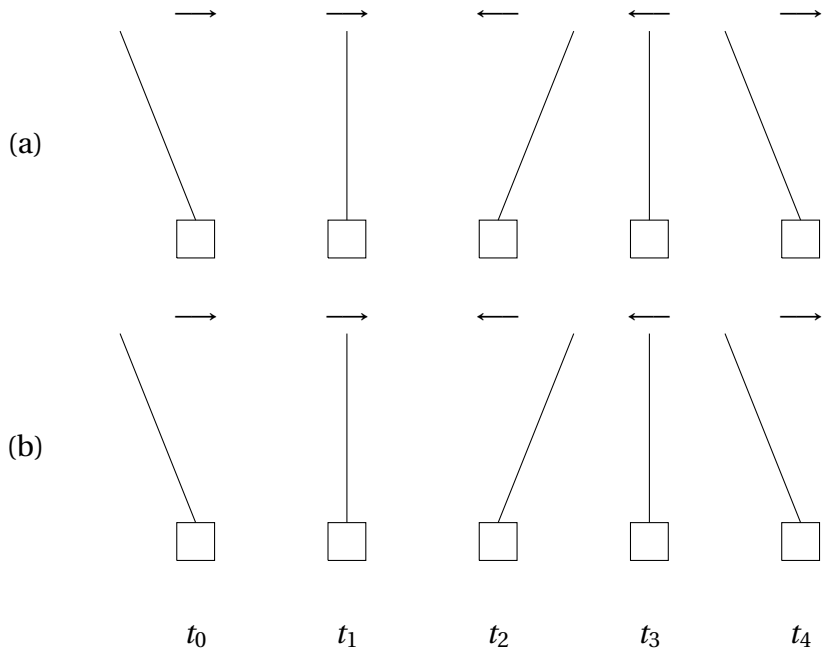

Figure 1.12 – In (a) and (b) two different metronomes are shown, which are photographed at times t_0, t_1, t_2, t_3, t_4, the arrow above each of the photographs shows the direction it has the instant after the photo was taken. In this case, the oscillators at each instant have the same direction, which is called synchronized. The fact that the times t_0 and t_4 are shown is to observe the periodicity of the oscillators.

where the parameter K determines the *coupling strength*.

Substituting the Equation (1.20) in Equation (1.19), it is the so-called *Kuramoto Model*, this is a simple model of N mutually coupled oscillators having different natural frequencies ω_i drawn from some probability density $\omega \mapsto g(\omega)$, with phases x_i, as in the following equation:

$$\frac{dx_i}{dt} = \omega_i + \frac{K}{N}\sum_{j=1}^{N}\sin\big(x_j - x_i\big). \tag{1.21}$$

Because this model describes the synchronization of a system, one of the natural questions has been how to quantify the degree of synchronization (there are a lot of examples, but you can see Fonseca and Abud 2018 for instance), that is why the dynamics of the Equation (1.21) has been analyzed in terms of the *order parameter*, then, the complex *mean field* of the population can be written as follows:

$$Z = X + iY = re^{i\Theta} = \frac{1}{N}\sum_{j=1}^{N} e^{ix_j}. \tag{1.22}$$

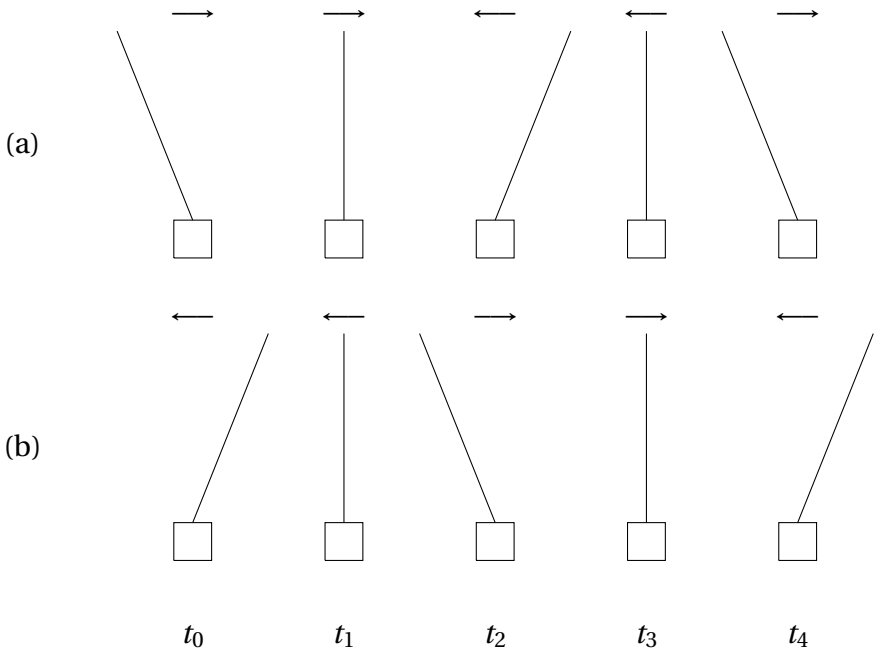

Figure 1.13 – In (a) and (b) two different metronomes are shown, which are photographed at times t_0, t_1, t_2, t_3, t_4, the arrow above each of the photographs shows the direction it has the instant after the photo was taken. In this case, the oscillators at each instant have the opposite direction, which is called phase locking. The fact that the times t_0 and t_4 are shown is to observe the periodicity of the oscillators.

The mean field, has amplitude r and phase Θ, as in the following equation:

$$r\cos(\Theta) = \frac{1}{N}\sum_{j=1}^{N}\cos(x_j), \qquad r\sin(\Theta) = \frac{1}{N}\sum_{j=1}^{N}\sin(x_j) \tag{1.23}$$

Equation (1.22), corresponds to the centroid of all the oscillators when they are represented as points on a unit circle. The magnitude r of the order parameter, also can be understood as a *measure of synchronization*: if all the oscillators are fully synchronized with identical angles $x_i(t)$, then $r = 1$, and if all the oscillators are separated on the unit circle, then $r = 0$. It is shown in Figure 1.15 examples of this synchronization measurement for two coupled oscillators, in (a) it is observed that the oscillators are in phase locking state, in (b) it is a state of incoherence and in (c) a synchronization state.

The Kuramoto model, from the Equation (1.21) has been applied to complex networks, in the sense that the involved oscillators will influence each other, depending on the connections that a network has, that is:

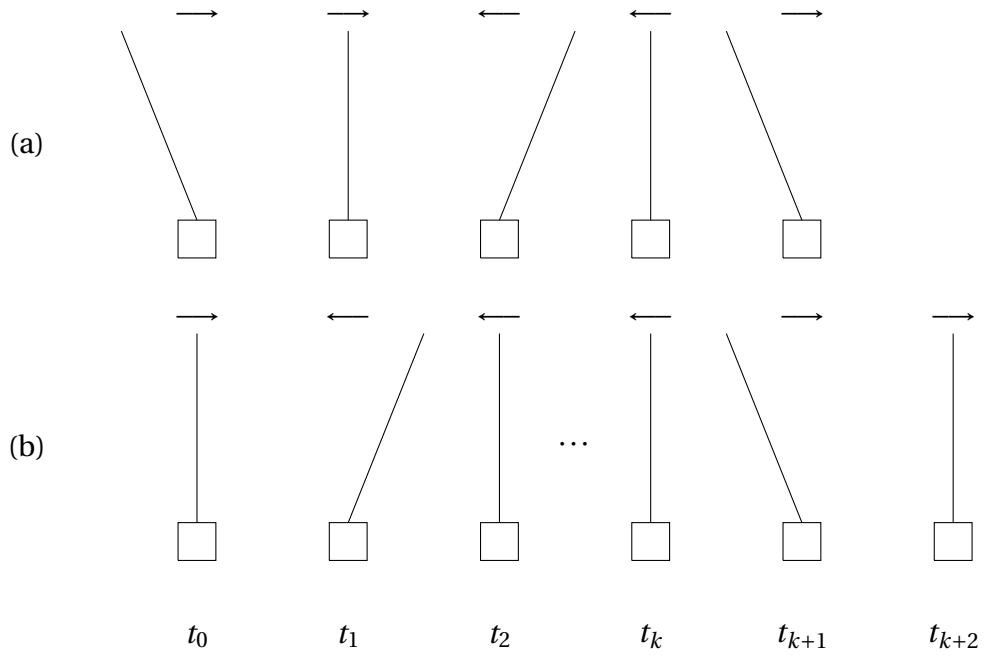

Figure 1.14 – In (a) and (b) two different metronomes are shown, which are photographed at times t_0, t_1, t_2, t_3, t_4, the arrow above each of the photographs shows the direction it has the instant after the photo was taken. In this case, the oscillators have their direction independently of each other, they go at their own pace and it is not possible to make a pattern of their behavior at different times.

$$\frac{dx_i}{dt} = \omega_i + \sigma \sum_{j \in \mathcal{V}(i)} \sin\big(x_j - x_i\big), \tag{1.24}$$

where $\mathcal{V}(i)$ denotes the *set of closest neighbors* of node i, the natural frequencies are distributed according to some probability density $\omega \mapsto g(\omega)$ and σ is the coupling strength with a suitable scale, such that the model has a good behavior when $N \to \infty$.

The Kuramoto model applied to different types of graphs has been widely studied, for example in DeVille and B. Ermentrout 2016; Delabays, Jacquod, and Dörfler 2019; Medvedev and Tang 2017; Moreno and Pacheco 2004; Gómez-Gardeñes, Moreno, and Arenas 2007, both for random and non-random graphs. Whether synchronization occurs depends on two factors: the coupling strength, and the difference between the frequencies of both oscillators. The coupling strength describes how weak or strong the interaction is. In the example of the metronomes on the swing, we can interpret it as a measure of the freedom that the strings allow them to move the board while they oscillate. Conversely, if the strings were rigid, then the movement of the metronomes would not affect the board and there would be no way for the two metronomes to

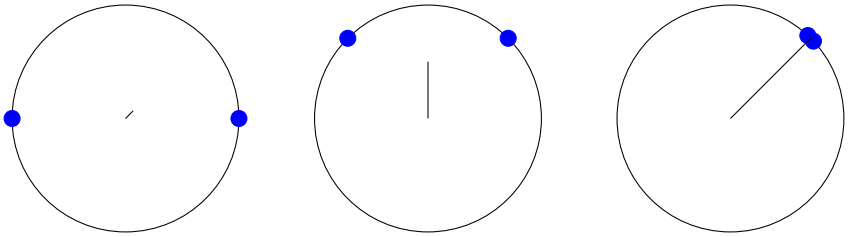

(a) (b) (c)

Figure 1.15 – In (a), (b) and (c) the angles that two oscillators have in three different situations are shown and the line that appears in the center of the circle towards the average of the angles shows the synchronization measure that exists between both oscillators, the first, that is (a), shows that the synchronization measure is zero, because the oscillators are in totally opposite directions, in other words, in phase locking. In (b), at the instant that the synchronization measurement was captured, it is greater than zero, because the angles seem to be close, which will not last long, because it is not an equilibrium state, so each of the angles will follow its path and the synchronization measurement will continue to change without stabilizing. In (c) it is shown that both angles are very close, so the synchronization measure corresponds to the length of the radius, that is, $r = 1$, which means that these oscillators are synchronized.

interact, so the coupling strength would tend to zero. On the other hand, if the strings are not fixed, but can vibrate or move with some ease, the interaction force would be increased. The other factor that allows synchronization to occur is the difference in natural frequencies between the oscillators describes how different they are. Then, measuring the coupling strength experimentally has some difficulty, but the frequency difference is easy to measure and to vary.

The synchronizing dynamics of the Laplacian flow is preserved in part by the Kuramoto flow neglecting the natural frequencies, written as follows:

$$\frac{dx_v}{dt} = \sigma \sum_{u \in V:\,(u,v)\in E} \sin(x_u - x_v). \tag{1.25}$$

Indeed, the diagonal is a global attractor for the Laplacian flow and, since the linearization of the Kuramoto flow around the diagonal is proportional to the Laplacian flow, applying a Hartman-Grobman argument Hartman 1960; Grobman 1959, it is concluded that it follows a similar converging dynamics in a small neighborhood of the diagonal.

1.1.5 Combinatorics

In this section, basic concepts of combinatorics will be introduced for the previous study of the paths towards the synchronization of the Laplacian system and the Kuramoto model, that are defined in previous sections.

It begins with a very simple concept, but which will be used repeatedly, the *binomial coefficient* is defined from a pair of positive integers N, k such that $k \leq N$. It is written $\binom{N}{k}$, and is given by the formula

$$\binom{N}{k} = \frac{N!}{k!(N-k)!}.$$

Which can be interpreted as the number of ways of k objects can be chosen from a total set of N objects. This concept is widely used and it will help to define more complex concepts as the following, that is the *Narayana number* T_N^k that is defined from a pair of positive integers $N, k in \mathbb{Z}$ such that $k \leq N$. This number is given by the formula:

$$T_N^k = \frac{1}{N}\binom{N}{k}\binom{N}{k-1}. \tag{1.26}$$

In the Table 1.1, the first seven lines of the Narayana numbers are shown, that is when $N = 1, ..., 7$, which generate the *Narayana triangle*.

			1			
		1		1		
	1		3		1	
1		6		6		1
1	10		20		10	1
1	15	50		50	15	1
1	21	105		175	105	21	1

Table 1.1 – The first 7 lines of the Narayana Triangle are shown in this representation which is generated from the Equation (1.26).

The Narayana numbers Narayana 1979 gives a solution to many counting problems in the area of combinatorics as in Stanley and Fomin 1999; Blanco and Petersen 2012 and there is a very complete documentation at Sloane 2021.

In the Equation (1.26), if a sum over all k in each row is done, then, the result is the *Catalan number* denoted as C_N, that is

$$C_N = \sum_{k=1}^{N} T_N^k,$$

which has several expressions as a closed formula, from them, the following is chosen:

$$C_N = \frac{1}{N+1}\binom{2N}{N}. \tag{1.27}$$

The first ten numbers of Catalan are listed below:

$$1, 2, 5, 14, 42, 132, 429, 1430, 4862, 16796.$$

Catalan numbers are the answer to dozens of problems in the area of combinatorics too, there is a very complete documentation at Sloane n.d. For example, this is the number of *Dyck paths* of order N, this is a staircase walk from $(0,0)$ to (N,N) that lies strictly below (or equal) to the diagonal. This case is equivalent to when the staircase walks are above (or equal) the diagonal.

In Figure 1.16 in (a), the Dyck path of dimension $N = 1$ is shown. In (b), the two Dyck paths in $N = 2$ are shown and in (c), the five corresponding to dimension 3. These numbers coincide with the first three digits of the list shown above about the values of the Catalan numbers.

A *parallelo-polyminoe* in the rectangular lattice of size $p \times q$ is a connected union of squares delimited by two increasing boundary functions $L, U : \{1, 2, \ldots, p\} \to \{0, 1, \ldots, q\}$ such that $L(1) = 0$, $U(p) = q$, and $L(n) < U(n-1)$ for each $2 \leq n \leq p$. In Figure 1.17 an example of parallelo-polyminoe in the lattice of size 14×10 is shown. The blue path defines the lower border function $L = (0,0,0,0,0,2,2,2,2,5,5,5,5,5)$, while the red one defines the upper border $U = (1,1,1,3,3,3,5,5,6,6,6,6,7,7)$. The number of parallelo-polyminoes in the lattice $p \times q$ is also related with the Narayana number.

Now, another important concept is presented. A *Golomb ruler* is a set of marks at integer positions along a ruler such that no two pairs of marks are the same distance apart. Formally, this rulers are defined as follows, the set $A = \{a_1, a_2, ..., a_N\} \subset \mathbb{Z}$, where $a_1 < a_2 < \cdots < a_N$, is a Golomb ruler if and only if for all $i, j, k, l \in \{1, 2, ..., N\}$ such that $i \neq j$ and $k \neq l$, $a_i - a_j = a_k - a_l \iff i = k$ and $j = l$. In other words, the *difference set* has all its elements distinct. The *order* of this Golomb ruler is N and its length is $a_N - a_1$.

In Figure 1.18 an example of two Golomb rulers is shown. In (a), there is the set $A = \{0, 1, 3\}$ that satisfies $x_3 - x_1 > x_3 - x_2 > x_2 - x_1$. In (b), there is $A = \{0, 2, 3\}$ such that $x_3 - x_1 > x_2 - x_1 > x_3 - x_2$. In both cases, $|A| = 3$. When the set of differences of two Golomb rules can be ordered in different ways, it is said that these Golomb rules are

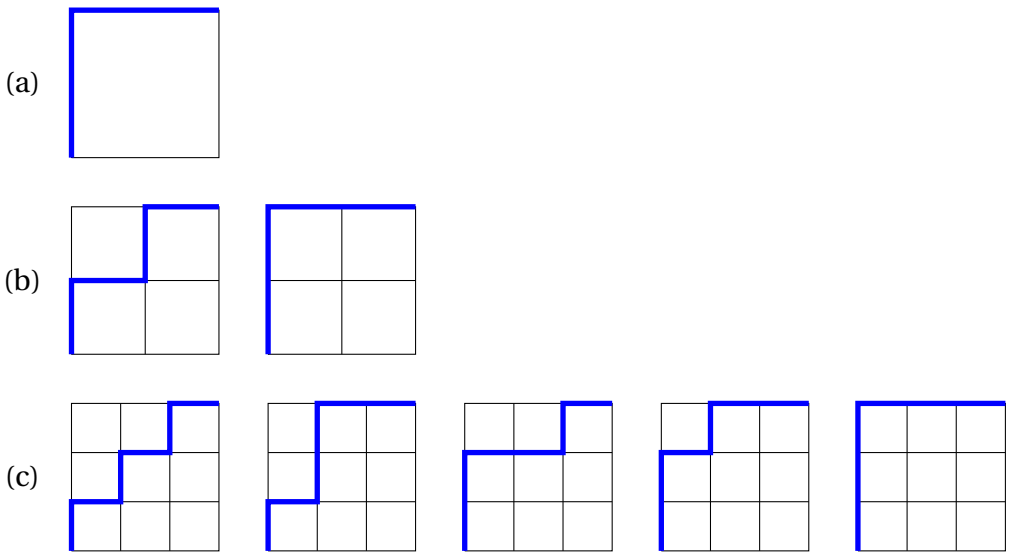

Figure 1.16 – In (a), (b) and (c), the different options of Dyck paths of order 1, 2 and 3, respectively, are shown. As can be seen in (a), the only option to build such a path of order 1 is to take one step up and one step to the right. In (b) there are two different options to build a Dyck path of order 2, the first is to intersperse steps up and to the right, and the second is to go as high as possible and then go as far to the right. Finally, in (c), the 5 options are shown to get from the coordinate $(0,0)$ to the coordinate $(3,3)$ in such a way that it is always above the diagonal, whose options they combine the exposed alternatives in the paths generated in (b).

combinatorially different.

Although there is still no closed formula to obtain these numbers, there are previous works as in Johnston 2014a; Beck, Bogart, and Pham 2011, in which they have counted the number of combinatorially different Golomb rulers with N markings which are shown below in Table 1.2. The example shown in Figure 1.18, also illustrates the two possibilities of Golomb rulers with $N = 3$ indicated in the table.

Another concept that is closely related, is the *Sidon set*. The set $A = \{a_1, a_2, ...\} \subset \mathbb{N}$, is a Sidon set in which all pairwise sums $a_i + a_j$ are different for $i \leq j$. The equivalence between the Golomb rulers and the Sidon finite sets has already been studied (see Dimitromanolakis 2002 for instance) and it is easy to prove by contradiction.

Suppose the set $A = \{a_1, a_2, ..., a_N\} \subset \mathbb{N}$ is a finite Sidon set but not a Golomb ruler. Since A is not a Golomb ruler, then there exist $i, j, k, l \in \{1, 2, ..., N\}$ such that $a_i - a_j = a_k - a_l$ whence it follows that $a_i + a_l = a_k + a_j$ which contradicts the fact that A is a finite Sidon set. In an analogous way it is proved that a Golomb Rule is a finite

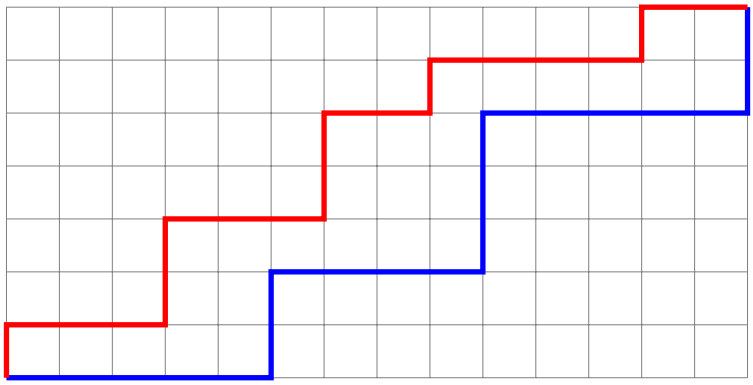

Figure 1.17 – Example of parallelo-polyminoe in the lattice of size 14×10. The blue path defines the lower border function $L = (0,0,0,0,0,2,2,2,2,5,5,5,5,5)$, while the red one defines the upper border $U = (1,1,1,3,3,3,5,5,6,6,6,6,7,7)$, as you can see there are no intersections on the paths, only at the beginning and at the end.

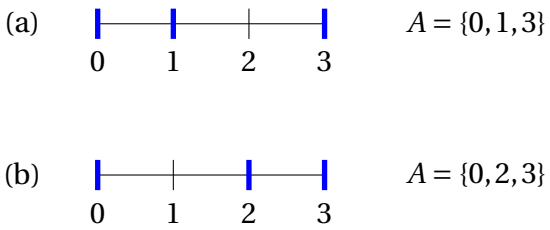

Figure 1.18 – Example of two combinatorially different Golomb rulers of order 3. In (a) and (b) two Golomb rulers are shown, both of order 3. These rules have an associated set that is denoted by the letter A that is written on the right side of each of them. Both rules are combinatorially different, because the differences between each of the elements have a different order. In (a), the set $A = \{0,1,3\}$ is presented, that satisfies $x_3 - x_1 > x_3 - x_2 > x_2 - x_1$. In (b), there is $A = \{0,2,3\}$ such that $x_3 - x_1 > x_2 - x_1 > x_3 - x_2$.

Sidon set.

With the definitions of these combinatorial objects the section of basic concepts is concluded. Now the methodological framework begins with the methodology proposed and used to build the paths to synchronization, for a system that acts on a fixed graph which it is known that synchronizes.

N	**Number Golomb rulers**
1	1
2	1
3	2
4	10
5	114
6	2608
7	107498
8	7325650
9	771505180

Table 1.2 – Combinatorially different Golomb rulers. This table shows the combinatorially different Golomb rulers from order 1 to order 9 which are the ones that have been calculated so far.

1.2 Path construction

In this section, the methodology used to build the paths towards synchronization is presented. This will be done from the subgraphs that can be generated from the main graph. There are previous works that measure the diffusion distance between networks in the Laplacian system as in Bao, You, and Lin 2018, but the proposal presented here is original.

To measure the degree of synchronization of the system, at a given time t, fist, a precision of $\epsilon > 0$ is set. The degree of synchronization by pairs of coordinates connected by the main graph will be observed.

Definition (Neighbors ϵ-synchronized)**.** *Let $G = (V, E)$ be the main graph, the configuration $x \in \mathbb{R}^{|V|}$, and let $u, v \in V$ such that $(u, v) \in E$. These neighbors are ϵ-synchronized if the distance between them is not greater than ϵ, that is:*

$$|x_u - x_v| \leq \epsilon.$$

In Figure 1.19 an example of the Laplacian flow as in Equation (1.15) is shown for $N = 2$ in the complete graph. The upper blue curve corresponds to the flow of $x_1(t)$ and the lower one to the flow of $x_2(t)$. Between red lines the ϵ-neighborhood is drawn. From the moment ($t \approx 2$), both flows enter the neighborhood, then they remain ϵ-synchronized.

A connection between two neighboring sites that are ϵ-close is said to be *active*, and it is defined a subnetwork containing all the active connections. The main objective of the present manuscript is to determine and describe the evolution of these subnetworks.

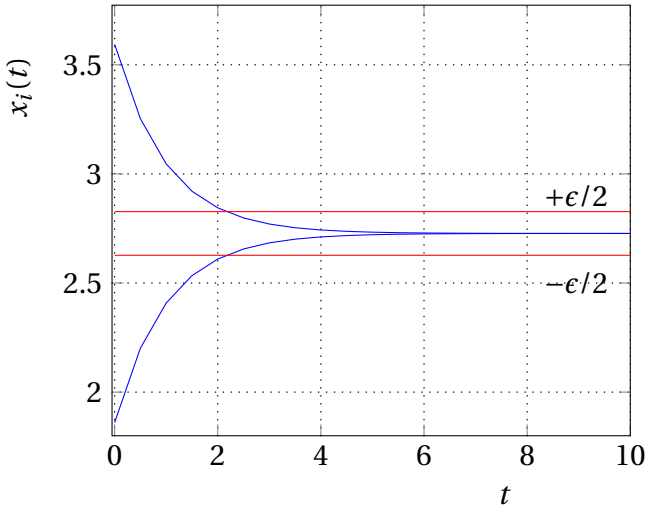

Figure 1.19 – Example of two neighbors ϵ-synchronized. Blue lines show the Laplacian flow of two coordinates from when they begin to interact, until they are synchronized, that is, until both acquire the same value. In red lines, is represented the neighborhood of size $\epsilon/2$ around the average of the values of said coordinates, when the flow enters this neighborhood, which is approximately at $t \approx 2$. These are neighbors ϵ-synchronized.

Definition (ϵ-synchronized subnetwork)**.** *To each fixed threshold $\epsilon > 0$, the graph $G = (V, E)$, and every configuration $x \in \mathbb{R}^{|V|}$, its associated ϵ-synchronized subnetwork $G_x = (V, E_x)$ is defined as follows. $E_x \subset E$ is the set of edges:*

$$E_x = \{(u, v) \in E : |x_u - x_v| \leq \epsilon\}. \tag{1.28}$$

Clearly, all possible ϵ-synchronized subnetworks G_x, associated with any $\epsilon > 0$, the graph $G = (V, E)$, and every configuration $x \in \mathbb{R}^{|V|}$ satisfy that they are subgraphs of G.

Definition (Feasible and unfeasible subgraphs)**.** *Let's consider the main graph $G = (V, E)$. A subgraph G' of G is feasible, if there exist $\epsilon > 0$, and at least one configuration $x \in \mathbb{R}^{|V|}$, such that its associated ϵ-synchronized subnetwork meets $G_x = G'$. Otherwise, the subgraph is said to be unfeasible.*

Due to the phenomenon studied in this thesis is the synchronization, the systems under consideration fulfills $G_{x(t)} = G$ for t large enough (which will also be denoted as $G_{x(t)} \to G$, when $t \to \infty$), when the initial condition is sufficiently close to the diagonal $\mathscr{D}$. This can also be seen in the example presented in Figure 1.19.

The graph G has $2^{|E|}$ subgraphs, then for each suitable initial condition $x \in \mathbb{R}^{|V|}$ there exists a finite sequence of switching times $t_0 = 0 < t_1 < t_2 < \cdots < t_\ell$ and a corresponding sequence of ϵ-synchronized subnetworks $(G_x, G_{x(t_1)}, \ldots, G_{x(t_\ell)})$ such that

$G_{x(t_\tau)} \neq G_{x(t_{\tau+1})}$, for each $0 \leq \tau < N$, and $G_{x(t)} = G_{x(t_\tau)}$ with $\tau = \max\{0 \leq j \leq \ell : t \geq t_j\}$. In other words, in the sequence of ϵ-subnetworks, no repeated consecutive subnetworks are found.

From the information provided by the sequences of ϵ-subnetworks, the *paths towards synchronization* are built.

Definition (Path towards synchronization)**.** *Lets consider a fixed threshold $\epsilon > 0$, the main graph $G = (V, E)$, and one configuration $x \in \mathbb{R}^{|V|}$. Also, consider its corresponding sequence of ϵ-synchronized subnetworks $(G_x, G_{x(t_1)}, \ldots, G_{x(t_\ell)})$. Its path towards synchronization $P = (V_P, E_P)$ (or just path to synchronization) is built as follows: Each ϵ-synchronized subnetwork is a vertex in V_P and the arrows in E_P indicate the order of appearance in the sequence. That is, $(G_{x(t_i)}, G_{x(t_{i+1})}) \in E_P$, for all $0 \leq i \leq \ell$.*

In Figure 1.19, there is an example for the Laplacian system in the complete graph K_2. For all times before $t_r = 2$, the two-vertex fully disconnected graph $\emptyset_2 = (V, \emptyset)$ shown in (a). After t_r, at any time cut, K_2 appears, as is shown in (b). Resulting in the sequence $\{\emptyset_2, K_2\}$ shown in Figure 1.20.

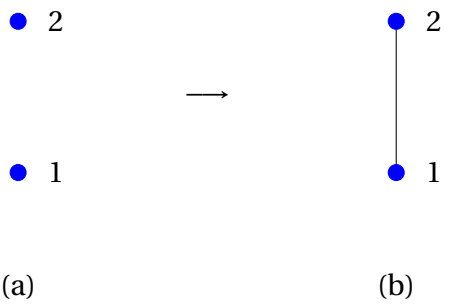

Figure 1.20 – Example of one path to synchronization. Here, the construction of the graphs represented in Figure 1.19 is shown. Before $t \approx 2$, the coordinates are separated by a length greater than ϵ, then, there is no edge is drawn in (a). From $t \approx 2$, they are already at a distance less than ϵ, then, an edge is drawn connecting vertices 1 and 2.

Definition (Typical path)**.** *A path towards synchronization associated with an initial condition $x \in \mathbb{R}^N$ that satisfies that all those increments $x_n - x_m$ are different from zero and pairwise different is called typical.*

The sequence of ϵ- synchronized subnetworks of G codify the progression of transient synchronizing patterns. It is important to keep in mind that if $\epsilon > 0$ sufficiently small is taken, all the possible synchronizing sequences can be obtained varying the initial condition $x \in \mathbb{R}^N$ inside the basin of attraction of the diagonal $\mathscr{D}$.

In Figure 1.21, two paths to synchronization that can be found in the Laplacian system acting on the complete graph K_3 are shown. The path shown in (a) is the same as shown in (b), by making the following label assignment $1 \mapsto 2 \mapsto 3 \mapsto 1$. This occurs in systems that act on networks that have some symmetries, such as the complete graph.

In the case of highly symmetric networks, instead of use directly the ϵ-synchronized subnetworks it is convenient to use another combinatorial structure that encodes the subnetwork and respects some of the symmetries that are preserved by the dynamics at the same time. In Figure 1.21, there are paths that could turn out to be redundant (in the sense that they do not provide more information than what is already available and they occupy memory when performing computations). Also, as it will be seen in the Section 2, this facilitates the description of the evolution of the ϵ-synchronized subnetworks.

It is proposed that the whole synchronizing dynamics on G can be compiled in a single combinatorial superstructure. I call this superstructure the *transition diagram*, where to each vertex is associated with a ϵ-synchronized subnetwork (it should be noted that this association is not necessarily injective), in such a way that the set of all paths in the transition diagram is equivalent to the set of all the observable sequences of ϵ-synchronized subnetworks.

Definition (The transition diagram)**.** *The transition diagram is a directed graph which is written as $\mathcal{T}_\epsilon = (V_\epsilon, A_\epsilon)$ whose vertices V_ϵ, are combinatorial objects containing all the information it is necessary to determine the ϵ-synchronized subnetworks, and its arrows, A_ϵ, are transitions between those structures, and they need to be consistent with the evolution of each ϵ-synchronized subnetwork.*

In Figure 1.22, the transition diagram for the Laplacian system applied to the complete graph K_3 is shown. Each of its vertices corresponds to a subgraph of K_3. In addition, all the transitions that occur can be observed. Each of the paths that appear in this transition diagram is realized by some initial condition $x \in \mathbb{R}^3$.

To study this dynamic of the paths to synchronization, it is enough to see the transition diagram with other labels that allow to encode the G_x (preferably in a simpler way). In Figure 1.22, it would be easier to analyze if a label to each subgraph is associated. An advantage of it will be taken soon to save information of the corresponding subgraph.

The association of objects in V_ϵ with ϵ-synchronized subnetworks is reached via a mapping:

$$\lambda : V_\epsilon \to \mathscr{E}_\epsilon, \tag{1.29}$$

which consists of labeling each vertex in the transition diagram with one ϵ- synchronized subnetwork.

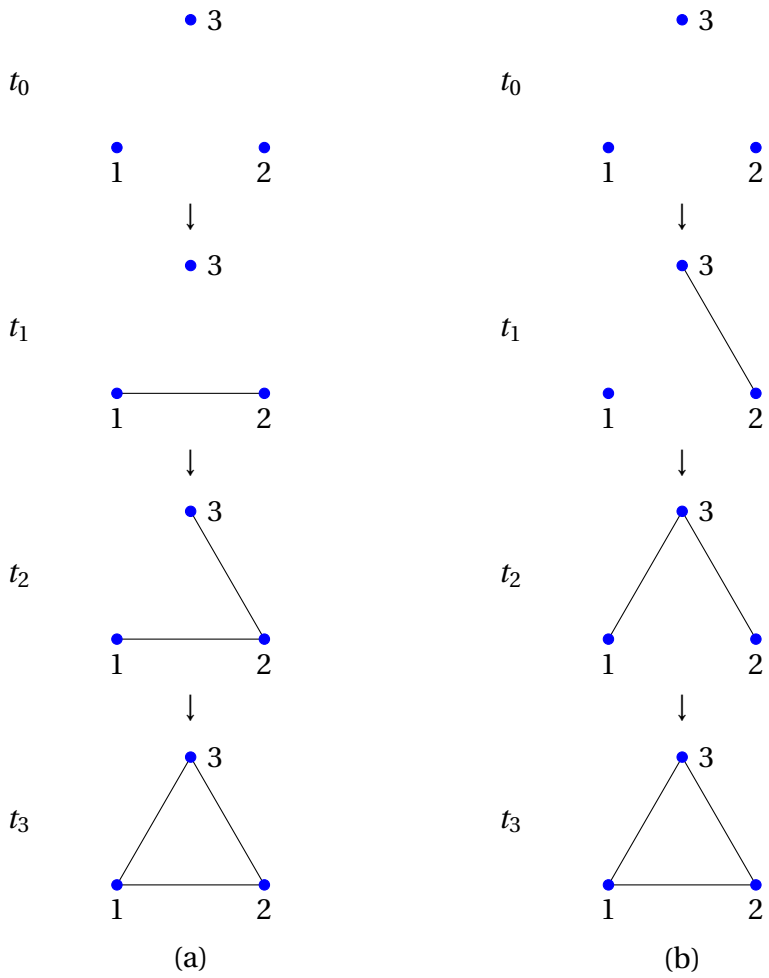

Figure 1.21 – Example of two different but symmetrical paths towards synchronization. In (a) and (b), two paths towards synchronization are shown considering the complete 3-dimensional graph K_3. Both have 4 times t_0, t_1, t_2, t_3 in which the different subgraphs that appear in each of the sequences can be noted whose transitions are represented by an arrow pointing down. In the case of (a), starting with the totally disconnected graph, then add the edge that joins vertices 1 and 2, then the one that joins vertices 2 and 3, and ends with the one that joins vertices 1 and 3. For (b), in the same way, starting with the totally disconnected graph, first the edge that joins vertices 2 and 3 appears, then the one that joins vertices 1 and 3 and ends with the one that joins vertices 1 and 2. One path can be obtained through another by rotating the labels of the graph so that $1 \to 2 \to 3 \to 1$.

Definition (Realizable sequence)**.** *The labelling defined by the mapping λ in Equation (1.29) is such that the sequence $(G_0, G_1, \ldots, G_\ell)$ is a realizable sequence of ϵ- synchronized subnetworks as long as there exists a path $v_0 \to v_1 \to \cdots \to v_\ell$ in $\mathcal{T}_\epsilon$ such that*

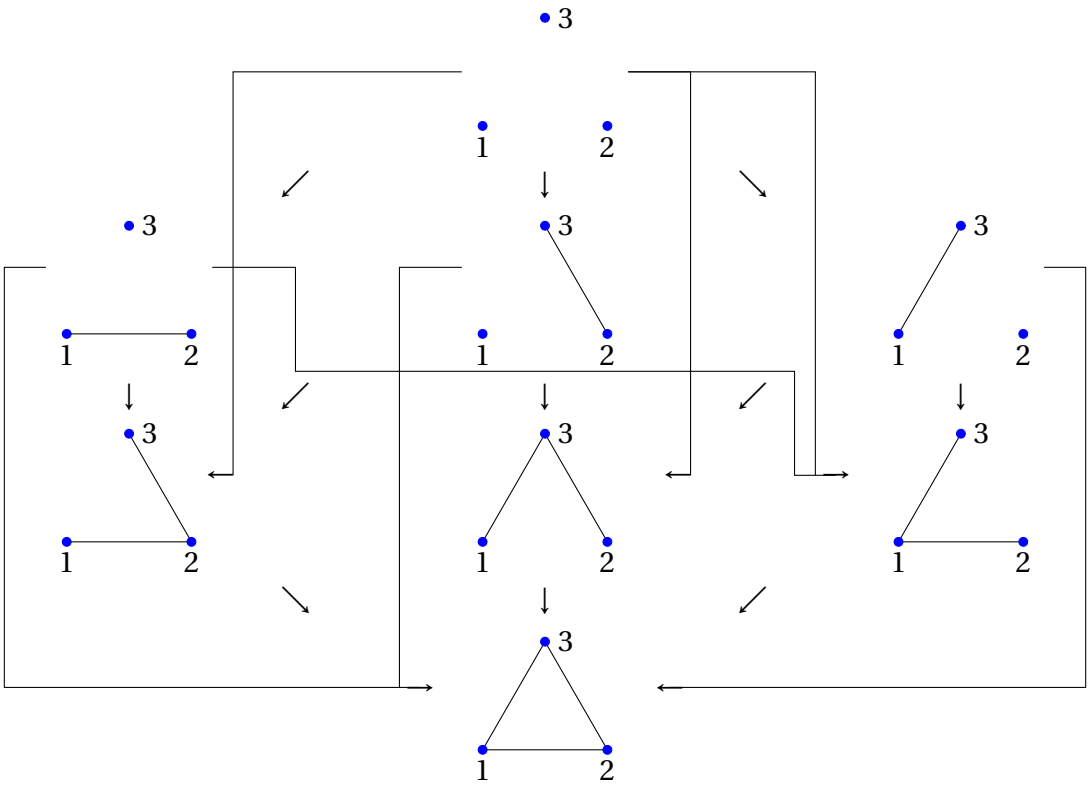

Figure 1.22 – The complete transition diagram of the Laplacian system in K_3 is shown. At the top, is the fully disconnected graph, and at the bottom, is the full 3-dimensional graph K_3. This transition diagram is made up of 8 vertices that are all the subgraphs that can be obtained from K_3, which are arranged by levels, depending on the number of edges that each of them has. Each of the arrows represents the transitions that can be observed. They are steps that jump one or two levels (a jump of three levels leads to a contradiction). Furthermore, this is a very rare case where all the arrows can be constructed following the rule that one graph is a subgraph of the next, with the only exception that the fully disconnected does not go to the fully connected.

$G_n = \lambda(v_n)$ *with* $0 \leq n \leq \ell$.

In general, the set $\mathscr{E}_\epsilon$ of all the ϵ-synchronized subnetworks changes with ϵ. Nevertheless, for ϵ sufficiently small, the set of ϵ-synchronized subgraphs defined by initial conditions in a small neighborhood of $\mathscr{D}$ becomes independent of ϵ. For example, in Figure 1.23, when two different values of ϵ are considered, different sequences are generated. For the neighborhood drawn in red, the sequence shown in Figure 1.20 is presented, which is $\{\emptyset_2, K_2\}$. For the neighborhood drawn in green, there is only $\{K_2\}$, because at any time, the flows are close enough to be connected.

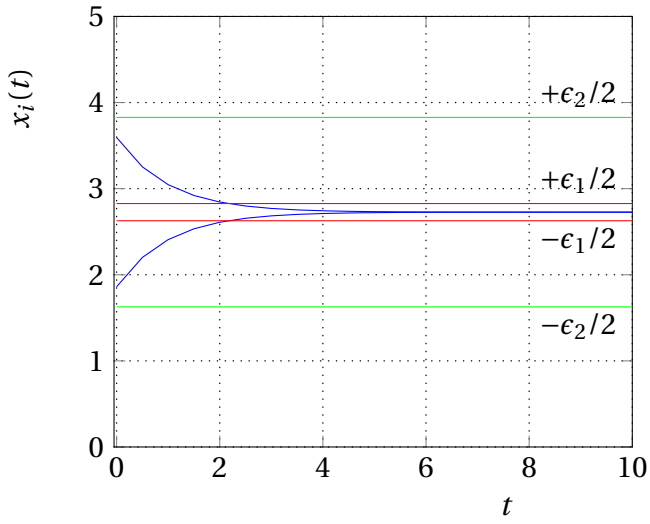

Figure 1.23 – Example when two neighbors ϵ-synchronized with different ϵ. The objective of this image is to show that when one changes the value of the precision $\epsilon > 0$, different sequences can be obtained, then, for some it can be considered a loss of information. For example, for the red neighborhood given by ϵ_1, the change that implies that at first the two coordinates were far apart can be observed, and then, they got close enough to get in synchronization. In the case of the green neighborhood given by ϵ_2, since it is too big, at no time did it notice that there was an approximation between the coordinates, because from the beginning, for this precision, they were already close enough.

In the case of the Laplacian flow, the set $\mathscr{E}_\epsilon$ of all possible ϵ-synchronized subnetworks is independent of ϵ as long as $\epsilon > 0$. It is natural to think that even if $\mathscr{E}_\epsilon$ is independent of ϵ, the corresponding transition diagram may change with ϵ. This, nevertheless, does not happen in the linear case, since for each initial condition $x \in \mathbb{R}^{|V|}$, the corresponding sequence $(G_x, G_{x(t_1)}, \ldots, G_{x(t_\ell)})$ of ϵ-synchronized subnetworks coincides with the sequence $(G_y, G_{y(t_1)}, \ldots, G_{y(t_\ell)})$ of ϵ'-synchronized subnetworks determined by $y = x\epsilon'/\epsilon$. Indeed, by Equation (1.28) and by the linearity of the system, $\{u, v\} \in E_x$ is equivalent to $|x_u - x_v| \leq \epsilon$, hence $|x_u - x_v| = \epsilon/\epsilon'|y_u - y_v| \leq \epsilon$, therefore $|y_u - y_v| \leq \epsilon'$, which is equivalent to $\{u, v\} \in E_y$. From this it follows that the set of ϵ-synchronized sequences does not depend on ϵ in the linear case.

Clearly, each ϵ-synchronized sequence can be realized by an infinite number of initial conditions. Due to the number of ϵ-synchronized sequences is finite, it is possible to realize some finite partition of the initial space, that is, the basin of attraction of the final synchronized state.

As it has been anticipated, the study is restricted only to the following families of networks the complete graph K_N, the complete bipartite graph $K_{N,N}$. And the following questions are addressed:

1. Given the underlying network, which subgraphs are realizable as ϵ-synchronizing subnetworks, how large is this set and how does it grow with the size N of the underlying graph?
2. Given an underlying network, what is the structure of the transition diagram? What is the longest path in this digraph and what is the distribution of path lengths?

2 Characterization of transition diagrams

Contents

This chapter contains the main results of the thesis, namely, the rigorous description and characterization of the transition diagrams of the path towards synchronization for the Laplacian flow. I treat the case of the Laplacian flow on the complete graph in full detail, while in the case of the bipartite complete graph, the characterization is restricted to paths starting at balanced initial conditions satisfying a condition whose precise definition I give below. The chapter contains as well a discussion concerning the transition diagram corresponding to the cycle graph.

2.1 The Laplacian flow on K_N

The first thing to be notices is the fact that not all the subgraphs of the complete graph are realizable as synchronization subgraph. The fact that the values of the coordinates of a configuration of the flow can be arranged in increasing order imposes a restriction on the presence or absence of edges in the corresponding synchronized subgraph. I will start by showing who the Laplacian flow in K_N preserves the order of the coordinates which suggests a natural coding for the synchronized subnetworks by integer increasing functions. This coding allows a complete description of all the path towards synchronization and therefore a detailed characterization of the corresponding transition diagram.

2.1.1 Coding

For the coding of the synchronized subnetworks of the completely connected network, I strongly use the fact that the as the configuration converges to the synchronized manifold, its coordinate differences monotonically tend to zero. We have the following.

Theorem (Monotonic convergence of coordinate differences)**.** *Let L_N denote the Laplacian matrix over the complete graph K_N, and consider the Laplacian flow given by*

$$\frac{dx}{dt} = L_N x, \quad x \in \mathbb{R}^N.$$

Then, for any initial condition $x(0) \in \mathbb{R}^N$ and each couple $\{n,m\} \in \{1,2,\dots,N\}^2$, we have

$$x_n(t) - x_m(t) = e^{-Nt}(x_n(0) - x_m(0)), \tag{2.1}$$

for all $t \in \mathbb{R}$.

Proof. Let e^n denotes the n-th vector of the canonical basis of $\mathbb{R}^N$. Since the Laplacian matrix L_N is symmetrical, as it can be readily verified from its definition in Equation (1.2), it can therefore be diagonalized. The collection $\{u^1, u^2, \dots, u^N\}$, where $u^1 := \sum_{n=1}^N \mathsf{e}^n$ and $u^n := \mathsf{e}^n - \mathsf{e}^1$ for $n \geq 2$, is an eigenbasis for L_N. Indeed, this collection is clearly a basis for $\mathbb{R}^N$ and a simple computation shows that

$$L_N e^n = \sum_{m=1}^N e^m - N e^n, \quad \text{for each } n \in \{1,2,\dots,N\}.$$

From this, it readily follows that

$$L_N u^1 = \sum_{n=1}^N L_N e^n = \sum_{n=1}^N \left(\sum_{m=1}^N e^N - N e^n \right) = \overline{0},$$

and for each $n \geq 2$,

$$L_N u^n = L_N \mathsf{e}^n - L_N \mathsf{e}^1 = \left(\sum_{m=1}^N e^m - N e^n \right) - \left(\sum_{m=1}^N e^m - N e^1 \right) = -N(e^n - e^1).$$

Therefore, 0 is a simple eigenvalue of L_N associated to the eigenvector u^1, while the other eigenvalue, -N, has degeneracy $(N-1)$. Notice that the synchronized manifold is precisely the linear span of the eigenvector u^1. The initial condition $x(0) \in \mathbb{R}^N$ decomposes in the eigenbasis as

$$x(0) = \bar{x}(0)\, u^1 + \sum_{n=1}^{N-1} (x(0)_{n+1} - \bar{x}(0))\, u^n,$$

where $\bar{x}(0) := \left(\sum_{n=1}^N x_n(0)\right)/N$ is nothing but the projection of $x(0)$ on the synchro-

nized manifold. The Laplacian flow can be easily integrated on this basis, and it gives

$$\begin{aligned} x(t) &= \bar{x}(0)\, u^1 + e^{-Nt} \sum_{n=1}^{N-1} (x_{n+1}(0) - \bar{x}(0))\, u^n, \\ &= \sum_{n=1}^{N} \left(\bar{x}(0)\left(1 - e^{-Nt}\right) + e^{-Nt} x_n(0)\right) \mathsf{e}^n, \end{aligned}$$

for all $t \in \mathbb{R}$. Hence, each coordinate converges to $\bar{x}(0)$ exponentially fast, while for each $m, n \in \{1, 2, \ldots, N\}$, we have

$$x_n(t) - x_m(t) = e^{-Nt}(x_n - x_m), \tag{2.2}$$

□

This monotone convergence of the differences has the following immediate implication on the construction of ϵ-synchronized subnetworks.

Corollary (Every link is synchronized from a certain time)**.** *For each initial condition $x(0) \in \mathbb{R}^N$, every $\epsilon > 0$, and each $n, m \in \{1, 2, \ldots, N\}$, the link $\{n, m\}$ belongs to the ϵ-synchronized subnetwork $G_{x(t)}$ for all*

$$t \geq t_{n,m} = \frac{\log|x_n - x_m| - \log(\epsilon)}{N}.$$

In other words, once an edge appears on a synchronized subnetwork, it never disappears.

The transition diagram inherits the invariance under permutation of vertices of K_N, which means that two paths towards synchronization are equivalent if the vertices of their synchronized subnetworks correspond under a permutation. Hence, without lost of generality, one may assume that $x_1(0) \leq x_2(0) \leq \cdots \leq x_N(0)$. I will call this type of initial conditions, ordered initial conditions. Another important consequence of Theorem 2.1.1 is the following.

Corollary (The coordinates' order is preserved)**.** *The Laplacian flow on K_N preserves the order of the coordinates, i.e., if $x(0) \in \mathbb{R}^N$ satisfies $x_1(0) \leq x_2(0) \leq \cdots \leq x_N(0)$, then $x_1(t) \leq x_2(t) \leq \cdots \leq x_N(t)$ for all $t > 0$.*

In view of this result, it is convenient to define the transition diagram not over the ϵ-synchronized subnetworks but over another combinatorial object that takes into account the fact that the coordinates' order is preserved by the flow. By doing so, the description of the transition diagrams will be greatly simplified since such a coding will allow to easily determine the order of apparition of new links in the synchronized subnetworks composing the synchronized sequence. From now on I will denote by

Id the identity function on the set $\{1,2,\ldots,N\}$.

Definition (Coding ordered initial conditions by increasing functions)**.** *Let $x \in \mathbb{R}^N$ be an ordered initial conditions. For each $\epsilon > 0$, define $\phi_{x,\epsilon} : \{1,2,\ldots,N\} \to \{1,2,\ldots,N\}$ by*

$$\phi_{x,\epsilon}(m) = \max\{n \geq m : x_n \leq x_m + \epsilon\}. \tag{2.3}$$

Clearly $\phi_{x,\epsilon} \geq Id$ for each ordered initial condition $x \in \mathbb{R}^N$ and every $\epsilon > 0$. In Figure 2.1 I present an example of the construction of function $\phi_{x,\epsilon}$ from the ordered initial condition $x \in \mathbb{R}^N$. The first line (a) represent the coordinates of $x = (x_1, x_2, x_3, x_4)$ as black dots on the line, while the superimposed boxes represent ϵ-neighborhoods. To construct the corresponding ϵ-synchronized subnetwork G_x, it is enough, according to Equation (1.28), to observe that x_1 and x_2 are inside the same ϵ-neighborhood, while x_3 and x_4 belong to another ϵ-neighborhood, disjoint to the previous one.This determines the links appearing on the ϵ-synchronized sub network, which is illustrated in (b), where a link between the vertices 1 and 2 as well as vertices 3 and 4 appear. In the last line (c), the increasing function $\phi_{x,\epsilon}$ associated with x is depicted. The information in $\phi_{x,\epsilon}$ can be read as follows: The furthest vertex connected to vertex 1 is vertex 2, vertex 2 does not reach vertex 3, and vertex 3 reaches vertex 4, which cannot reach further vertices since it is the last one.

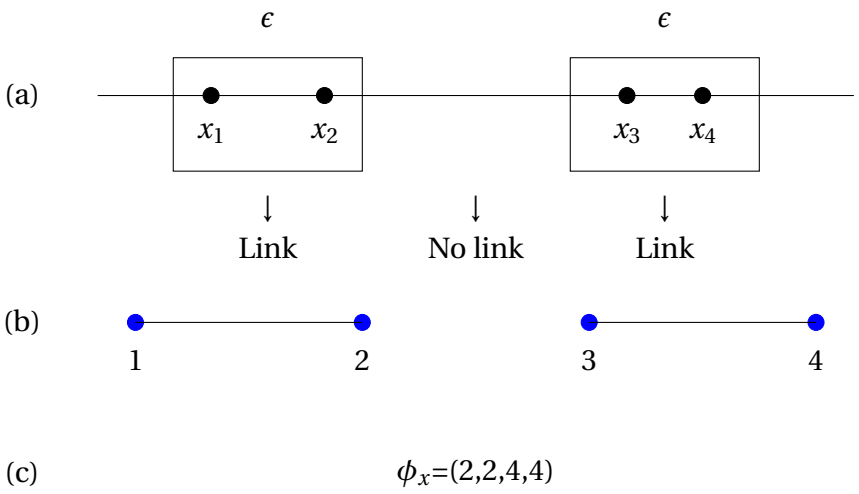

Figure 2.1 – In (a), a graphic representation of the coordinates of an ordered initial condition, where coordinates that are ϵ-close are encircled in a box. In (b), the corresponding ϵ-synchronized subnetwork is shown. Finally, in (c), the resulting increasing function $\phi_{x,\epsilon}$ codifying the initial condition is shown.

Notice that if for certain $t > 0$ we have $x_j(t) - x_i(t) < \epsilon$, then $x_\ell(t) - x_k(t) < \epsilon$ for

each $i \le k < \ell \le j$. Hence, for each ordered configuration, if a link is included in the ϵ-synchronized subnetwork, then all the intermediate links (links joining intermediated vertices with respect to the prescribed order) should belong to the subnetwork as well. For instance, in the ϵ-synchronized subnetwork depicted in Figure 2.2, vertex 2 and 5 are connected, which means that $|x_5 - x_2| < \epsilon$, therefore all the couples $\{i, j\}$ with $2 \le me, j \le 5$ are necessarily included in the same ϵ-synchronized subnetwork. In what follows, to avoid tiring the eyes, I will draw only the links joining the farthest connected vertices, understanding that each couple of intermediated vertices form a link in the same network.

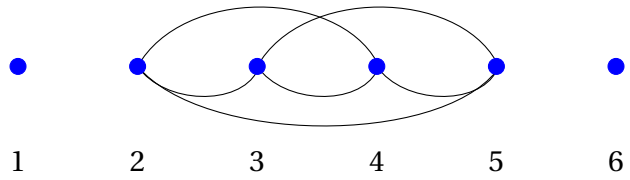

Figure 2.2 – This figure shows the ϵ-synchronized subnetwork defined by an ordered initial condition $x \in \mathbb{R}^6$. Since vertices 2 and 5 are connected, then all the couples of intermediated vertices form a link, that is, vertices 2 and 3, 3 and 4, 4 and 5, 2 and 4 and 3 and 5 define links in the same subnetwork. To avoid writing so many arrows, only the links joining the farthest connected vertices will be drawn, understanding that the intermediated links are included in the same subnetwork.

Theorem (The coding is faithful)**.** *Let $\epsilon > 0$ and let $N \in \mathbb{N}$. Consider the collection*

$$\Phi_N := \{\phi : \{1, \dots, N\} \to \{1, \dots, N\} \text{ increasing and s. t. } \phi \ge Id\}. \tag{2.4}$$

There is a one-to-one correspondence between the set of all ϵ-synchronized subnetworks of K_N defined by ordered initial conditions, and increasing functions in Φ_N. The correspondence $\phi \mapsto G_\phi$ is the following. For $\phi \in \Phi_N$, G_ϕ is the subnetwork containing all the links

$$\{\{m, n\} : \min(m, n) \le \phi(\max(n, m))\}. \tag{2.5}$$

Proof. If the subnetwork G_x is the ϵ-synchronized subnetwork for a given ordered initial condition $x \in \mathbb{R}^N$, then the increasing function $\phi_{x,\epsilon}$ defined by Equation (2.3) is precisely the one satisfying Equation (2.5). Hence, $G_x \mapsto \phi_{x,\epsilon}$ is the inverse of the correspondence in the statement of the theorem, which proves that the correspondence is injective.

In order to prove that the correspondence $\phi \mapsto G_\phi$ is subjective, it is enough to exhibit, given an increasing function $\phi \in \Phi_N$, an ordered initial condition x such that $\phi = \phi_{x,\epsilon}$. For this it is convenient to use a representation of ϕ as a disjoint union of

directed trees.
Let $\mathrm{Fix}(\phi) := \{1 \le n \le N : \phi(n) = n\}$. Associate, to each $n \in \mathrm{Fix}(\phi)$, the directed tree T_n rooted at n, with vertices $V_n := \bigcup_{l=0}^{h(n)} \phi^{-l}(\{n\})$, and edges $A_n := \{(k, \phi(k)) : k \in V_n \setminus \{n\}\}$. The vertex set V_n splits into $h(n)+1$ disjoint levels, $V_n^l := \phi^{-l}(\{n\})$, $0 \le l \le h(n)$. The number $h(n)$ is the high of T_n.

The maximal paths in T_n are completely determined by their starting vertices, which must be leaves. Let $\ell_n^1 < \ell_n^2 < \cdots < \ell_n^{w(n)}$ be the leaves of T_n. Its number, $w(n)$, is the width of the tree T_n. Since ϕ is increasing and such that $\phi \ge \mathrm{Id}$, then every element in the l-th level, V_n^l, is greater than all the elements in the l'-th level, $V_n^{l'}$ whenever $l < l'$. It implies that the length $l(m)$ of the path starting at m and ending at the root, is a decreasing function of m.

Each maximal path in T_n starts at a leaf and the longest of those paths have length $h(n)$ and start at leaves in the highest level. Furthermore, all vertices in T_n belong to a maximal path, which means that it is reachable from a leaf.

Now, given $\phi : \{1, 2, \ldots, N\} \to \{1, 2, \ldots, N\}$ increasing and such that $\phi \ge \mathrm{Id}$, let $\{T_{n_k} : 1 \le k \le R\}$ be the associated collection of directed trees and $n_1 < n_2 < \cdots < n_R$ in $\mathrm{Fix}(\phi)$ the corresponding roots. Let $x \in \mathbb{R}^N$ such that $x_{n_1} = \epsilon\, h(n_1)$, and for each $1 \le k < R$:

$$x_{n_{k+1}} = x_{n_k} + (h(n_k) + 2)\,\epsilon. \tag{2.6}$$

In this way, the value of x_n is fixed for each $n \in \mathrm{Fix}(\phi)$ in such a way that $x_{n_k} + \epsilon < x_{n_{k+1}} - h(n_{k+1})\,\epsilon$ for each $1 \le k < R$. Now, for each $n \in \mathrm{Fix}(\phi)$, let $\ell_n^1 < \ell_n^2 < \cdots < \ell_n^{w(n)}$ be the leaves of T_n. For each $1 \le j \le w(n)$ and $0 \le k \le l(n_j)$ for which $x_{\phi^k(\ell_n^j)}$ is not yet defined, let:

$$x_{\phi^k(\ell_n^j)} = x_n - (l(n_j) - k)\,\epsilon + (j-1)\,\frac{\epsilon}{w(n)}. \tag{2.7}$$

Remember that $l(n_j)$ is the length of the maximal path starting at ℓ_n^j. It is not difficult to verify that Equations (2.6) and (2.7) define an ordered initial condition $0 = x_1 < x_2 < \cdots < x_N = \sum_{k=1}^{R} (h(n_k) + 2)$, such that $\phi_x = \phi$. □

By establishing the equivalence of these objects, it is then possible to search for properties of one that may be useful in the study of the other.

Lemma. *(Increasing functions and Dyck paths) The collection Φ_N is equivalent to the set of Dyck paths of order N and length $2N$.*

Proof. Indeed, a Dyck path of order N and length $2N$ is a sequence $(0,0), (0,n_1), (1,n_2), \ldots, (N-1, N), (N,N)$ determining a path in the the lattice $\{0,1,\ldots,N\} \times \{0,1,\ldots,N\}$ such that $n_1 \le n_2 \le \cdots \le N$ and such that $n_k \ge k$ for each $0 < k < N$. To this Dick path associate the function $\phi : \{1,2,\ldots,N\} \to \{1,2,\ldots,N\}$ such that $\phi(k) = n_k$ for $1 \le k < N$, and $\phi(N) = N$. Clearly this is a one-to-one correspondence between Dyck paths, and functions in Φ_N. □

In this way, ϵ-synchronized subnetworks and increasing functions above the diagonal can be used interchangeably and better yet, at the convenience of the problem that is addressed.

As mentioned in Section 1.1.5, the set of Dick paths has a cardinality given by the Catalan numbers (Stanley and Fomin 1999). The formula shown below is one of the most important relationships found in this thesis.

Theorem (The number of states in the transition diagram)**.** *The number of functions in Φ_N is the N-th Catalan number, i.e.,*

$$|\Phi_N| = C_N := \frac{1}{N+1}\binom{2N}{N}. \tag{2.8}$$

In Figure 2.3 I show a concrete example of the correspondence between functions in Φ_3 and ϵ-synchronized subnetworks of K_3. There I show as well, the abridges representation on the ϵ-synchronized networks. In the first column I show the increasing functions in Φ_N, then, in the second column the abridged representation of the corresponding ϵ-synchronized subnetwork. In the last column, the the actual ϵ-synchronized subnetwork is depicted. In this way, it will be clearer when passing from the transition diagram with vertices representing subgraphs, to the same transition diagram with increasing functions in Φ_N as states. The coding in terms of increasing functions in Φ_N will allow to analyse the paths in the transition digraph step by step. Notice that $|\Phi_3| = \frac{1}{4}\binom{6}{3} = 5$, which precisely corresponds to the number of rows in Figure 2.3, the total number of ϵ-synchronized subnetworks of K_3, defined by ordered configuration.

Figure 2.4, I show the complete list of increasing functions in Φ_4 accompanied by the abridged representation of the corresponding synchronized subnetwork. Note that $|\Phi_4| = \frac{1}{5}\binom{8}{4} = 14$, which corresponds precisely to the number of increasing functions depicted in the figure.

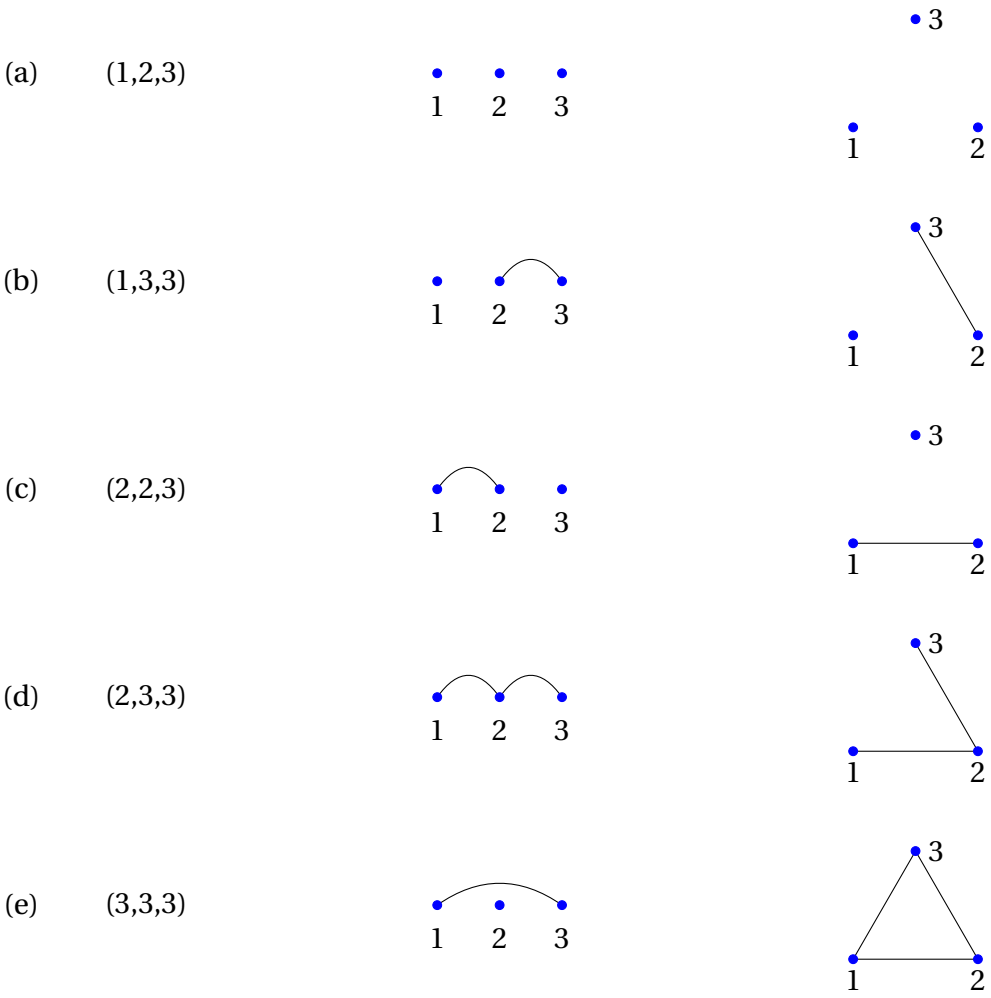

Figure 2.3 – The complete list of increasing functions in Φ_3 accompanied by the abridged representation of the corresponding synchronized subnetwork, and the actual synchronized subnetwork.

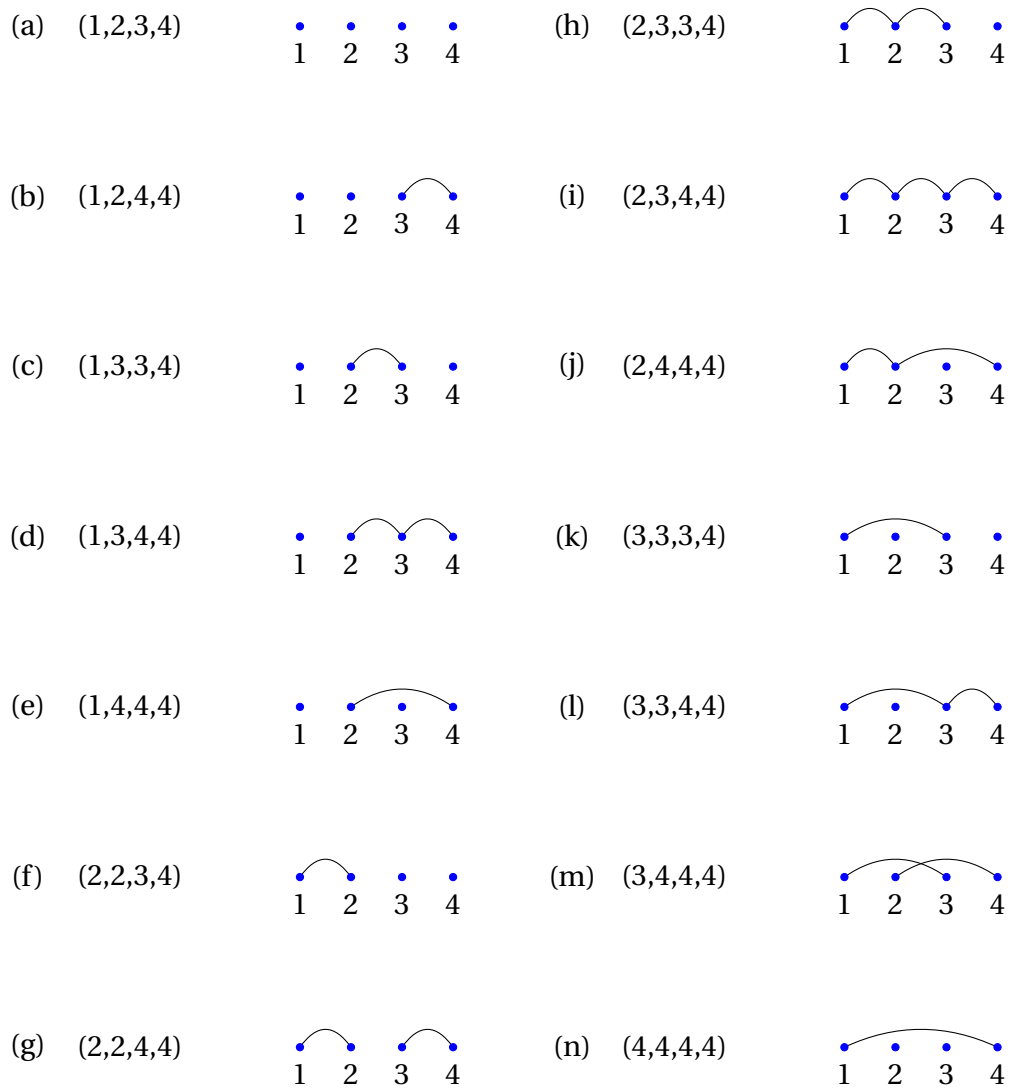

Figure 2.4 – The complete list of increasing functions in Φ_4 accompanied by the abridged representation of the corresponding synchronized subnetwork.

2.1.2 Unfeasible synchronized subnetworks

This section is devoted to the analysis of subnetworks of K_N which cannot correspond to ϵ-synchronized subnetworks. Indeed, since synchronized subnetworks correspond to increasing functions above the diagonal, while an arbitrary subnetwork would need much more information to be defined, it turns out that the majority of subnetworks of K_N are unfeasible as synchronized subnetworks. Below I will give explicit sufficient conditions for a given subnetwork to be unfeasible as synchronized subnetwork.

As noted in the Section 1.2, all subgraphs of K_3 are synchronized subnetworks. Hence, we I start my analysis from $N = 4$. In this dimension, there are two clear examples, shown in Figure 2.5, of unfeasible subnetworks. None of the subgraphs in (a) and (b), neither the subgraphs obtained by permutation of vertices, correspond to synchronized subnetworks of K_4, i.e., there is no configuration $x \in \mathbb{R}^4$ for which G_x is one of those subnetworks.

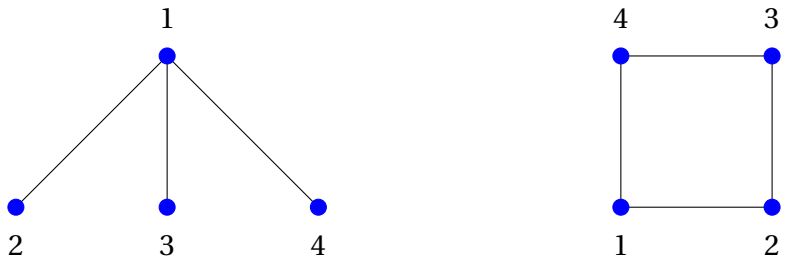

Figure 2.5 – In (a) and (b), the two kinds of subnetworks which are unfeasible as synchronized subnetworks of K_4. The subnetwork in (a) is named 3-star, while the subgraph in (b) is named 4-cycle.

Proposition (Unfeasible synchronized subnetworks of K_4)**.** *There is no initial condition $x \in \mathbb{R}^4$ such that G_x is either a 3-star or a 4-cycle.*

Proof. Consider the 3-star depicted in Figure 2.5 (a), denote it S, and suppose that $x \in \mathbb{R}^N$ is such that $S = G_x$ for some $\epsilon > 0$. If so is the case, then necessarily $\{x_2, x_3, x_4\} \subset B_\epsilon(x_1)$. In this case, either $|x_2 - x_3| < \epsilon$, $|x_3 - x_4| < \epsilon$ or $|x_2 - x_4| < \epsilon$, but this implies that at least one of the links $\{2,3\}, \{3,4\}$ or $\{2,4\}$ belong to G_x, therefore G_x strictly contains S. The same argument applies to any subnetwork obtained form S by permutation of vertices.

Now consider the 4-cycle shown in Figure 2.5 (b), detonate it C, and suppose that $x \in \mathbb{R}^N$ is such that $S = G_x$ for some $\epsilon > 0$. If so is the case, then $|x_1 - x_3| > \epsilon$ and

$\{x_2, x_4\} \subset B_\epsilon(x_3) \cap B_\epsilon(X_1)$. This implies that $|x_2 - x_4| < \epsilon$, and therefore the link $\{2,4\}$ belong to G_x, implying that G_x strictly contains C. Once again, the argument applies to any subnetwork obtained from C by permutation of vertices. □

A consequence of this result is the following.

Corollary (Unfeasible synchronized subnetworks of K_N for $N > 4$)**.** *If a subnetwork G of K_N contains a 3-star or a k-cycle, for $k \geq 4$, as induced subgraphs, then G is unfeasible as synchronized subnetwork K_N.*

Proof. The proof of this corollary follows the lines of the proof of Proposition 2.1.2. The contradiction when supposing the occurrence of a 3-star is exactly the same as in the proposition. The same can be said when it is a 4-cycle that occurs as an induced subgraph. Then, suppose that G_x contains a k-cycle, for $k \geq 5$, as an induced subgraph. Let $n_1, n_2, \ldots, n_k$ be the vertices defining the induced k-cycle, ordered in such a way that $x_{n_1} < x_{n_2} < \cdots < x_{n_k}$. Then $x_{n_{j-1}} > x_{n_j} - \epsilon$, $x_{n_{j+1}} < x_{n_j}$, and $x_{n_{j+1}} > x_{n_{j-1}} + \epsilon$ for each $j = 2, 3, \ldots, k-1$. But since $n_1, n_2, \ldots, n_k$ induce a k-cycle, necessarily $x_{n_k} < x_1 + \epsilon$, which implies that the subgraph of G_x induced by the vertices $n_1, n_2, \ldots, n_k$, strictly includes the k-cycle since it includes all the links $\{n_i, n_j\}$ for each $1 \leq i, j \leq k$. □

The previous corollary supplies a tool, easy to implement, to discriminate subgraphs which cannot be obtained as synchronized subnetworks.

Let me close this subsection by highlighting the fact that not all subgraphs of the complete graph K_N, when the dimension is greater than 3, can be obtained as synchronized subnetworks and establishing which subnetworks are feasible and computing how many of them there are is not a trivial problem. This problem was completely solved by using a clever coding of the feasible synchronized subnetworks. This was made in the Subsection 2.1.1, while in this subsection we present easily verifiable conditions ensuring that a subgraph is unfeasible as synchronized subnetwork.

2.1.3 Paths towards synchronization

The coding established in Subsection 2.1.1 allows to rigorously determine all the paths to synchronization in the transition diagram of the Laplacian flow on K_N. The analysis is restricted to initial conditions in $\mathbb{R}^N$ satisfying a condition, ensuring that its synchronized subnetworks never add more than one link at a time. The restriction to this class of initial conditions, which are predominant in a geometric and probabilistic sense, allows to specify necessary and sufficient conditions for a sequence of increasing functions in Φ_N to codify a path towards synchronization. In this way it is possible to characterize, from a combinatorial point of view, the full transition diagram and to obtain bounds for the number of paths towards synchronization. Exact computations, relaying on extensive numerical computations, are available only for dimensions less than or equal nine. Finally, two types of distributions associated with path lengths

and the out degrees in the transition diagram of are shown.

As mentioned above in Subsection 2.1.1, the switching times $t_1 < t_2 < \cdots < t_\ell$ are completely determined by the increments $x_n - x_m$, with $m < n$. I will only consider typical paths to synchronization, which I defined in Subsection 1.2. Non-typical paths are defined by initial conditions satisfying a system of linear equations of the kind $x_m = x_n$ or $x_m + x_n = x_k + x_\ell$. Hence, non-typical paths clearly correspond to a set of initial conditions of zero Lebesgue measure, which justifies the imposed restriction.

The restriction to typical paths allows to reduce the transition digraph shown in Figure 1.22, which contains all possible paths to synchronization for the Laplacian flow in K_3, to the more simple diagram shown in Figure 2.6, which contains only the typical paths. The fact that all increments of coordinates in the initial condition are different, eliminate jumps larger than one level in the transition diagram. This is an easier diagram to read and it represents all the paths towards synchronization, except for initial conditions in a set of zero Lebesgue measure.

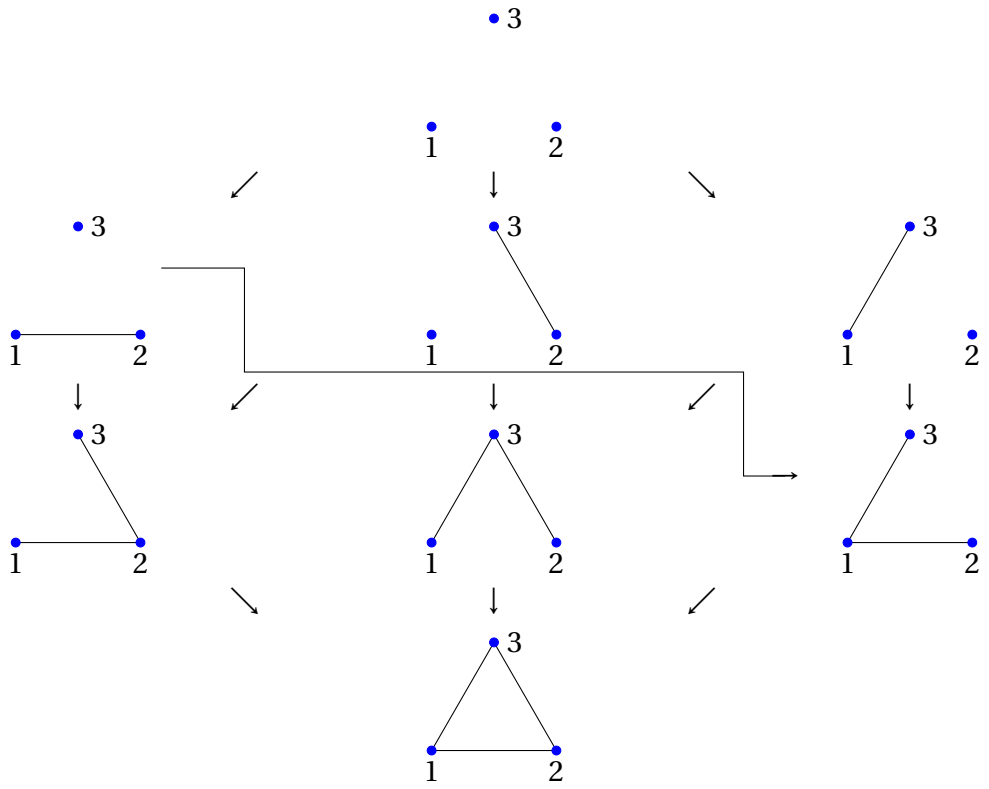

Figure 2.6 –
Transition diagram of the Laplacian flow in K_3 for typical initial conditions.

By using the coding of synchronizing subnetworks, a path to synchronization be-

comes a sequence of increasing functions in Φ_N. Denote by δ_n, the characteristic function of the singleton $\{n\} \subset \{1,2,\dots,N\}$. The following result characterizes such sequences.

Definition (Admissible sequence of increasing functions)**.** *A sequence $(\phi_0,\phi_1,\dots,\phi_\ell)$ in Φ_N is said to be admissible if it satisfies the following two conditions:*

a) for each each $0 \le \tau < \ell$, there exists $n_\tau \in \{1,2,\dots,N\}$ such that $\phi_{\tau+1} = \phi_\tau + \delta_{n_\tau}$,

b) $\phi_\ell(n) = N$ for all $n \in \{1,2,\dots,N\}$.

It is not difficult to see that, for each typical initial condition $x(0) \in \mathbb{R}^N$, the corresponding sequence $(\phi_{x(0),\epsilon}, \phi_{x(\tau_1),\epsilon}, \dots, \phi_{x(\tau_\ell),\epsilon}) \in \Phi_N$ is admissible. Here $\tau_1 < \tau_2 < \cdots < \tau_\ell$ is the sequences of switching times for the initial condition $x(0)$ and since the initial condition is typical, then at each switching time only one new link is added to the synchronized subnetwork, which means that the increasing function codifying the subnetwork increases by one and only one site. Clearly, the last subnetwork in the path has to be K_N, represented by the constant function $\phi = N$. On the other hand, not all the admissible sequences codify a path to synchronization.

Definition (Realizable sequence of increasing functions)**.** *A sequence $(\phi_0,\phi_1,\dots,\phi_\ell)$ in Φ_N is said to be realizable if there exists a typical initial condition $x(0) \in \mathbb{R}^N$, with switching times $\tau_1 < \tau_2 < \cdots < \tau_\ell$, such that $\phi_k = \phi_{x(\tau_k),\epsilon}$ for each $0 \le k \le \ell$.*

The following is the complete characterization of the set of realizable sequences of increasing functions.

Theorem (Characterization of the realizable sequences of increasing functions)**.** *Let $(\phi_0,\phi_1,\dots,\phi_\ell)$ be an admissible sequence of increasing functions in Φ_N, and for each $1 \le \tau \le \ell$, let $n_\tau \in \{1,2,\dots,N\}$ be the τ-th jump site of the sequences, i.e., $\phi_{\tau+1} - \phi_\tau = \delta_{n_\tau}$. In order for $(\phi_0,\phi_1,\dots,\phi_\ell)$ to be realizable, it is necessary and sufficient that there exists a typical configuration $x \in \mathbb{R}^N$ such that the differences*

$$\Delta := \{\Delta_{n,k} := x_{n+k} - x_n : 1 \le n < n+k \le N\}, \tag{2.9}$$

are ordered in such a way that the τ-th smallest increment in Δ is $\Delta_{n_\tau,k}$.

Proof. et $(\phi_0,\phi_1,\phi_2,\dots,\phi_\ell) \in \Phi_N$ be an admissible sequence and $n_1,n_2,\dots,n_\ell$ the corresponding sequence of jump sites, i.e., $\phi_{\tau+1} - \phi_\tau = \delta_{n_\tau}$ for each $1 \le \tau \le \ell$. Suppose that $x(0) \in \mathbb{R}^N$ is typical and such that the τ-th smallest increment in $\{\Delta_{n,k} := x_{n+k} - x_n : 1 \le n < n+k \le N\}$ is $\Delta_{n_\tau,k}$. Consider the sequence $(\phi_{x(0),\epsilon}, \phi_{x(\tau_1),\epsilon}, \dots, \phi_{x(\tau_\ell),\epsilon}) \in \Phi_N$ determined by the initial condition $x(0)$. This sequence is admissible and, since $x_m(t) - x_n(t) = (x_m(0) - x_n(0))\, e^{-Nt}$ for each $1 \le n < m \le N$ and $t \in \mathbb{R}$, then the k-th increment necessarily takes place at the site n_k. Therefore the admissible sequence $(\phi_0,\phi_1,\phi_2,\dots,\phi_\ell) \in \Phi_N$, defined by the sequence of jump sites $n_1,n_2,\dots,n_\ell$ is realizable. On the other hand, if the admissible sequence $(\phi_0,\phi_1,\dots,\phi_\ell)$ in Φ_N is realizable, then there exists a typical initial condition $x(0) \in \mathbb{R}^N$ such that $\phi_\tau = \phi_{x(\tau),\epsilon}$ for each $1 \le \tau \le \ell$. Furthermore, since $x_m(t) - x_n(t) = (x_m(0) - x_n(0))\, e^{-Nt}$ for each

$1 \leq n < m \leq N$ and $t \in \mathbb{R}$, necessarily the k-th increment in $(\phi_0, \phi_1, \ldots, \phi_\ell)$ takes place at the site n_k satisfying $\phi_{x(\tau_{k+1},\epsilon)} - \phi_{x(\tau_k,\epsilon)} = \delta_{n_k}$. □

Consider the Laplacian flow in K_3, and take typical ordered initial conditions $x = (x_1, x_2, x_3) \in \mathbb{R}^3$, (that is $x_1 < x_2 < x_3$, and all the differences $|x_i - x_j|$ for all i, j and $i \neq j$, are different from zero and pairwise different). Use the codification of synchronized subnetworks by increasing functions, defined in Figure 2.3. Using this labelling, in Figure 2.7 I depict the transition diagram which results in a simplified version of the one presented in Figure 2.6. In this simplified version, only one of all redundant paths obtained by permutation of vertices is retained. Clearly, this diagram contains all the relevant information, for example, the length of the longest path, the out degree of a state, and the diversity of paths.

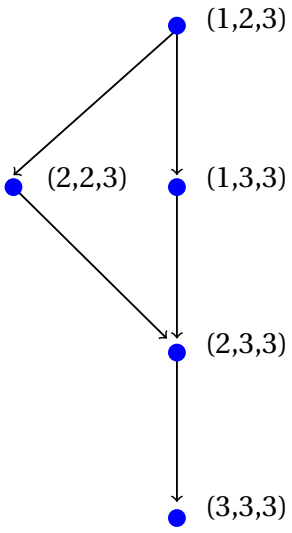

Figure 2.7 – Transition diagram of the Laplacian flow on K_3, labelled by increasing functions. It consists of 5 states and 5 arrows. At the top the state $(1,2,3)$, corresponding to the totally disconnected graph of dimension 3. At the bottom, the state $(3,3,3)$, corresponding to the K_3. This transition diagram represents all the paths to synchronization defined by typical ordered initial conditions and constitutes a simplification of digraph in Figure 2.6.

Recall that $\Delta_{n,k}$ denotes the increment $x_{n+k} - x_n$ in the coordinates of an initial condition x. The increments of each typical initial condition in $\mathbb{R}^3$ can only fit one of two possible increment orderings:

$$\Delta_{1,1} < \Delta_{1,2} < \Delta_{2,1},$$
$$\Delta_{1,2} < \Delta_{1,1} < \Delta_{2,1}.$$

These two possible ordering determine the only two distinguishable paths shown

in Figure 2.7, both starting at the disconnected network represented by $(1,2,3)$, and ending at K_3, represented by $(3,3,3)$. The two realizable paths are the following.

$$(1,2,3) \to (2,2,3) \to (2,3,3) \to (3,3,3),$$
$$(1,2,3) \to (1,3,3) \to (2,3,3) \to (3,3,3).$$

It is therefore verified in this case that different realizable paths correspond to different order types.

It should be noted that not all transitions $G \to G'$, where G' is obtained from G by the addition of a new link, appear in paths to synchronization. This is precisely the basis of the difference between admissible and realizable paths. The following example illustrates the differences between admissible path and realizable path, in the case of K_4. In Figure 2.8, each row represents a subgraph of K_4 (it is understood that vertices are labels from left to right from 1 to 4) and each blue arrow represents a transition $G \to G'$, where G' is obtained from G by the addition of a new link. The column (a) shows an admissible, but not realizable path, while in column (b), the path is realizable. The path in the first column cannot be obtained from any initial condition. Indeed, from step 4 on, the transitions depicted are incompatible with the first three transitions. In this case, the first three steps force in step 4 to add a link joining the first vertex with the third one, then the third one with the last one, as it is in the path depicted in the column (b).

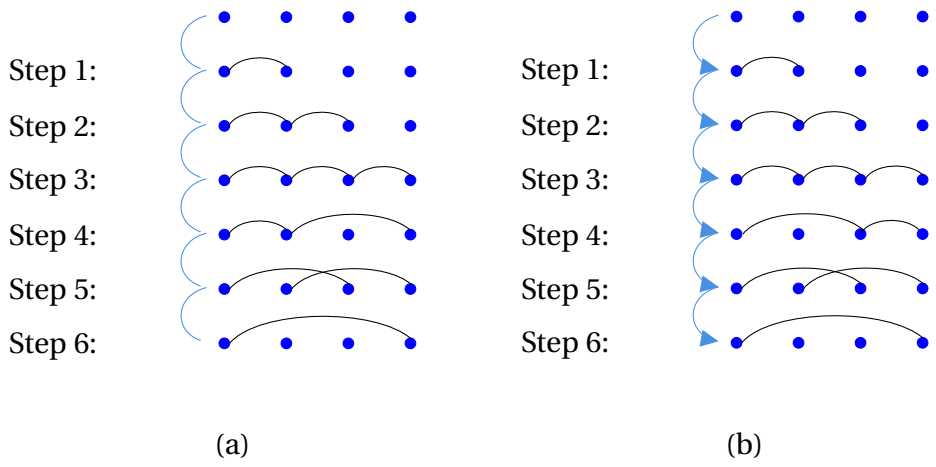

Figure 2.8 – In (a), an admissible path to synchronization which is incompatible with any initial condition. A realizable path, starting with the same first three steps, will force the last steps to be as in the path depicted (b).

There is a total of 16 admissible paths towards synchronization for the Laplacian flow on K_4, all of them shown in the table below. Each letter refers to the notation of

configurations used in Figure 2.4.

$$
\begin{array}{ll}
(a \to f \to h \to k \to l \to m \to n) & (a \to f \to h \to i \to l \to m \to n) \\
(a \to f \to h \to i \to j \to m \to n) & (a \to f \to g \to i \to l \to m \to n) \\
(a \to f \to g \to i \to j \to m \to n) & (a \to c \to h \to k \to l \to m \to n) \\
(a \to c \to h \to i \to l \to m \to n) & (a \to c \to h \to i \to j \to m \to n) \\
(a \to c \to d \to i \to l \to m \to n) & (a \to c \to d \to i \to j \to m \to n) \\
(a \to c \to d \to e \to j \to m \to n) & (a \to b \to g \to i \to l \to m \to n) \\
(a \to b \to g \to i \to j \to m \to n) & (a \to b \to d \to i \to l \to m \to n) \\
(a \to b \to d \to i \to j \to m \to n) & (a \to b \to d \to e \to j \to m \to n)
\end{array}
$$

There is a total of 10 realizable paths towards synchronization for the Laplacian flow on K_4, each of them corresponding to each one of the 10 different order types of the increments of a typical initial condition. These 10 order types are depicted in Table 2.1.

$\Delta_{1,1} < \Delta_{2,1} < \Delta_{3,1} < \Delta_{1,2} < \Delta_{2,2} < \Delta_{1,3}$	$\Delta_{1,1} < \Delta_{2,1} < \Delta_{1,2} < \Delta_{3,1} < \Delta_{2,2} < \Delta_{1,3}$
$\Delta_{1,1} < \Delta_{3,1} < \Delta_{2,1} < \Delta_{1,2} < \Delta_{2,2} < \Delta_{1,3}$	$\Delta_{2,1} < \Delta_{1,1} < \Delta_{3,1} < \Delta_{1,2} < \Delta_{2,2} < \Delta_{1,3}$
$\Delta_{2,1} < \Delta_{1,1} < \Delta_{1,2} < \Delta_{3,1} < \Delta_{2,2} < \Delta_{1,3}$	$\Delta_{2,1} < \Delta_{3,1} < \Delta_{1,1} < \Delta_{2,2} < \Delta_{1,2} < \Delta_{1,3}$
$\Delta_{2,1} < \Delta_{3,1} < \Delta_{2,2} < \Delta_{1,1} < \Delta_{1,2} < \Delta_{1,3}$	$\Delta_{3,1} < \Delta_{1,1} < \Delta_{2,1} < \Delta_{2,2} < \Delta_{1,2} < \Delta_{1,3}$
$\Delta_{3,1} < \Delta_{2,1} < \Delta_{1,1} < \Delta_{2,2} < \Delta_{1,2} < \Delta_{1,3}$	$\Delta_{3,1} < \Delta_{2,1} < \Delta_{2,2} < \Delta_{1,1} < \Delta_{1,2} < \Delta_{1,3}$

Table 2.1 – The ten different order types of the increments for typical initial conditions in $\mathbb{R}^4$.

Each order type uniquely determines a realizable path towards synchronization. All of the paths are organized in the transition diagram depicted in Figure 2.9. The synchronized subnetworks are codified by increasing functions, as shown in Figure 2.4. At the top of the diagram it is the identity function $(1,2,3,4)$, which codifies the completely disconnected graph. All the paths finish at the constant function $(4,4,4,4)$, which codifies the fully connected graph.

Since each realizable path to synchronization is determined by an order type in the increments of coordinates of a typical initial condition, the counting the number of such paths amounts to count the total number of different order types. The order types are related to combinatorial objects already considered in the literature. These are the so called Golomb rulers already defined in Subsection 1.1.5.

Corollary (An equivalent problem for the number of realizable paths)**.** *The total number of realizable paths toward synchronization is the number combinatorially distinct Golomb rulers, i.e.,*

$$\textit{Number of paths towards synchronization for } K_N = \textit{Golomb}(N).$$

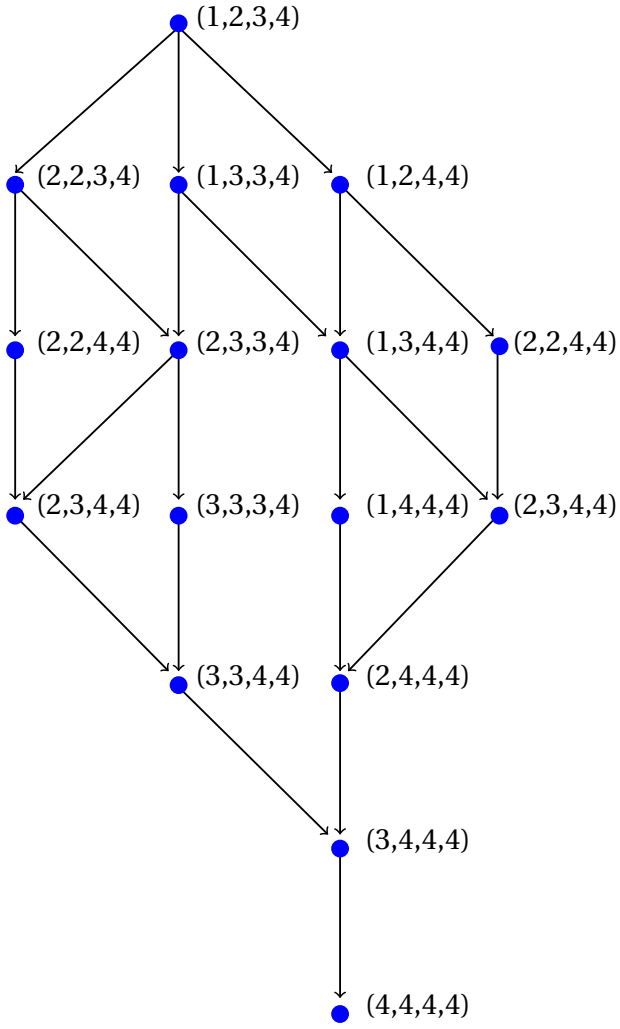

Figure 2.9 – The synchronized subnetworks are codified by increasing functions. At the top, the function $(1,2,3,4)$ codifies the totally disconnected graph of dimension 4, and at the bottom, the function $(4,4,4,4)$ codifies the complete graph of dimension 4. Each path in this transition diagram corresponds to an order type of the increments of initial conditions $x = (x_1, x_2, x_3, x_4) \in \mathbb{R}^4$ such that $x_1 < x_2 < x_3 < x_4$.

Proof. As proved above, each realizable path to synchronization correspond to a order type of coordinate increments in Δ. As mentioned in Section 1.1.5, a Golomb ruler with N marks is a vector $a \in \mathbb{Z}^N$ with $a_1 < a_2 < \cdots < a_N$, such that no two increments $a_{n+k} - a_n$, where $1 \leq n < N$ and $1 \leq k \leq N - n$ coincide. Hence, a Golomb ruler is nothing but a typical initial condition with integer coordinates. A Golomb ruler can be associated each typical initial condition $x \in \mathbb{R}^N$, as follows. Since x is typical, then both $\epsilon_1 = \min\{\Delta_{n,k} : 1 \leq n < N, 1 \leq k < N - n\}$ and $\epsilon_2 = \min\{|\Delta_{n,k} - \Delta_{m,\ell}| : (m,k) \neq (n,\ell)$:

$1 \leq n < N, 1 \leq k < N-n, 1 \leq m < N, 1 \leq \ell < N-m\}$ are strictly positive. Let $p \in \mathbb{N}$ be such that $p \cdot \min(\epsilon_1, \epsilon_2/4) > 1$, and for each $1 \leq n \leq N$ let $q_n := \max\{q \in \mathbb{Z} : q/p \leq x_n\}$. The vector $q = (q_1, q_2, \ldots, q_N) \in \mathbb{Z}^N$ is the desired Golomb ruler. Indeed, since $p\epsilon_1 > 1$, then for each $1 \leq n < N$, then

$$q_n \leq p\, x_n \leq p\,(x_{n+1} - \epsilon_1) \leq q_{n+1} + 1 - p\epsilon_1 < q_{n+1}.$$

On the other hand, whenever $\Delta_{n,k} > \Delta_{m,\ell}$, then

$$(q_{n+k} - q_n) - (q_{m+\ell} - q_m) \geq p(\Delta_{n,k} - \Delta_{m,\ell} - 4/p) > p(\epsilon_2 - 4/p) > 0.$$

Furthermore, two Golomb rulers are combinatorially equivalent if they determine the same ordering in their differences, which means that $a, b \in \mathbb{R}^N$ are equivalent if and only if $((a_{n+k} - a_n) - (a_{m+\ell} - a_m))((b_{n+k} - b_n) - (b_{m+\ell} - b_m)) > 0$ for each $1 \leq m, n < N$ and $1 \leq k < n$, $1 \leq \ell < m$. Hence, the number Golomb(N) of combinatorially different Golomb rulers with N marks, coincides with the number of paths to synchronization. □

The growth of the number of paths towards synchronization can be seen as a measure of complexity, similar to the topological complexity of dynamical systems (Blanchard, Host, and Maass 2000). The topological complexity counts the growth of the number of distinguishable trajectories as a function of time, while in this case, Golomb(N) counts the number of distinguishable paths towards synchronization as a function the dimension of the system.

Theorem (Bounds for $Golomb(N)$)**.** *Following bounds hold for each $N \in \mathbb{N}$,*

$$(N-1)! \leq Golomb(N) \leq \left(\frac{N(N+1)}{2}\right)! \frac{\prod_{i=1}^{N-1} i!}{\prod_{i=1}^{N}(2i-1)!} \leq \binom{N}{2}!.$$

Proof. The upper bound directly derives from the upper bound for the number of orderings of pairwise multiplications which can be found in (Johnston 2014b). Indeed, A Golomb ruler $a \in \mathbb{Z}$ is also characterized by the fact that all the sums $a_m + a_n$ are different. For this, notice that, given a collection $A = \{a_1, a_2, \ldots, a_N\}$ of natural numbers,

$$\{\text{sign}((a_{n+k} - a_n) - (a_{m+\ell} - a_m)) = \text{ sign}((a_{n+k} + a_m) - (a_{m+\ell} + a_n)),$$

For each $1 \leq m, n \leq N$ and $k, \ell \in \mathbb{N}$ such that $1 \leq n+k, m+\ell \leq N$. Hence, the number of combinatorially different Golomb rules is noting but the number of different orderings for the set of sums $S = \{a_m + a_n : 1 \leq m < n \leq N\}$. On the other hand, this number is to the number of different orderings for the set of products $P = \{a_m\, a_n : 1 \leq m < n \leq N\}$.

the equivalence is readily established by taking the logarithm. N. Johnston proved that

$$\text{Number of orderings for} P \leq \left(\frac{N(N+1)}{2}\right)! \frac{\prod_{i=1}^{N-1} i!}{\prod_{i=1}^{N}(2i-1)!}.$$

His argument goes as follows. Let $M_N \in \mathscr{M}(\mathbb{N})_{N\times N}$ be such that each (i,j)-element is $a_i a_j$. For instance, when $N=5$, there is the following symmetric matrix,

$$M_5 = \begin{pmatrix} a_1^2 & a_1a_2 & a_1a_3 & a_1a_4 & a_1a_5 \\ a_2a_1 & a_2^2 & a_2a_3 & a_2a_4 & a_2a_5 \\ a_3a_1 & a_3a_2 & a_3^2 & a_3a_4 & a_3a_5 \\ a_4a_1 & a_4a_2 & a_4a_3 & a_4^2 & a_4a_5 \\ a_5a_1 & a_5a_2 & a_5a_3 & a_5a_4 & a_5^2 \end{pmatrix}.$$

As $a_1 < a_2 < \cdots < a_N$, then the rows and columns of the upper-triangular part of M_N are increasing. The upper bound can be obtained by counting the number $T(N)$ of ways which the numbers $1,2,\ldots,N(N+1)/2$ (representing the rank index of a particular product), can be arranged in $N(N+1)/2$ places in the upper-triangular part of a matrix, in such a that the rows and columns of that upper-triangular part are increasing. This number was obtained by M. R. Thrall in (Thrall 1952), and is precisely

$$T(N) = \left(\frac{N(N+1)}{2}\right)! \frac{\prod_{i=1}^{N-1} i!}{\prod_{i=1}^{N}(2i-1)!}, \tag{2.10}$$

Clearly $\binom{N}{2}! \geq T(N)$. A lower bound can be obtained by counting all the orderings of the products of consecutive increments, $a_{i+1} - a_i$ for $1 \leq i \leq N-1$, whose $N-1$ values can be ordered arbitrarily. □

Since the number of combinatorially different Golomb rulers and the number of paths to synchronize coincide, the bounds obtained above apply to the number of paths to synchronize as well. This number is relevant quantum entanglement (Hildebrand 2007). The sequence Golomb(N) appears in the On-line Encyclopedia of Integer Sequences (OEIS), under the entry A237749 (Johnston 2014a), where the first nine terms, which we reproduce in Table 2.2, are explicitly computed. Notice that for dimensions 3 and 4, they coincide with the number of paths computed in the examples examined previously in this section.

Let me stress the fact that the computation of a closed formula for Golomb(N) remains an open problem. In Figure 2.10, a graphic comparison of the bounds just discussed is shown. The black line corresponds to the exact computation of the number of combinatorially different Golomb rules up to $N=9$. The dashed lines are the bounds established in the previous theorem. Notice how the trivial upper bound, $\binom{N}{2}!$, departs from the exact behavior.

The characterization of the paths towards synchronization developed so far, allows

N	Golomb(N)
1	1
2	1
3	2
4	10
5	114
6	2608
7	107498
8	7325650
9	771505180

Table 2.2 – Number of combinatorially different Golomb rulers.

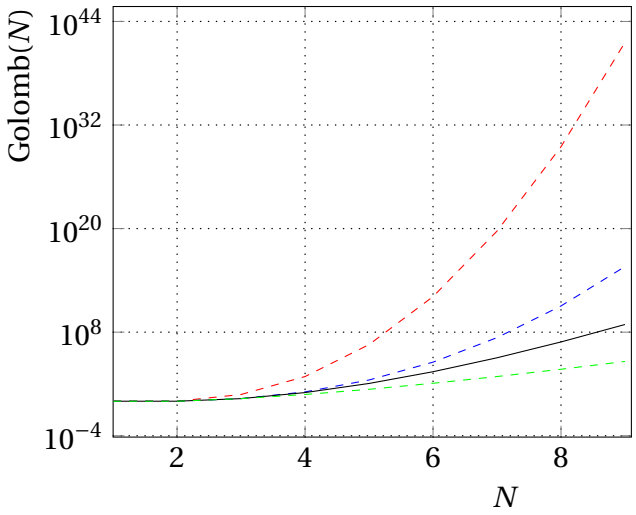

Figure 2.10 – Bounds for the number of combinatorially different Golomb rules. The black line corresponds to the exact computation of the number of combinatorially different Golomb rules. The dashed lines are the bounds shown established in Theorem 2.1.3. The red line and the green line are the trivial upper and lower bounds $\binom{N}{2}!$ and $(N-1)!$ respectively. The blue line is the bound given by (2.10).

to compute certain characteristics of the transition diagram such as, the number of synchronized sequences of fixed length ℓ, and the distribution of lengths of the all paths towards synchronization. From these computations, the mean length and the most frequent length of the paths can be obtained. Furthermore, the behavior of these quantities for increasingly large dimensions can be extrapolated.

As it can be seen in all the examples, the transition diagram for K_N has a hierarchical structure having the disconnected subnetwork, codified by the identity function

$\mathrm{Id} := (1,2,\ldots,N) \in \Phi_N$, at the top, and the complete graph, codified by the constant function $\mathbf{N}(n) = N$, where $1 \le n \le N$, at the bottom.

Proposition (The maximum length of a paths to synchronization)**.** *The maximal length of a synchronizing sequence in the transition diagram of the Laplacian flow on K_N is*

$$l_{\max} = N(N-1)/2.$$

Proof. A path defined by a typical initial condition is such that at each step only one new edge appears in the synchronized subnetwork. At level ℓ, counting from top to bottom, all the subnetworks which can be reached from the disconnected subnetwork after exactly ℓ steps are placed. These subnetworks are precisely those having exactly ℓ edges, therefore they are codified by increasing functions $\phi \in \Phi_N$ such that

$$\sum_{n=1}^{N} (\phi(n) - n) = \ell.$$

From here, the maximal length of a synchronizing sequence is

$$l_{\max} = \sum_{n=1}^{N} (N - n) = N(N-1)/2.$$

□

It is easy to characterize the synchronized subnetworks which are starting points of a path to synchronization of a given length. To compute their number, it is enough to note the following. The number $F_N(\ell)$ of synchronized subnetworks starting a sequence of length ℓ is given by the number of Dyck paths of order N, with length $2N$ and area $N^2 - \ell$, that is,

$$F_N(\ell) := \left| \left\{ \phi \in \Phi_N : \sum_{n=1}^{N} \phi(n) = N^2 - \ell \right\} \right|. \tag{2.11}$$

This problem has been treated in the literature. The generating polynomial defined by these quantities is,

$$\begin{aligned} P_N(t) &:= \sum_{\phi \in \Phi_N} t^{\,\mathrm{area}(\phi)}, \\ &= \sum_{\ell=0}^{\frac{N(N-1)}{2}} F_N(\ell)\, t^{\frac{N(N-1)}{2} - \ell}, \end{aligned}$$

where $\mathrm{area}(\phi) := \sum_{n=1}^{N} (\phi(n) - n)$ denotes the area under the Dyck path determined by the increasing function ϕ. These generating polynomials can be computed by using

the recurrence relation,

$$P_N(t) = \sum_{n=0}^{N-1} t^n \, P_n(t) \, P_{N-n-1}(t) \tag{2.12}$$

derived in (Carlitz and Riordan 1964), with initial condition $P_0 = 0$ (see (Blanco and Petersen 2012) as well). The fraction $F_N(\ell)/C_N$, can be interpreted as the probability of choosing a path to synchronisation of length ℓ, by selecting randomly, uniformly, a synchronization subnetwork. Here C_N is the total number of synchronized subnetworks which, as shown above, coincides with the N-th Catalan number.

Although there is no closed formula for $F_N(\ell)$, the recurrence relation above allows to directly compute the distributions $\ell \to F_N(\ell)$, and determine their asymptotic behavior. In the Table 2.3 I depict some $F_N(\ell)$ for $2 \le N \le 8$.

N	$F_N(\ell)$
2	(1,1)
3	(1,1,2,1)
4	(1,1,2,3,3,3,1)
5	(1,1,2,3,5,5,7,7,6,4,1)
6	(1,1,2,3,5,7,9,11,14,16,16,17, 14,10,5,1)
7	(1,1,2,3,5,7,11,13,18,22,28,32,37,40,44,43,40,35,25,15,6,1)
8	(1,1,2,3,5,7,11,15,20,26,34,42,53,63,73,85,96,106,113,118,118,115,102,86,65,41,21,7,1)

Table 2.3 – Number $F_N(\ell)$ of functions $\phi \in \Phi_N$, codifying synchronizing subnetworks, which are starting configurations of a synchronizing path of length ℓ.

Definition (The normalized cumulative distribution)**.** *Let $F_N(\ell)$ be the number of synchronized subnetworks which are starting configurations of a path of length ℓ synchronized in the transition diagram of K_N. The normalized cumulative distribution of starting points of paths of a given length, $f_N : [0,1] \to [0,1]$, is defined by*

$$f_N(x) = \frac{1}{C_N} \sum_{n \le x \times N(N-1)/2} F_N(x), \tag{2.13}$$

where F_N is given by Equation (2.11) and C_N is the N-th Catalan number previously defined.

By using the recurrence in Equation (2.12), I numerically computed $f_N(x)$ for increasing values of N, and observe that f_N approaches an absolutely continuous limit distribution $x \mapsto f(x)$. Its density, defined as $\rho(x) := d\,f(x)/dx$, approaches a smooth curve as the one shown in Figure 2.11. It can be observed that for N sufficiently large and $\delta > 0$ sufficiently small, the proportion of starting points of paths of length $N(N-1)(x \pm \delta)/2$ is approximatively $\rho(x)\,\delta$. The numerical computations, as shown in

the same figure, suggest that the function ρ is continuous, unimodal, and negatively skewed.

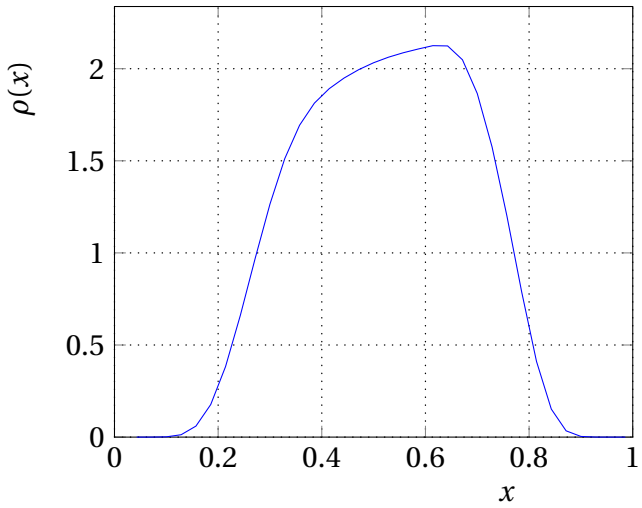

Figure 2.11 – Density $x \to \rho(x)$, of starting points of paths of normalized length x.

Summarizing, the transition diagram for the Laplacian flows on K_N can be decomposed into levels

$$\mathrm{L}_0, \mathrm{L}_1, \ldots, \mathrm{L}_{\frac{N(N-1)}{2}},$$

in such a way that each path to synchronization passes through levels of increasing index until it reaches the level $N(N-1)/2$, which is composed solely by the complete graph K_N, representing the full synchronization.

Proposition (About the mode and the mean of the normalized cumulative distribution of path lengths)**.** *Consider the system L_N, and $F_N(\ell)$ the number of synchronized sequences of length ℓ. The number of ϵ-synchronized subnetworks at each level increases monotonously from* 1 *to the following expression:*

$$mode_N(\ell) \approx 0.632\,\frac{N(N-1)}{2}. \tag{2.14}$$

And, the mean length of these paths towards synchronization is smaller than the most frequent length, that is:

$$\langle \ell \rangle_N < \ mode_N(\ell). \tag{2.15}$$

Proof. A typical initial condition starting at level L_n, will take $N(N-1)/2 - n$ steps to attain the complete graph. Furthermore, the number of subnetworks at level $n = N(N-1)/2 - \ell$ is given by $F_N(\ell)$, defined by Equation (2.11). Then, the number of ϵ-synchronized subnetworks at each level increases monotonously from 1 to the following expression:

$$\begin{aligned} \text{mode}_N(\ell) &:= \max_{1\leq \ell \leq N(N-1)/2} F_N(\ell), \\ &\approx 0.632\,\frac{N(N-1)}{2}, \end{aligned}$$

and then decreases monotonously to 1 as shown in Figure 2.11. Hence, being the distribution of those lengths negatively skewed, the mean length of these paths towards synchronization is smaller than the most frequent length and then:

$$\begin{aligned} \langle \ell \rangle_N &:= \frac{\sum_{\ell=1}^{N(N-1)/2} \ell\, F_N(\ell)}{C_N}, \\ &\approx 0.523\,\frac{N(N-1)}{2}, \\ &< \text{mode}_N(\ell). \end{aligned}$$

□

From the calculations shown in this section, an idea of some characteristics of a typical synchronization path in the Laplacian system of the complete graph K_N can be obtained, for example, if a random ordered initial condition $x \in \mathbb{R}^N$ is taken, then its associated synchronization path would most likely be of length as in Equation (2.14).

Proposition (About the degree distribution of the L_N transition diagram)**.** *The degree distribution of the L_N transition diagram associated to typical ordered initial conditions, is given by the Narayana triangle (described by the Equation (1.26)) read by lines.*

By setting the dimension $N = 100$, the following histogram shown in Figure 2.12 it is generated which is unimodal and symmetric.

As a conclusion of this section, there are two different types of paths that can be generated from sequences of increasing functions that satisfy that are greater than another by one unit at a single coordinate value. When they only meet this condition are called admissible paths, moreover, when they satisfied a specific order dictated by the differences between the coordinates then, they are realizable paths. This is a famous problem equivalent to compute the number of combinatorially distinct Golomb rulers, for which there is no closed formula, and it seems to be a NP-hard problem. Despite of this, bounds of its growth with respect to the dimension N can still be given. On the other hand, it is shown that the longest path that can be found in the transition diagram of L_N precisely matches the number of edges of K_N. Furthermore, the number of paths towards synchronization of size ℓ is given by the number of Dyck paths of order N with length $2N$ and area $N^2 - \ell$, which its probability density function for N sufficiently large is given, and from which the behavior for the mode

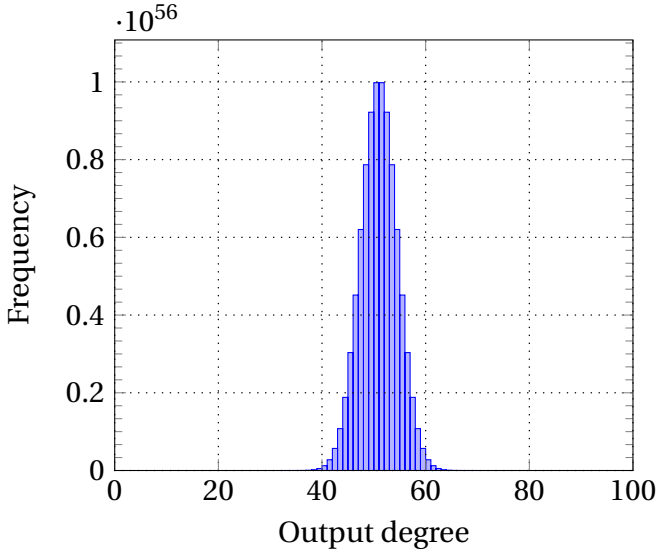

Figure 2.12 – $L(M_{K_{100}})$ transition diagram degree distribution. The degree distribution for the L_N transition diagram, is given by the Narayana triangle described by the Equation (1.26) read by lines, in this case, when $N = 100$ the distribution is shown.

and the mean path length is obtained. Finally, the degree distribution of the transition diagram of L_N is given by the lines of the Narayana triangle. Once again, the coding done through the increasing functions allow to formally describe the behavior of this transition diagram.

2.1.4 Discussion

In this section it is formally and rigorously analyzed the behavior of the transition diagram of the Laplacian system applied to the complete graph of dimension N. To achieve this objective, a coding of the subgraphs of K_N was proposed, which preserves the dynamics of the system and turns out to be very useful because it transforms it into a combinatorial problem that has been widely studied before.

One of the advantages of using this coding is that it automatically generates the subgraphs that are feasible for a set of initial conditions. Despite of this, it was considered pertinent to give the two conditions that a subgraph of K_N must meet to be feasible by an initial condition, the first is that it must not strictly contain 3-stars and the second is that it must not induce k-cycles for $k \geq 4$, this with the aim of giving an idea of how many states that could be thought to be feasible for K_N actually are not.

Moreover, two key simplifications are made for the analytical study of the transition

diagram of L_N. The first is when defining the coding of the subgraphs that are formed from initial conditions, whose coordinates are in strictly increasing order, then, that the set of associated ϵ-synchronized subnetworks have a bijection with the set of increasing functions. This simplification allows to focus the attention on the diversity of states generated by considering a single symmetry of the complete graph. On the other hand, the second simplification made in this section is when the typical initial conditions in the space $\mathbb{R}^N$ are considered, that is, when the differences between the coordinates are different from zero and pairwise different. This type of initial conditions faithfully represents space, because for example, if they were generated randomly, on the one hand, the probability of finding an initial condition with two or more exactly equal coordinates is zero, and on the other hand, the probability that two differences of the coordinates coincide is also zero. Typical initial conditions generate typical paths, which are the ones with the longest lengths, that is, if they start forming the totally disconnected subgraph, then they will reach synchronization in $N(N-1)/2$ steps.

By considering these two simplifications in the space of initial conditions, it is possible to establish the two rules by which two increasing functions will be consecutive on a path towards synchronization. The first is that an increasing function will follow another if they differ by only one coordinate and only by one unit. From this condition admissible paths are generated. The second condition is that the sequence of increasing functions must correspond to a specific order of the increments of a typical initial condition. This second condition generates feasible paths.

The problem of counting how many realizable paths there are in each dimension is equivalent to counting the number of combinatorially distinct Golomb rulers, which is a famous open problem, for which some analytical and numerical bounds have been provided. Furthermore, the number of combinatorially distinct Golomb rulers has only been possible to calculate up to dimension nine, due to the great memory demand that the computation of the Golomb rulers requires.

To end this discussion, it should be noted that having this coding allow to associate characteristics of the combinatorial objects that have a relevant meaning in terms of the study of the transition diagram, which are listed below.

Combinatorial concept	Transition diagram property
Catalan number	Possible states
Combinatorially different Golomb rulers	Number of paths towards synchronization
Number of Dyck paths of order N and area $N^2-\ell$	Number of synchronized sequences of length ℓ
N-th line of Narayana triangle	Degree distribution of L_N

2.2 The transition diagram of $L(M_{K_{N,N}})$

This section is devoted to the analysis of the transition diagram of the Laplacian system on the complete bipartite graph. This study is organized as follows. To begin with, the coding used to describe the states and the paths towards synchronization is presented. Then, the subgraphs which are unfeasible as synchronized subnetworks of the complete bipartite graph are studied. Finally, the way to generate the paths to synchronization for the Laplacian, as well as an estimation of their diversity and distribution are presented.

2.2.1 Coding

The coding of the subgraphs of the complete bipartite graph and the monotonic dynamics that they follow on their path to synchronization was carried out, taking advantage of the fact that the coordinate differences tend monotonically to zero for initial conditions in a domain of the space. So, the following definition is needed.

Definition (Balanced initial condition)**.** *Consider the initial condition $x \in \mathbb{R}^{2N}$, and let*

$$\bar{x} := \frac{\sum_{n=1}^{2N} x_n}{2N},\ \bar{x}_1 := \frac{\sum_{n=1}^{N} x_n}{N} \text{ and } \bar{x}_2 := \frac{\sum_{n=1}^{N} x_{N+n}}{N}. \tag{2.16}$$

A balanced initial condition is such that:

$$\bar{x}_1 = \bar{x}_2.$$

Through this section, the Laplacian matrix of $K_{N,N}$ will be denoted simply by L.

Theorem (Monotony of the coordinate differences)**.** *Consider the Laplacian flow on the complete bipartite graph, where the coordinates $\{1,2,\ldots,N\}$ correspond to vertices in one party of the graph while $\{N+1,N+2,\ldots,2N\}$ are the vertices of the other party.*

Then all the difference $x_i(t) - x_j(t)$, with $1 \le i, j \le N$, converge monotonously and at the same speed to zero, if and only if $x(0)$ is a balanced initial condition.

Proof. The Laplacian matrix on $K_{N,N}$ has the following entries

$$L(i,j) \quad = \quad \begin{cases} 1, & \text{if } N < i \le 2N \text{ and } 0 < j \le N \\ & \text{or } N < j \le 2N \text{ and } 0 < i \le N, \\ -N, & \text{if } i = j,\ 1 \le i, j \le 2N, \\ 0, & \text{otherwise.} \end{cases}$$

As it was said in Section 1.1.2, an eigenbasis can be computed in terms of the canonical basis of $\mathbb{R}^{2N}$ and written as the set:

$$\mathscr{B} = \{u^m, v^n, w^n :\ 1 \le m \le 2,\ 1 \le n \le N-1\},$$

where

$$u^1 = \sum_{k=1}^{2N} \mathsf{e}^k, \quad u^2 = \sum_{k=1}^{N} (\mathsf{e}^k - \mathsf{e}^{k+N}),$$

and for each $n \ge 1$,

$$v^n = \mathsf{e}^{n+1} - \mathsf{e}^1, \quad w^n = \mathsf{e}^{N+n+1} - \mathsf{e}^{N+1},$$

The Laplacian system acts on this basis as follows:

$$Lu^1 = 0, \quad Lu^2 = -2N\,u^2, \quad Lv^n = -N\,v^n \text{ and } Lw^n = -N\,w^N, \text{ for } 1 \le n \le N-1.$$

An initial condition $x \in \mathbb{R}^{2N}$ can be decomposed as:

$$x = \bar{x}\,u^1 + (\bar{x}_1 - \bar{x})\,u^2 + \sum_{n=1}^{N-1} \left((x_{n+1} - \bar{x}_1)\,v^n + (x_{N+n+1} - \bar{x}_2)\,w^n\right),$$

therefore, for all $t \in \mathbb{R}$:

$$\begin{aligned} x(t) &= \bar{x}\,u^1 + e^{-2Nt}(\bar{x}_1 - \bar{x})\,u^2 + e^{-Nt} \sum_{n=1}^{N-1} \left((x_{n+1} - \bar{x}_1), v^n + (x_{N+n+1} - \bar{x}_2)\,w^n\right), \\ &= \sum_{n=1}^{N} \left(\left(1 - e^{-Nt}\right)\left(\bar{x} - e^{-Nt}\bar{x}_1\right) + e^{-Nt}x_n\right)\mathsf{e}^n \\ &\qquad + \sum_{n=1}^{N} \left(\left(1 - e^{-Nt}\right)\left(\bar{x} - e^{-Nt}\bar{x}_2\right) + e^{-Nt}x_{N+n}\right)\mathsf{e}^{N+n}. \end{aligned}$$

From here it follows that:

$$\begin{aligned} x_n(t) - x_{N+m}(t) &= e^{-Nt}\left(x_n - x_{N+m} + \left(1 - e^{-Nt}\right)(\bar{x}_1 - \bar{x}_2)\right), && (2.17) \\ x_n(t) - x_m(t) &= e^{-Nt}\,(x_n - x_m), && (2.18) \\ x_{N+n}(t) - x_{N+m}(t) &= e^{-Nt}\,(x_{N+n} - x_{N+m}), \end{aligned}$$

for all $t \in \mathbb{R}$ and each $1 \leq m, n \leq N$.

Hence, the distance between coordinates in the same party of the complete bipartite graph $K_{N,N}$ decreases monotonously, while the distances between coordinates at different parties will oscillates once, and then decreases to zero. Clearly, all the differences decreases monotonously if and only if the initial condition $x(0) \in \mathbb{R}^{2N}$ satisfies $\bar{x}_1 = \bar{x}_2$, and in this case all the differences go to zero at the same speed, namely $e^{-N\,t}$ □

This property has immediate consequences in the construction of the ϵ-synchronized subnetworks.

Corollary (Preservation of links)**.** *For each balanced initial condition $x \in \mathbb{R}^{2N}$, and every $\epsilon > 0$, the edges $\{n, m\}$ is included in the ϵ-synchronized subnetwork $G_{x(t)}$ for all*

$$t \geq t_{n,m} := \frac{\log|x_n - x_{N+m}| - \log(\epsilon)}{N}.$$

Without loss of generality, assume that the coordinates of the initial condition are ordered as $x_1 \leq x_2 \leq \cdots \leq x_N$, $x_{N+1} \leq x_{N+2} \leq \cdots \leq x_{2N}$, that is, each of its parties is ordered in an increasing way.

Corollary (About coordinate order preservation)**.** *If $x \in \mathbb{R}^{2N}$ is a balanced initial condition such that $x_1 \leq x_2 \leq \cdots \leq x_N$, $x_{N+1} \leq x_{N+2} \leq \cdots \leq x_{2N}$, then $x_1(t) \leq x_2(t) \leq \cdots \leq x_N(t)$ and $x_{N+1}(t) \leq x_{N+2}(t) \leq \cdots \leq x_{2N}(t)$ for all $t \in \mathbb{R}$.*

Proof. Equation (2.18) ensures that $x_1(t) \leq x_2(t) \leq \cdots \leq x_N(t)$ and $x_{N+1}(t) \leq x_{N+2}(t) \leq \cdots \leq x_{2N}(t)$ for all $t \in \mathbb{R}$. □

In Figure 2.13, in (a), a non-balanced initial condition is shown. The dashed line represents the average value of the coordinates at each party. In (b), a balanced initial condition is depicted.

Similarly as in Section 2.1.1, in order to take advantage of the fact that the Laplacian flow preserves the order of the coordinates at each party, the transition diagram is defined not over the ϵ-synchronized subnetworks but over combinatorial objects that encode the ϵ-synchronized subnetworks respecting this order. This will simplify the description the transition diagram, mainly in the monotonous case which is achieved when the initial condition $x \in \mathbb{R}^{2N}$ is balanced.

The ϵ-synchronized subnetwork G_x defined by balanced initial condition $x \in \mathbb{R}^{2N}$ such that $x_1 \leq x_2 \leq \cdots \leq x_N$, $x_{N+1} \leq x_{N+2} \leq \cdots \leq x_{2N}$, is encoded by the couple of

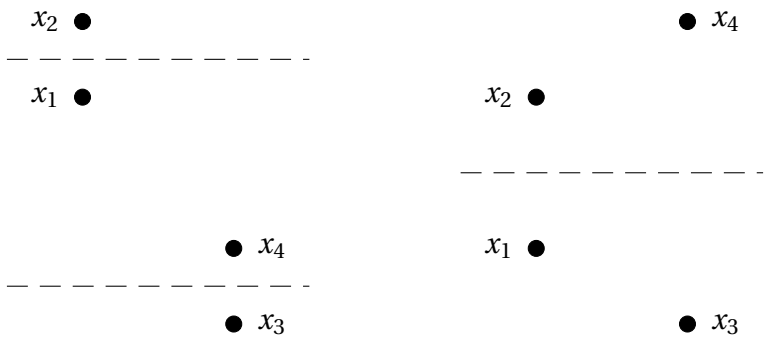

(a) (b)

Figure 2.13 – In (a) and (b) examples of initial conditions in $\mathbb{R}^4$ are shown. The height represents the value of the coordinate, which are grouped according to the party that they belong to. The dashed lines represent the average of the coordinates at each party. In (a), it is observed that the averages of different, while in (b) it is observed that both averages coincide. Initial conditions that satisfy the case shown in (b) are called balanced initial conditions.

functions $\alpha_x, \omega_x : \{1,2,\ldots,N\} \to \{0,1,2,\ldots,N+1\}$ given by:

$$\alpha_x(n) = \begin{cases} \min\{\ell \leq N : x_n - \epsilon \leq x_{N+\ell}\} & \text{if } x_{2N} \geq x_n - \epsilon, \\ N+1 & \text{if } x_{2N} < x_n - \epsilon, \end{cases} \tag{2.19}$$

$$\omega_x(n) = \begin{cases} \max\{\ell \leq N : x_n + \epsilon \geq x_{N+\ell}\} & \text{if } x_{N+1} \leq x_n + \epsilon, \\ 0 & \text{if } x_{N+1} > x_n + \epsilon. \end{cases} \tag{2.20}$$

It should be noted that $\operatorname{im}(\alpha_x) \subset [1, N+1]$ while $\operatorname{im}(\omega_x) \subset [0, N]$.

Both functions are increasing and such that $\alpha_x(n) \leq \omega_x(n)+1$ for each $1 \leq n \leq N$. An example of the construction of the increasing functions from a given initial condition is presented in Figure 2.14. Firstly in (a), an example of the relative position of the coordinates of $x = (x_1, x_2, x_3, x_4)$ for each of its parts on different sides with black dots is illustrated, the first two coordinates to the left and the last two coordinates to the right. The angles that open from the first two coordinates indicate their ϵ-neighborhood. To construct the subgraph G_x, according to Equation (2.21), it is enough to observe that x_3 is inside the ϵ-neighborhood of x_1, and x_4 is inside the ϵ-neighborhood of x_2, hence, in (b), vertices 1 and 3 are connected as well as vertices 2 and 4. Finally, in (c), the increasing functions determined by $x \in \mathbb{R}^4$ are shown. The first function α_x codified the fact that x_3 is the first coordinate of the second part inside the angle opening from x_2 and similarly x_4 with respect to x_2. On the other hand, the second function ω_x, indicates that x_3 is the last coordinate of the second part inside the angle

opening from x_1 and analogously x_4 with respect to x_2. Therefore, the two increasing functions associated with the initial condition are built.

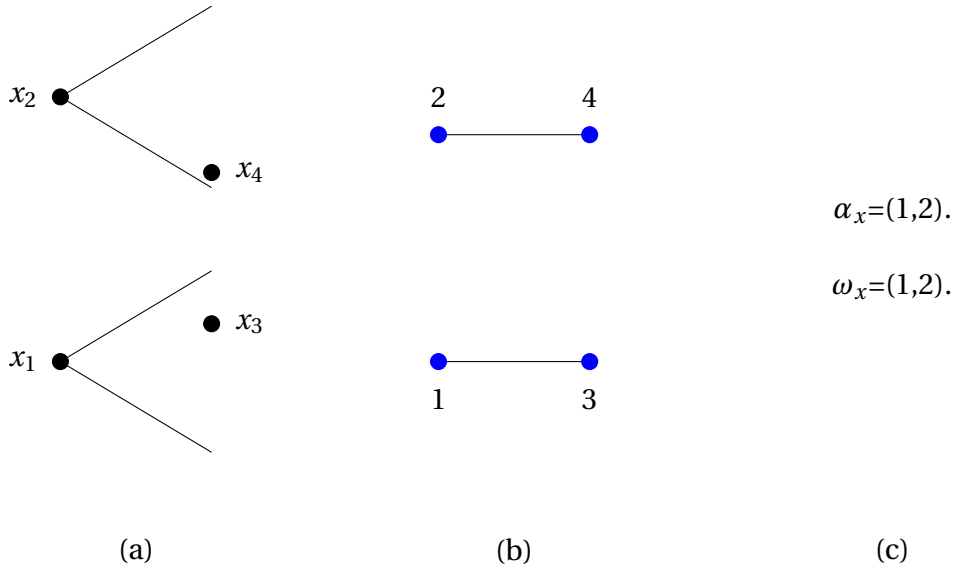

Figure 2.14 – Construction of the increasing functions α_x and ω_x from a given initial condition $x \in \mathbb{R}^4$. In (a), a representation of the values of an initial condition $x \in \mathbb{R}^4$ are shown, and these values are grouped according to the party they belong to. At the coordinates x_1 and x_2, a fan opens towards second party. This is to represent the ϵ-neighborhood around the coordinates x_1 and x_2. In (b), an edge joining the vertices whose coordinates are ϵ-close is drawn. In (c), the increasing functions codifying this configuration presented. The function α_x codified the fact that, x_3 is the first coordinate of the second party above $x_1 - \epsilon$, and similarly x_4 with respect to x_2. The function ω_x indicates that x_3 is the last coordinate of the second party below $x_1 + \epsilon$, and analogously for x_4 with respect to x_2.

Now the following set of increasing functions is defined. Note that the domain of the increasing function has dimension N and the image has dimension $N+2$.

$$I_N := \{\phi : \{1,\dots,N\} \to \{0,\dots,N+1\} : \phi(n+1) \geq \phi(n) \text{ for all } 1 \leq n < N\}.$$

From I_N, it can be defined the following collection of pairs of increasing functions:

$$\Phi_{N,N} := \{(\alpha,\omega) \in I_N \times I_N : \ \mathrm{im}(\alpha) \subset [1,N+1],\ \mathrm{im}(\omega) \subset [0,N] \text{ and } \alpha \leq \omega + 1\}.$$

This collection codifies all the synchronized subgraphs.similar

Theorem (The coding is faithful)**.** *There is a one-to-one correspondence between* $\Phi_{N,N}$ *and the collection of all* ϵ*-synchronized subnetworks of* $K_{N,N}$ *compatible with an or-*

dered initial conditions $x_1 \leq x_2 \leq \cdots \leq x_N$, $x_{N+1} \leq x_{N+2} \leq \cdots \leq x_{2N}$. *The correspondence is given as follows. To each* $(\alpha,\omega) \in \Phi_{N,N}$ *associate the subnetwork* $G_{(\alpha,\omega)} \subset K_{N,N}$, *with edges*

$$E_{(\alpha,\omega)} = \{(n, N+m) : 1 \leq n, m \leq N, \text{ and } \alpha(n) \leq m \leq \omega(n)\}. \tag{2.21}$$

This correspondence is consistent with the fact that $(\alpha,\omega) = (\alpha_x,\omega_x)$ *if and only if* $G_{(\alpha,\omega)} = G_x$.

Proof. The correspondence in Equation (2.21) establishes a mapping from $\Phi_{N,N}$ to the collection of ϵ-synchronized subnetworks defined by ordered initial conditions. In this case, the this correspondence realizes the λ mapping defined in Equation (1.29).

To begin with, notice that each ϵ-synchronized subnetwork G_x, when codified by a couple of increasing functions as prescribed by Equations (2.19) and (2.19), necessarily produced a couple $(\alpha_x,\omega_x) \in \Phi_{N,N}$.

Assume now that $(\alpha,\omega) \in \Phi_{N,N}$. In order to prove that it codifies an ϵ-synchronized subnetwork it is enough to exhibit a point $x \in \mathbb{R}^{2N}$ such that, according to Equations (2.19) and (2.20), $\alpha = \alpha_x$ and $\omega = \omega_x$. The point $x \in \mathbb{R}^{2N}$ can be constructed as follows. For $1 \leq n \leq N$, define the set

$$\mathscr{A}_n := \{1 \leq m \leq N : \alpha(n) \leq m \leq \omega(n)\}.$$

Define recursively n_k and m_k, such that

$$n_1 = 1 \text{ and } m_1 = \max\{m \geq n_1 : \mathscr{A}_n \cap \mathscr{A}_{n+1} \neq \emptyset, \text{ for each } n_k \leq n < m\},$$

then, for each $k > 1$,

$$n_{k+1} = m_k + 1 \text{ and} m_{k+1} = \max\{m \geq n_{k+1} : \mathscr{A}_n \cap \mathscr{A}_{n+1} \neq \emptyset, \text{ for each } n_k \leq n < m\}.$$

Clearly this recursion finishes at the stage ℓ such that $m_\ell = N$. With this integers define the partition $\{1,2,\ldots,N\} = \bigsqcup_{k=1}^{\ell} I_k$, where for each $1 \leq k \leq \ell$, $I_k = \{n_k, n_k+1, \ldots, m_k\}$. For each $1 \leq k \leq \ell$, let $\Delta : I_k \to I_k$ be such that

$$\Delta(n) = \max\{m \in I_k : \mathscr{A}_n \cap \mathscr{A}_m \neq \emptyset\}.$$

Notice that $\Delta(n) \geq n$ and $\Delta(n) = n$ if and only if $n = n_k = m_k$. To Δ can be associated to a directed tree T_k with vertices in I_k, rooted at m_k, and arrows $n \mapsto \Delta(n)$. The structure of these trees is similar to that of the trees described in proof of Theorem **??** for the complete graph K_N. Notice that

$$n_k \mapsto \Delta(n_k) \mapsto \cdots \mapsto \Delta^j(n_k) \mapsto \cdots \mapsto m_k = \Delta^{h_k}(n_k),$$

is the maximal path in T_k and for each $1 \leq j \leq h_k$ let $V_j = \Delta^{-j}(\{m_k\})$ be the j-th level

of T_k. Clearly

$$\min V_j = \Delta^{h_k - j}(n_k) \text{ and } \max V_j < \min V_{j-1},$$

for each $0 \leq j \leq h_k$.

Now assume that x_{n_k} is given. With this, define

$$n_{k,j} := \min V_j \text{ and } x_{n_{k,j}} := x_{n_k} + j\epsilon,$$

for each $1 \leq j \leq h_k$. Now, for $n_{k,j} \leq n < n_{k,j-1}$, let

$$x_n = x_{n_{k,j}} + \frac{(n - n_{k,j})\,\epsilon}{n_{j-1} - n_{k,j}}.$$

In this way, all the coordinates of vertices in the first party can be defined from $x_{n_1}, x_{n_2}, \ldots, x_{n_\ell}$, which will be fixed below. Meanwhile, for each $1 \leq k \leq \ell$, let $\delta_k := \frac{1}{2}\min_{n_k \leq n < m_k}(x_{n+1} - x_n)$. Notice that by construction, $\alpha(n) <\leq \omega(n) \leq \alpha(n+1)$, for each $n \in \{n_k, n_k + 1, \ldots, nm_k - 1\}$. For n this interval such that $\alpha(n) \leq m < \alpha(n+1)$, define

$$x_{N+m} = x_n - (\epsilon - \delta_k) \in (x_n - \epsilon, x_n + \epsilon),$$

therefore $\alpha(n) \leq m < \alpha(n+1)$ and $\omega(n-1) < m \leq \omega(n)$ as required. For the remaining values of $n \in \{n_{k,1}, n_{k,1} + 1, \ldots, n_{k,0} - 1$, where $\omega(n) < m \leq \omega(n+1)$, define

$$x_{N+m} = x_n + (\epsilon - \delta_k) \leq x_n + \epsilon$$

which implies that $\omega(n) < m \leq \omega(n+1)$ as required. In the degenerated case, when $\alpha(m_k) \leq m \leq \omega(n_{k,1})$, define $x_{N+m} = (x_{n_{k,1}} + x_{m_k})/2$. This allows to define all the coordinates of the vertices in the second party, from $x_{n_1}, x_{n_2}, \ldots, x_{n_\ell}$. In order to complete the specification of all the coordinates, fix $x_1 = x_{n_1} = 0$ and for each $1 \leq k \leq \ell$ let $x_{n_k} := x_{m_{k-1}} + 3\epsilon$. Finally, for each $m \notin \bigcup_{n=1}^{N} \mathscr{A}_n$, let $k(m) := \min\{1 \leq k \leq \ell : \alpha(n_k) > m\}$ and define $x_{N+m} := x_{N+\alpha(n_k)} - 3\frac{\epsilon}{2}$. If $\omega(N) < N$, then define $x_{N+m} := x_{m_\ell} + 3\frac{\epsilon}{3}$. With this, the construction of the initial condition associated with the two increasing functions is finalized, ensuring that that $\alpha = \alpha_x$ and $\omega = \omega_x$. □

The pairs of increasing functions in $\Phi_{N,N}$ can be related to know and well studied combinatorial objects.

The collection of pair of increasing functions $\Phi_{N,N}$ is equivalent to the set of parallelo-polyminoes inscribed in a rectangle size $N+1 \times N+2$. Since the number of parallelo-polyminoes in the lattice of size $p \times q$ is given by the Narayana number (Barcucci, Frosini, and Rinaldi 2005) (see Section 1.1.5 for the definition of the paralello-polyminoes and its number). The formal result is the following.

Theorem (Equivalence between $\Phi_{N,N}$ and a collection of parallelo-polyminoes)**.** *There is a one-to-one correspondence between $\Phi_{N,N}$ and the collection of parallelo-polyminoes inscribed in a rectangle size $N+1 \times N+2$.*

Proof. Let $(\alpha,\omega) \in \Phi_{N,N}$ be given. A parallelo-polyminoe in $\{0,1,\ldots,N+1\}\times\{0,1,\ldots,N+1\}$ can be associated to this couple as follow. Define the functions $L, U : \{1,\ldots,N+1\} \to \{0,1,\ldots,N+1\}$ can be associated, to this couple as follow,

$$L(n) = \begin{cases} 0 & \text{for } n = 1, \\ \alpha(n-1)-1 & \text{for } 2 \le n \le N+1, \end{cases} \tag{2.22}$$

and

$$U(n) = \begin{cases} \omega(n)+1 & \text{for } 1 \le n \le N, \\ N+1 & \text{for } n = N+1. \end{cases} \tag{2.23}$$

These two functions define the lower and upper border of a parallelo-polymino in $\{0,1,\ldots,N+1\}\times\{0,1,\ldots,N+1\}$. Furthermore, given su a parallelo-polymino, the corresponding couples $(\alpha,\omega)\Phi_{N,N}$ satisfying the equations above can be determined. The correspondence is therefore one-to-one. □

Lemma. *The number of pairs of increasing functions in a rectangle size $N+1\times N+2$ is given by the Narayana number. In view of the previous theorem,*

$$|\Phi_{N,N}| = T_{N+1}^{2N+1} := \frac{1}{2N+1}\binom{2N+1}{N+1}\binom{2N+1}{N}. \tag{2.24}$$

2.2.2 Unfeasible subgraphs of $K_{N,N}$

Given the characteristics of the pairs of increasing functions and the way they consistently codes ordered and balanced initial conditions in the sense of ϵ-synchronized subnetworks, it turns out that some subgraphs of $K_{N,N}$ remain uncoded, precisely because they are unfeasible. Below are described these types of subgraphs.

To begin, an interesting note is that for the complete bipartite graph case, unlike the case exposed in Section 2.1.2, initial conditions in the form of a 3-star or a 4-cycle can be feasible. It is easy to find initial conditions, as is shown in Figure 2.15, for which these subnetworks arise as synchronized subnetworks of $K_{3,3}$.

To be more precise, consider the complete bipartite graph $K_{3,3}$ and fix $\epsilon > 0$. To build the subgraph depicted in Figure 2.15 (a), it is required that $|x_1 - x_5| \le \epsilon$, $|x_2 - x_5| \le \epsilon$ and $|x_3 - x_5| \le \epsilon$, and there is no constraint, for $|x_2 - x_1|$. An explicit initial condition for this ϵ-synchronized subgraph is $x_1 = x_2 = x_3 = x_5 = 0$ and $x_4 = -3\epsilon$, $x_6 = 3\epsilon$. In the case of Figure 2.15 (b), it is needed that that $|x_1 - x_5| \le \epsilon$, $|x_2 - x_5| \le \epsilon$, $|x_2 - x_4| \le \epsilon$ and $|x_1 - x_4| \le \epsilon$, and there are any constraints for $|x_1 - x_2|$. An explicit initial condition realizing this subnetwork is $x_1 = x_2 = x_4 = x_5 = 0$ and $x_3 = 3\epsilon$, $x_6 = 6\epsilon$.

Although these two subgraphs are feasible in the case of the complete bipartite graph in any dimension, there is another subgraph that is unfeasible, the 6-cycle. An example of this subgraph is shown in Figure 2.16.

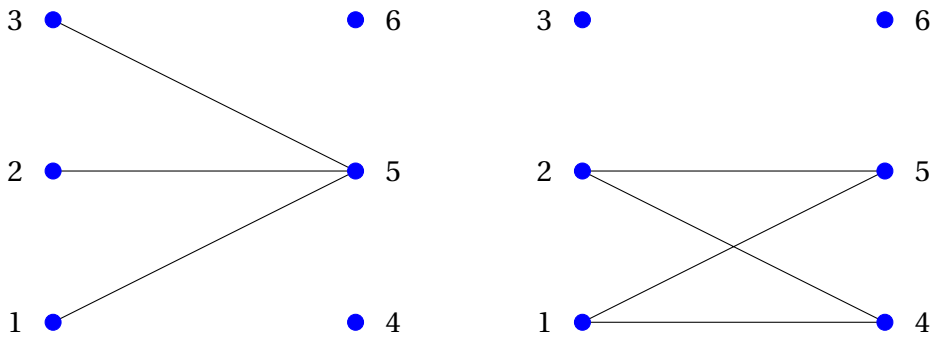

(a) (b)

Figure 2.15 – The subgraphs presented in (a) and (b) correspond to the 3-star and the 4-cycle respectively. Considered as subgraphs of $K_{3,3}$, there is no impediment to find initial condition on $\mathbb{R}^6$, for which they are the corresponding ϵ-synchronized subnetworks, unlike in the case of K_6.

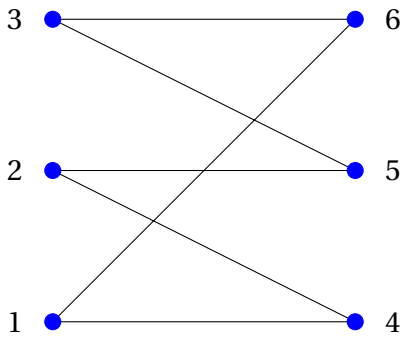

Figure 2.16 – The figure shows a 6-cycle, which can be considered as a subgraph of $K_{3,3}$ or as a subgraph of K_6. In both cases it is unfeasible since there is no initial condition for which it is the corresponding ϵ-synchronized subnetwork.

Proposition (An unfeasible subgraphs for $K_{3,3}$)**.** *Let $\epsilon > 0$. Consider the network $K_{3,3}$ and there, the 6-cycle $1-6-3-5-2-4-1$ as depicted in Figure Figure 2.16. There is no initial condition $x \in \mathbb{R}^6$ such that this subgraph is the corresponding ϵ-synchronized subnetwork.*

Proof. Consider $x = (x_1, x_2, x_3, x_4, x_5, x_6) \in \mathbb{R}^6$. If the cycle $1-6-3-5-2-4-1$ is the synchronized subnetwork defined by x, then necessarily

$$|x_6 - x_1|, |x_6 - x_3|, |x_5 - x_2|, |x_5 - x_3|, |x_4 - x_1|, |x_4 - x_2| \leq \epsilon.$$

At the same time, it is required that

$$|x_6 - x_2|, |x_5 - x_1|, |x_4 - x_3| > \epsilon.$$

There are no restrictions for the distances $|x_3 - x_1|$, $|x_3 - x_2|$, $|x_2 - x_1|$, $|x_6 - x_4|$, $|x_6 - x_5|$ and $|x_5 - x_4|$, since this graph is considered a subgraph of $K_{3,3}$.

Suppose x_1 is the smallest coordinate of x, then $x_4, x_6 \in [x_1, x_1 + \epsilon]$. Besides, $x_2 \in [x_1, x_4 + \epsilon]$. Since $|x_2 - x_6| > \epsilon$, then necessarily $x_1 < x_6 < x_4 < x_1 + \epsilon < x_6 + \epsilon < x_2 \leq x_4 + \epsilon$. Now, since $|x_3 - x_6| \leq \epsilon$, then necessarily $x_3 \in [x_6, x_2]$. Notice that $x_4 \in [x_6, x_2]$ as well. If $x_3 < x_4$, then, $x_3, x_4 \in [x_1, x_1 + \epsilon]$, which contradicts the fact that $|x_3 - x_4| > \epsilon$. If on the contrary $x_3 > x_4$, then $x_3 > x_6 + \epsilon$ which is again a contradiction. □

The important fact to highlight in this section is that not all the subgraphs of the complete bipartite graph $K_{N,N}$ (when the dimension is greater than 6), are feasible for some initial condition, therefore, establish how many states its transition diagram has is not a trivial problem, which could be calculated exactly in Section 2.2.1, when a symmetry of the graph and balanced initial conditions are considered.

2.2.3 Paths towards synchronization

In this section the paths towards the synchronization of the Laplacian flow on $K_{N,N}$ are studied, using the coding established in Section 2.2.1. To begin with, the conditions that the pairs of increasing functions must fulfill to they can be consecutive to form a path towards synchronization are mentioned. In addition, concrete example for dimensions four are presented. It needs to be noted that the transition diagram contains all the paths towards synchronization starting at balanced initial conditions, but it also contains paths which are not compatible with any balanced initial condition. In general, a bound is presented for the number of paths towards synchronization of the Laplacian flow on $K_{N,N}$. Finally, two types of distributions associated to path lengths in the corresponding transition diagram are shown.

Due to the equivalence given by the Equation (2.5), each sequence of ϵ-synchronized subnetworks defined by an ordered and balanced initial condition is faithfully codified by the corresponding sequences of couples of increasing functions given by the Equations (2.19) and (2.20). As mentioned above in Section 2.2.1, for a balanced initial condition $x \in \mathbb{R}^{2N}$, all the differences $x_{N+m}(t) - x_n(t)$ converge to 0 monotonously and at the same speed. In this case, each one of the maps $t \mapsto \alpha_{x(t)}$ and $t \mapsto \omega_{x(t)}$ are coordinate-wise monotonous, and they converge respectively to the constant functions $\mathbf{1}(n) = 1$ and $\mathbf{N}(n) = N$ at time:

$$t_{1,N} := \frac{\log|x_1 - x_{2N}| - \log(\epsilon)}{N}.$$

The sequence of switching times $0 < t_1 < t_2 < \cdots < t_\ell$ is such that $(\alpha_{x(t_\tau)}, \omega_{x(t_\tau)}) \neq (\alpha_{x(t_{\tau+1})}, \omega_{x(t_{\tau+1})})$. Denote as α_{t_τ} by α_τ, and the corresponding for ω. For a typical initial condition, at each switching time, only one of the functions α_τ or ω_τ changes and it changes only at one site.

Lemma. *The sequence of couples of increasing functions*

$$((\alpha_0,\omega_0),(\alpha_1,\omega_1),\ldots,(\alpha_\ell,\omega_\ell)),$$

that form a path to synchronization is completely determined by the initial couple (α_0,ω_0)*, the jump sites* $n_1,n_2,\ldots,n_\ell \in \{1,2,\ldots,N\}^\ell$ *and binary labels* $q_1,q_2,\ldots,q_\ell \in (-1,+1)^\ell$ *as follows:*

$$(\alpha_{\tau+1},\omega_{\tau+1}) = \begin{cases} (\alpha_\tau - \delta_{n_\tau},\omega_\tau) & \text{if } q_\tau = -1, \\ (\alpha_\tau,\omega_\tau + \delta_{n_\tau}) & \text{if } q_\tau = +1. \end{cases} \tag{2.25}$$

To the couple $(\alpha_\tau,\omega_\tau)$*, a parallelo-polyminoe according to Equations* (2.22) *and* (2.23) *can be associated. In the transition* $(\alpha_\tau,\omega_\tau) \rightarrow (\alpha_{\tau+1},\omega_{\tau+1})$*, the area inside the corresponding parallelo-polyminoe increases by one unit until the greatest area.*

There is an example of this transition in Figure 2.17, the parallelo-polyminoes only differ by one unit of area.

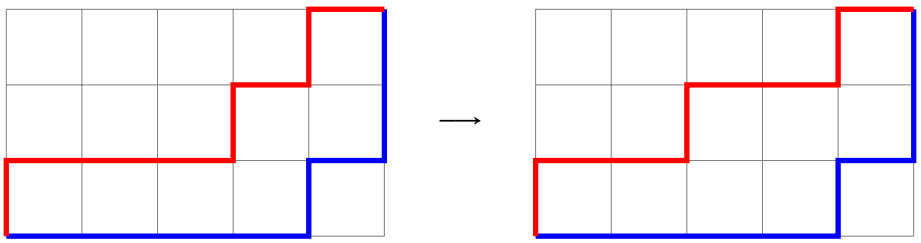

$U = (1,1,1,2,3)$.
$L = (0,0,0,0,1)$.

(a)

$U = (1,1,2,2,3)$.
$L = (0,0,0,0,1)$.

(b)

Figure 2.17 – Example of the transition between parallelo-polyminoes. In (a) and (b), two parallelo-polyminoes and their respective increasing functions that generate them U (red line) and L (blue line) are shown. From the parallelo-polyminoe shown in (a), there is a step to the parallelo-polyminoe shown in (b). In its U-functions, there is only one unit increase in one coordinate. Which translates to an increase of an area unit between them, in other words, this is how it looks the transition between parallelo-polyminoes.

Definition. *A sequence* $((\alpha_0,\omega_0),(\alpha_1,\omega_1),\dots,(\alpha_\ell,\omega_\ell)) \in \Phi_{N,N}$ *is admissible if*

a) for each $1 \le \tau < \ell$ *there exists* $n_\tau \in \{1,2,\dots,N\}$ *cush that either* $\alpha_{\tau+1} = \alpha_\tau - \delta_{n_\tau}$ *and* $\omega_{\tau+1} = \omega_\tau$, *or* $\alpha_\tau = \alpha_\tau$ *and* $\omega_{\tau+1} = \omega_\tau + \delta_{n_\tau}$,

b) $\omega_\ell(n) = N$ *and* $\alpha_\ell(n) = 0$ *for all* $1 \le n \le N$.

A realizable sequences $((\alpha_0,\omega_0),(\alpha_1,\omega_1),\dots,(\alpha_\ell,\omega_\ell))$ *is an admissible sequences determined by a balanced initial condition* $x \in \mathbb{R}^{2N}$.

Proposition (Characterization of the paths to synchronization)**.** *An admissible sequences* $((\alpha_0,\omega_0),(\alpha_1,\omega_1),\dots,(\alpha_\ell,\omega_\ell))$, *with that the corresponding sequence of jump sites and signs* $((n_1,q_1),(n_2,q_2),\dots,(n_\ell,q_\ell))$ *as defined in* (2.25), *is realizable if there exists a balance initial condition* $x \in \mathbb{R}^{2N}$ *such that* $\alpha_x = \alpha_0$, $\omega_x = \omega_0$, *and such that*

a) $|x_{N+m_1} - x_{n_1}| < |x_{N+m_2} - x_{n_2}| < \cdots < x_{N+m_1\ell} - x_{n_\ell}|$, *and*

b) $q_\tau = sign(x_{N+m_\tau} - x_{n_\tau})$ *for each* $1 \le \tau \le \ell$.

The statement is a direct consequence of the definition.

Notice that all the possible orderings of the differences $\{\Delta := \{\Delta_{n,m} := x_{N+m} - x_n \, 1 \le n,m \le N\}$ defined by an initial condition $x \in \mathbb{R}^{2N}$, are not necessarily compatible with a balanced initial condition. If it is assumed that the dynamics towards synchronization is completely determined by this ordering as in the balanced case, a transition diagram with vertices in the set $\Phi_{N,N}$ with maximal paths starting at the couples (α,ω) (codifying the disconnected subnetwork), and ending at the couple (**1**, **N**) (codifying the complete bipartite graph $K_{N,N}$), is obtained. This digraph contains all the paths towards synchronization starting at balanced initial conditions, as well as some paths which are not compatible with any balanced initial condition.

For instance, in $N = 2$, there are 20 realizable possible orderings $\{\Delta_{n,m} : 1 \le n,m \le N\}$, written in Table 2.4, defining 20 paths towards synchronization represented in the transition diagram of Figure 2.19. Nevertheless, there are 4 orderings, and therefore 4 paths towards synchronization, which are incompatible with a balanced initial condition. Each one of the functions α,ω, are codified by a two-digit string. There are six starting configurations, underlined in the diagram, all of them coding the disconnected network. The ending vertex, (11,22), is the couple codifying the complete bipartite graph $K_{2,2}$. In red it is indicated the starting couples which are incompatible with a balanced initial condition. In this case, by erasing the elements in red color, the transition diagram codifying all the paths towards synchronization for balanced initial conditions is obtained.

In Figure 2.18, the coordinate arrangements that are incompatible with a balanced initial conditions are shown. In (a), for $x_1 < x_2 < x_3 < x_4$ and, in (b), for $x_3 < x_4 < x_1 < x_2$ are depicted. In general, there are 2 arrangements of initial conditions, $x_1 < \cdots < x_N < x_{N+1} < \cdots < x_{2N}$ and $x_{N+1} < \cdots < x_{2N} < x_1 < \cdots < x_N$, which are incompatible with a balanced initial condition. These arrangements define maximal paths starting at vertices (**1**, **0**) and (**N+1**, **N**), which for the case $N = 2$, that is for

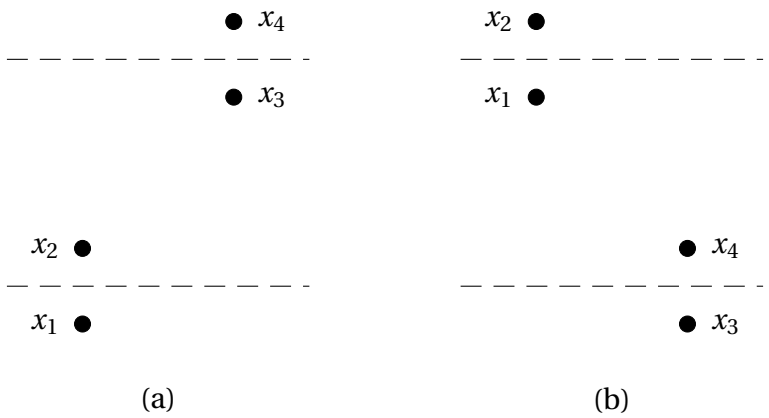

Figure 2.18 – Arrangements incompatible with a balanced initial conditions in $\mathbb{R}^4$. Of all the arrays of 4 components $(x_1, x_2, x_3, x_4) \in \mathbb{R}^4$ that can be generated that satisfy $x_1 < x_2$ and $x_3 < x_4$, there are two arrays that cannot be generated by balanced initial conditions. In (a), the case in which $x_1 < x_2 < x_3 < x_4$ is shown. In (b)m the case $x_3 < x_4 < x_1 < x_2$ is shown. It can be observed that the average of the two parts can not be the same.

$L(M_{K_{2,2}})$ transition diagram, is indicated in red in the following Figure 2.19.

Coordinates	Differences	Signs
$x_1 < x_2 < x_3 < x_4$	$\lvert\Delta_{2,1}\rvert < \lvert\Delta_{2,2}\rvert < \lvert\Delta_{1,1}\rvert < \lvert\Delta_{1,2}\rvert$	$(+1,+1,+1,+1)$
	$\lvert\Delta_{2,1}\rvert < \lvert\Delta_{1,1}\rvert < \lvert\Delta_{2,2}\rvert < \lvert\Delta_{1,2}\rvert$	$(+1,+1,+1,+1)$
$x_1 < x_3 < x_2 < x_4$	$\lvert\Delta_{2,1}\rvert < \lvert\Delta_{2,2}\rvert < \lvert\Delta_{1,1}\rvert < \lvert\Delta_{1,2}\rvert$	$(-1,+1,+1,+1)$
	$\lvert\Delta_{2,2}\rvert < \lvert\Delta_{2,1}\rvert < \lvert\Delta_{1,1}\rvert < \lvert\Delta_{1,2}\rvert$	$(+1,-1,+1,+1)$
	$\lvert\Delta_{2,2}\rvert < \lvert\Delta_{1,1}\rvert < \lvert\Delta_{2,1}\rvert < \lvert\Delta_{1,2}\rvert$	$(+1,+1,-1,+1)$
	$\lvert\Delta_{2,1}\rvert < \lvert\Delta_{1,1}\rvert < \lvert\Delta_{2,2}\rvert < \lvert\Delta_{1,2}\rvert$	$(-1,+1,+1,+1)$
	$\lvert\Delta_{1,1}\rvert < \lvert\Delta_{2,1}\rvert < \lvert\Delta_{2,2}\rvert < \lvert\Delta_{1,2}\rvert$	$(+1,-1,+1,+1)$
	$\lvert\Delta_{1,1}\rvert < \lvert\Delta_{2,2}\rvert < \lvert\Delta_{2,1}\rvert < \lvert\Delta_{1,2}\rvert$	$(+1,+1,-1,+1)$
$x_1 < x_3 < x_4 < x_2$	$\lvert\Delta_{1,1}\rvert < \lvert\Delta_{2,2}\rvert < \lvert\Delta_{1,2}\rvert < \lvert\Delta_{2,1}\rvert$	$(+1,-1,+1,-1)$
	$\lvert\Delta_{2,2}\rvert < \lvert\Delta_{1,1}\rvert < \lvert\Delta_{2,1}\rvert < \lvert\Delta_{1,2}\rvert$	$(-1,+1,-1,+1)$
$x_3 < x_4 < x_1 < x_2$	$\lvert\Delta_{1,2}\rvert < \lvert\Delta_{1,1}\rvert < \lvert\Delta_{2,2}\rvert < \lvert\Delta_{2,1}\rvert$	$(-1,-1,-1,-1)$
	$\lvert\Delta_{1,2}\rvert < \lvert\Delta_{2,2}\rvert < \lvert\Delta_{1,1}\rvert < \lvert\Delta_{2,1}\rvert$	$(-1,-1,-1,-1)$
$x_3 < x_1 < x_4 < x_2$	$\lvert\Delta_{1,2}\rvert < \lvert\Delta_{1,1}\rvert < \lvert\Delta_{2,2}\rvert < \lvert\Delta_{2,1}\rvert$	$(+1,-1,-1,-1)$
	$\lvert\Delta_{1,1}\rvert < \lvert\Delta_{1,2}\rvert < \lvert\Delta_{2,2}\rvert < \lvert\Delta_{2,1}\rvert$	$(-1,+1,-1,-1)$
	$\lvert\Delta_{1,1}\rvert < \lvert\Delta_{2,2}\rvert < \lvert\Delta_{1,2}\rvert < \lvert\Delta_{2,1}\rvert$	$(-1,-1,+1,-1)$
	$\lvert\Delta_{1,2}\rvert < \lvert\Delta_{2,2}\rvert < \lvert\Delta_{1,1}\rvert < \lvert\Delta_{2,1}\rvert$	$(+1,-1,-1,-1)$
	$\lvert\Delta_{2,2}\rvert < \lvert\Delta_{1,2}\rvert < \lvert\Delta_{1,1}\rvert < \lvert\Delta_{2,1}\rvert$	$(-1,+1,-1,-1)$
	$\lvert\Delta_{2,2}\rvert < \lvert\Delta_{1,1}\rvert < \lvert\Delta_{1,2}\rvert < \lvert\Delta_{2,1}\rvert$	$(-1,-1,+1,-1)$
$x_3 < x_1 < x_2 < x_4$	$\lvert\Delta_{1,1}\rvert < \lvert\Delta_{2,2}\rvert < \lvert\Delta_{1,2}\rvert < \lvert\Delta_{2,1}\rvert$	$(-1,+1,+1,+1)$
	$\lvert\Delta_{2,2}\rvert < \lvert\Delta_{1,1}\rvert < \lvert\Delta_{2,1}\rvert < \lvert\Delta_{1,2}\rvert$	$(+1,-1,-1,+1)$

Table 2.4 – Increment orders at opposite parties, and corresponding signs for typical initial conditions in $\mathbb{R}^4$. The twenty different orderings of the differences between coordinates at opposite parties, and corresponding signs, for a typical initial conditions in $\mathbb{R}^4$.

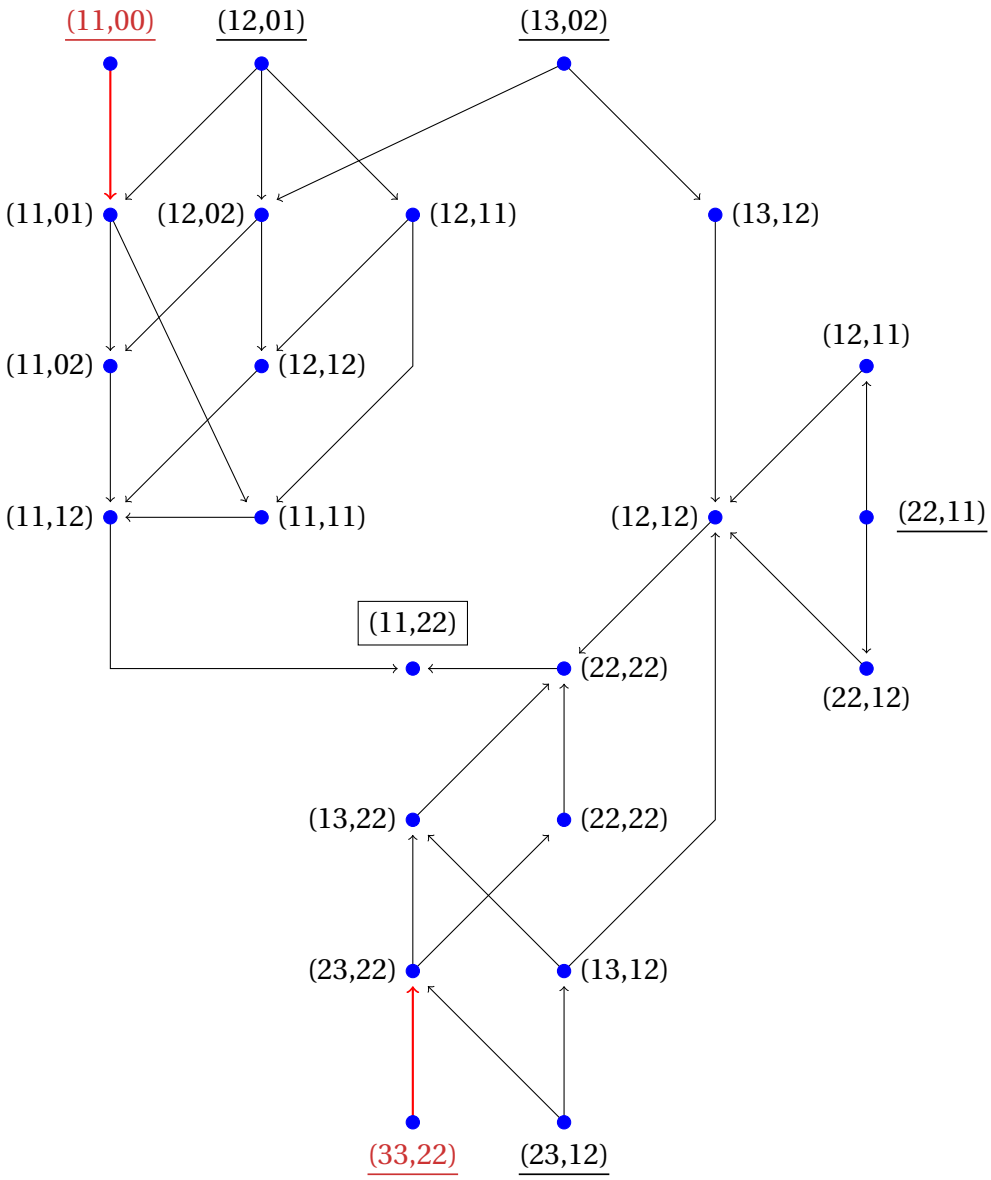

Figure 2.19 – Transition diagram of $L(M_{K_{2,2}})$ with labels assigned by the corresponding increasing functions is shown. This is composed of 23 vertices and 31 edges. The vertices where a path can start (so that it is as long as possible), are underlined: $(22,11),(12,01),(13,02),(23,12),(11,00),(33,22)$. The vertices that are in red are those that correspond to initial conditions that are not balanced. And in the middle, the vertex $(1,1,2,2)$ that corresponds to the complete bipartite graph $K_{2,2}$, is placed. This transition diagram corresponds to the ordered initial conditions $x = (x_1, x_2, x_3, x_4) \in \mathbb{R}^4$ such that $x_1 < x_2$ and $x_3 < x_4$, which are the ones that keep the monotony.

Now, the number of paths towards synchronization in the Laplacian flow over the complete bipartite graph $K_{N,N}$ is estimated.

Theorem (About the number of paths to synchronization)**.** *Consider the system $L(M_{K_{N,N}})$. The number of paths to synchronization associated with balanced, typical, and ordered initial conditions is bounded by the following expression:*

$$(2N-1)! < \sharp\, \textit{Paths towards sync in } L(M_{K_{N,N}}) \leq \left(\binom{2N}{N} - 2\right) \textit{Golomb}(2N). \tag{2.26}$$

Proof. For each one of the arrangements $x_{i_1} < x_{i_2} < \cdots < x_{i_{2N}}$, obtaining by interplacing the first N coordinates with respect to the last N coordinates while maintaining the order inside each group of coordinates. There are, as has been mentioned in the previous Section 2.1, Golomb$(2N)$ different orderings for the differences $x_{i_k} - x_{i_\ell}$. Each one of these orderings give again a path towards synchronization, but in this case, the path does not depend on the differences between coordinates of the same group, that means, first N or last N coordinates. Furthermore, there are two coordinate arrangements which are incompatible with a balanced initial condition, when $x_1 < x_2 < \cdots < x_{2N}$ and when $x_{N+1} < x_{N+2} < \cdots < x_{2N} < x_1 < x_2 < \cdots < x_N$.

On the other hand, a lower bound can be obtained by counting all the orderings of the first differences $x_{i+1} - x_i$ for $1 \leq i \leq 2N-1$. □

Once again, the growth of the number of paths towards synchronization with respect to N defines a complexity function analogous to the topological complexity as a function of time.

Similar to the case presented in Section 2.1, the number of paths towards synchronization of a given length, in this case written as $F_{N,N}(\ell)$, is given by the number of pairs of increasing functions $(\alpha,\omega) \in \Phi_{N,N}$ such that the corresponding parallelopolyminoe has an interior area of $(N+1)^2 - \ell$ units. Hence,

$$F_{N,N}(\ell) := \left| \left\{ (\alpha,\omega) \in \Phi_{N,N} : \sum_{n=1}^{N+1} (U(n) - L(n)) = (N+1)^2 - \ell \right\} \right|. \tag{2.27}$$

Here, $L, U : \{1,\ldots,N+1\} \to \{0,1,\ldots,N+1\}$ are the polyminoe border functions defined from the couple of increasing functions (α,ω) by the Equations (2.23) and (2.22), mentioned before. In the Table 2.5 the numbers that generate the distributions $F_{N,N}(\ell)$ for the first dimensions $2 \leq N \leq 8$ are shown.

For each N and $0 \leq \ell \leq N$, the integer $F_{N,N}(\ell)$ coincides with the ℓ-th term of the sequence of Sloans (it can be found by writing the entry A000712 of the On-line Encyclopedia of Integer Sequences (Sloane 2022), which among other things, counts

N	$F_{N,N}(\ell)$
2	(1,2,5,6,6)
3	(1,2,5,10,16,24,31,36,30,20)
4	(1,2,5,10,20,32,53,78,111,146,187,216,243,240,210,140,70)
5	(1,2,5,10,20,36,61,98,153,228,327,454,611,798,1005,1236,1466,1688,1862,1980, 1971,1850,1540,1120,630,252)
6	(1,2,5,10,20,36,65,106,173,268,409,600,867,1212,1671,2244,2966,3826,4868, 6056,7422,8906,10519,12166,13830,15352,16704,17656,18133,17890,16903, 14966,12306,8988,5670,2772,924)
7	(1,2,5,10,20,36,65,110,181,288,449,680,1013,1474,2107,2958,4088,5558,7450, 9842,12820,16488,20932,26246,32507,39790,48116,57538,67984,79414,91653, 104578,117806,131096,143865,155692,165779,173530,177877,178282,173616, 163632,147855,127092,102060,75432,49434,27720,12012,3432)
8	(1,2,5,10,20,36,65,110,185,296,469,720,1093,1618,2369,3400,4824,6732,9296, 12654,17054,22694,29912,38976,50333,64320,81489,102242,127219, 156850, 191841,232602,279832,333830,395204,464030,540737,625028,716966,815766, 920990,1031168,1145253,1260882,1376172,1487820,1593022,1687242,1766791, 1826112,1860845,1865122,1834995,1765746,1656541,1506540,1320987,1106748, 877470,647592,437118,260832,132132,51480,12870)

Table 2.5 – Number $F_{N,N}(\ell)$ of couples $(\alpha,\omega) \in \Phi_{N,N}$ codifying a ϵ-synchronized sub-networks starting in a path towards synchronization of length ℓ.

the number of couples of integer partitions $P = (p_1 \geq p_2 \geq \cdots \geq p_k)$, $Q = (q_1 \geq q_2 \geq \cdots \geq q_r)$, such that

$$\sum_{i=1}^{k} p_i + \sum_{j=1}^{r} q_j = \ell. \tag{2.28}$$

Indeed, to each couple of integer partitions (P,Q), it can be associated a unique couple $L,U : \{1,2,\ldots,N+1\} \to \{0,1,\ldots,N+1\}$ of upper and lower border functions such that $U(i) = N+1-p_i$ and $L(N+2-j) = q_j$.

Clearly the previous sum presented in Equation (2.28), occurs if and only if the area of the parallelo-polyminoe with border functions L and U is exactly $(N+1)^2 - \ell$.

The correspondence between integer partitions and border functions cannot go further than $\ell = N$, since for $\ell = N+1$ the couple $((N+1),(0))$ of partitions does not define admissible border functions in the considered rectangle.

On the opposite extreme, $F_{N,N}(N^2)$ counts all the parallelo-polyminoes in $\{0,1,\ldots,N+1\} \times \{0,1,\ldots,N+1\}$ composed of $2N+1$ squares. These squares are arranged in a path going from $(0,0)$ to $(N+1,N+1)$, the next square place at the left or on top of the previous one. In Figure 2.20 an example for $N = 4$ is depicted, of this array of squares a path from $(0,0)$ to $(5,5)$ which is made up of 9 squares is shown, which coincides with the notes mentioned above.

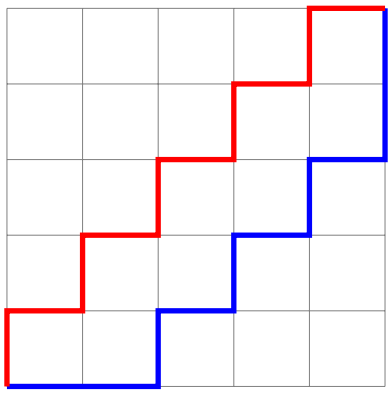

$U = (1,2,3,4,5)$.
$L = (0,0,1,2,3)$.

Figure 2.20 – Example of parallelo-polyminoe in a path from $(0,0)$ to $(5,5)$. Parallelo-polyminoe in a path from $(0,0)$ to $(5,5)$ and the functions U and L that form it are shown. If $N = 4$ is fixed, and it is constructed such that the next square place at the left or on top of the previous one, it is verified that is made up of $2N+1 = 9$ squares.

Each one of these arrangements can therefore be codified into a sequence:

$$(a_1, a_2, \ldots, a_{2N}) \in \{L, T\}^{2N},$$

with exactly N entries equal to T. From this an exact formula can be written.

$$F_{N,N}(N^2) = \binom{2N}{N}. \tag{2.29}$$

Proposition (About the normalized cumulative distribution of path lengths)**.** *Consider the system $L(M_{K_{N,N}})$, and $F_{N,N}(\ell)$ the number of synchronized sequences of length ℓ. The normalized cumulative distribution, $f_{N,N} : [0,1] \to [0,1]$, is given by:*

$$f_{N,N}(x) = \frac{1}{|\Phi_{N,N}|} \sum_{n \leq x \times N^2} F_{N,N}(x), \tag{2.30}$$

where the number $F_{N,N}$ is given by Equation (2.27) and the number $|\Phi_{N,N}|$ was defined in (2.2.1).

In this case, there are numerically computed $f_{N,N}(x)$ for increasing N, and observe how it approaches a limit distribution $x \mapsto \mathrm{f}(x)$ whose density $\varrho(x) := d\ \mathrm{f}(x)/dx$ approaches the curve depicted in Figure 2.21, which means that for N sufficiently large and $\delta > 0$ sufficiently small, the number of paths of length $N^2(x \pm \delta)/2$ is approximatively $\varrho(x)\,\delta$. As in the case of the Laplacian flow applied to the complete graph K_N,

the numerical computation suggests that ϱ is continuous, unimodal, and negatively skewed.

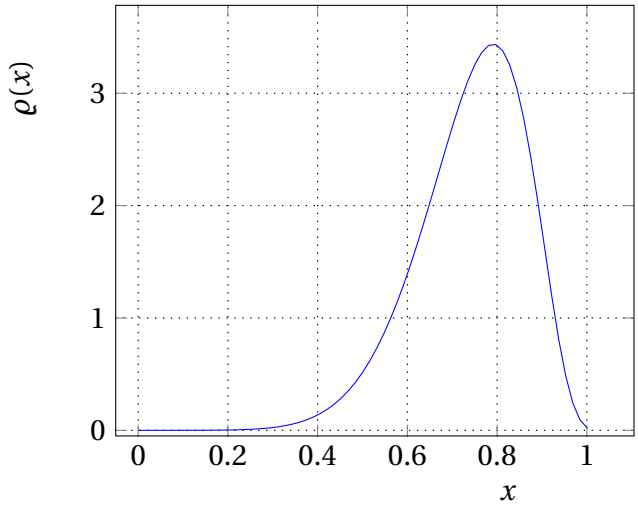

Figure 2.21 – The probability density function $\varrho(x)$ of the asymptotic distribution of the normalized length of a path towards synchronization.

Throughout this section, it is emphasized that in the case of $K_{N,N}$ there is not complete panorama of its paths towards synchronization, since this methodology, and therefore this analysis, is limited to the initial conditions that are balanced, because they are the initial conditions that keep the monotony of the system. In addition, currently there are no results in combinatorics that allow to make calculations for arbitrarily large sizes N. Nevertheless by directly computing these distributions for low dimensions, it is a very fast convergence of the normalized distribution $f_{N,N}$.

Proposition (About the mode and the mean of the normalized cumulative distribution of path lengths)**.** *Consider the system $L(M_{K_{N,N}})$, and $F_{N,N}(\ell)$ the number of synchronized sequences of length ℓ. The number of ϵ-synchronized subnetworks at each level has an unimodal distribution with has a maximum at:*

$$mode_{N,N}(\ell) \approx 0.74118\, N^2. \tag{2.31}$$

And the mean length of these paths being larger than the most frequent length, that is:

$$\langle \ell \rangle_{N,N} > \ mode_{N,N}(\ell). \tag{2.32}$$

Proof. The number of ϵ-synchronized subnetworks at each level has an unimodal distribution with has a maximum at:

$$\begin{aligned} \text{mode}_{N,N}(\ell) &:= \max_{1\leq \ell \leq N^2} F_{N,N}(\ell), \\ &\approx 0.74118\, N^2. \end{aligned}$$

The distribution is negatively skewed, and the mean length of these paths being larger than the most frequent length, as it is shown in the following expression:

$$\begin{aligned} \langle \ell \rangle_{N,N} &:= \frac{\sum_{\ell=1}^{N^2} \ell\, F_{N,N}(\ell)}{T(2N+1, N+1)}, \\ &\approx 0.8125\, N^2, \\ &> \text{mode}_{N,N}(\ell). \end{aligned}$$

□

This distribution is depicted in Figure 2.21. Also, the estimations shown in Equations (2.31) and (2.32) were obtained by using a relatively low ($N = 8$) dimension. As mentioned above, despite this low dimension an accurate qualitative behavior of the asymptotic distribution can be obtained. Which means that it is possible to qualitatively describe a typical synchronization path for the Laplacian of the complete bipartite graph $L(M_{K_{N,N}})$, starting at a random balanced ordered initial condition $x \in \mathbb{R}^{2N}$. For instance, this kind of path towards synchronization would most likely be of the length indicated in Equation (2.31).

As a conclusion of this section, for two pairs of increasing functions to be consecutive on a path towards synchronization then, respective two of them must be equal and the other pair must differ by one unit of area (if it corresponds to the upper function, it must go up, and if it corresponds to the lower function, must go down), in this way a sequence of jump sites and the direction (up or down) are assigned. These realizable sequences are compatible with balanced initial conditions and are completely determined by the differences between the two parties of the coordinates, of which clearly not all correspond to balanced initial conditions. Then the famous problem that computes the number of combinatorially distinct Golomb rulers in dimension $2N$, is necessary to make an adjustment to constrain the paths to synchronization bound (in the case of the Laplacian flow applied to the complete bipartite graph). Furthermore, the number of paths towards synchronization of size ℓ is computationally given for the first eight dimensions, which its probability density function for N sufficiently large is given, and from which the behavior for the mode and the mean path length is obtained. Once again, the coding done through the couples of increasing functions allow to formally describe a part of the space of initial conditions by their transition diagram.

2.2.4 Discussion

In this section it is formally and rigorously analyzed the behavior of the transition diagram of the Laplacian system applied to the complete bipartite graph of dimension $2N$. To achieve this objective, a coding of the subgraphs of $K_{N,N}$ was proposed, which preserves the monotonic dynamics of the system and turns out to be very useful because it transforms it into a combinatorial problem that has been widely studied before.

One of the advantages of using this coding is that it automatically generates the subgraphs that are feasible for a set of initial conditions. Despite of this, it was considered pertinent to give the examples that show that not all the subgraphs of $K_{N,N}$ are feasible. Then, it can be stated that when $N \geq 3$ not all subgraphs of the complete bipartite graph are feasible for some initial condition on the respective space $\mathbb{R}^{2N}$.

Moreover, two key simplifications for the analytical study of the transition diagram of $L(M_{K_{N,N}})$ are made. The first, defining the coding of the subgraphs that are formed from initial conditions, for whose two groups of coordinates are in strictly increasing order, such that, the set of associated ϵ-synchronized subnetworks have a relation with the set of the couples of increasing functions. This simplification allows to focus the attention on the diversity of states generated by considering a single symmetry of the complete bipartite graph. On the other hand, the second simplification made in this section is: balanced initial conditions in the space $\mathbb{R}^{2N}$ are considered (that is, the mean of the two parts of the coordinates are equal). This type of initial conditions represents all the monotonous dynamics of space. As in the previous case, typical initial conditions generate typical paths, which are the ones with the longest lengths, that is, if they start forming the totally disconnected subgraph, then they will reach synchronization in N^2 steps.

By considering these two simplifications in the space of initial conditions, it is possible to establish the rules by which two pairs of increasing functions will be consecutive on a path towards synchronization. That is, respective two of them must be equal and the other pair must differ by one unit of area, if it corresponds to the upper function, it must go up, and if it corresponds to the lower function, must go down, in this way a sequence of jump sites and the direction (up or down) are assigned.

These realizable sequences are compatible with balanced initial conditions, and they are completely determined by the differences between the two parties of the coordinates. Clearly, not all correspond to balanced initial conditions. The problem of counting how many realizable paths there are in each dimension $2N$ is equivalent to counting the number of combinatorially distinct Golomb rulers (but in this case, with an adjustment), which is a famous open problem. Some analytical and numerical bounds have been provided in low dimensions (due to the great memory demand that the computation of the Golomb rulers requires).

To end this discussion, it should be noted that having this coding allow to associate characteristics of the combinatorial objects that have a relevant meaning in terms of the study of the transition diagram, which are listed below.

Combinatorial concept	**Transition diagram property**
Narayana number	Possible states
Combinatorially different Golomb rulers	Number of paths towards synchronization
Number of parallelo-polyminoe with interior area $(N+1)^2-\ell$	Number of synchronized sequences of length ℓ

2.3 The transition diagram of $L(M_{C_N})$

In this section it is formally and rigorously analyzed the behavior of the transition diagram of the Laplacian system applied to the cycle graph of dimension N. This study is organized as follows: to begin with, the two dynamics are shown in the Laplacian system with respect to the dimension. Then, the feasible subgraphs that the cycle graph has been shown. Finally, a bound for the maximum length of the paths that are observed in the associated transition diagram is presented.

As mentioned in the Section 1.1 (specifically in Equations (1.12) and (1.13)), the eigensystem of the Laplacian system applied to the cycle graph $L(M_{C_N})$ (in this Section it is written just as L), has the symmetries inherited by the graph in question, besides there is a difference in the behavior of the system depending on the parity of the dimension N. When the system has an even dimension, it behaves in one way, and when it has an odd dimension, it behaves in another way. This can be inferred when the flow of an initial condition of the space is analyzed, as it is done in the following.

To begin, any initial condition $x \in \mathbb{R}^N$ can be written as a linear combination of the eigenbasis $\mathscr{B}_L = \{v_1, v_2, ..., v_N\}$ of $L(M_{C_N})$, for some coefficients $\alpha_i \in \mathbb{R}$, where $1 \leq i \leq N$, as the following expression:

$$x = \sum_{i=1}^{N} \alpha_i \, |v_i\rangle \, .$$

On the other hand, its flow meets:

$$\begin{aligned} x(t) &= \sum_{i=1}^{N} \alpha_i e^{\lambda_i t} |v_i\rangle, \\ &= \sum_{i=1}^{N-1} \alpha_i e^{\lambda_i t} |v_i\rangle + \alpha_N |v_N\rangle, \\ &= \alpha_N |v_N\rangle + \sum_{i=1}^{\lfloor \frac{N-1}{2} \rfloor} e^{\lambda_i t}(\alpha_i |v_i\rangle + \alpha_{N-i} |v_{N-i}\rangle) \\ &\quad + \alpha_{i^*} e^{\lambda_{i^*} t} |v_{i^*}\rangle. \end{aligned}$$

Where the i^* term only appears when the dimension N is even, and is defined as following:

$$i^* = \frac{N}{2} + 1.$$

Therefore, with this fact, it can be inferred that depending on the parity of the dimension N, the Laplacian system applied to the cycle graph have a different dynamic.

On the other hand, the flow at each coordinate meets:

$$\begin{aligned} x_j(t) &= \alpha_N + \sum_{i=1}^{\lfloor \frac{N-1}{2} \rfloor} e^{\lambda_i t}(\alpha_i v_i^j + \alpha_{N-i} v_{N-i}^j) + \alpha_{i^*} e^{\lambda_{i^*} t} v_{i^*}^j, \\ &= \alpha_N + \sum_{i=1}^{\lfloor \frac{N-1}{2} \rfloor} e^{\lambda_i t} \left(\alpha_i \cos\left(\frac{2\pi j i}{N}\right) + \alpha_{N-i} \cos\left(\frac{2\pi j (N-i)}{N}\right)\right) \\ &\quad + \alpha_{i^*} e^{\lambda_{i^*} t} v_{i^*}^j, \\ &= \alpha_N + \sum_{i=1}^{\lfloor \frac{N-1}{2} \rfloor} e^{\lambda_i t} \cos\left(\frac{2\pi j i}{N}\right)(\alpha_i + \alpha_{N-i}) + \alpha_{i^*} e^{\lambda_{i^*} t} v_{i^*}^j. \end{aligned}$$

And also, by the symmetry of the function $\cos(x)$ and the considered interval $\left(0, \frac{2\pi(N-1)}{N}\right)$, the eigenvectors are equal by couples as the following relation $v_i = v_{N-i}$ for $1 \leq i \leq \lfloor \frac{N-1}{2} \rfloor$. The symmetry of the eigenvalues and the eigenvectors make that the flow of the coordinates also have a symmetric behavior.

One of the most important notes related to the dynamics of the cycle graph is that all its subgraphs are feasible for some initial condition.

Theorem (About the states number in $L(M_{C_N})$ transition diagram)**.** *The number of states number in $L(M_{C_N})$ transition diagram is:*

$$\sharp \textit{ Vertices in the transition diagram of } L(M_{C_N}) = 2^{N-1}. \tag{2.33}$$

Proof. The simplest way to construct an initial condition $x \in \mathbb{R}^N$ that meets the requirements of a given subgraph is: if vertex i is connected to vertex j, then $x_i = x_j$ and make sure that when there is no edge, the vertices are further apart than the corresponding $\epsilon > 0$. □

On the other hand, due to the way in which the eigenvalues and eigenvectors in the spectrum of $L(M_{C_N})$ are defined, the differences of the coordinates are not monotone, then, they are crossings between them. This causes that the flow of the transition diagram is not in a single direction (as it has been observed in the two previous cases, whichever vertex was chosen at the beginning, the next step was closer to the node that represents complete synchronization), that is, there are cycles or returns from low levels to high levels. Also, for this reason, the number of steps towards synchronization often exceeds the total number of edges of C_N which is $N-1$.

As a conclusion of this section, since the Laplacian system applied to the cycle graph does not have a monotone dynamic quickly to find, it was not possible to provide a coding in terms of increasing functions as in the previous cases. However, it was possible to provide the number of possible states, and a lower bound for the depth of the transition diagram. It is hoped that in the future a good coding will be achieved in such a way that it will be possible to describe its transitory dynamics in a combinatorial way.

2.4 The transition diagram of the Kuramoto model

In this section it is formally and rigorously analysed the behavior of the transition diagram of the Kuramoto model applied to the complete graph of dimension N and the complete bipartite graph of dimension $2N$. This study is organized as follows: first, a discussion is made of why and when it is possible to use the same coding in terms of increasing functions from the case of the Laplacian system to the case of the Kuramoto model in the complete graph. Finally, in the same way, it is discussed, and the conditions to use the same coding in terms of pairs of increasing functions from the case of the Laplacian system to the case of the Kuramoto model in the complete bipartite graph are given.

Although the above presented results in Section 2.1 concern the Laplacian flow, they can be applied in a particular region when the Kuramoto flow is considered. In the case of complete graph K_N, the transition diagram obtained from the Laplacian flow describes most of the paths towards synchronizations stating in a small neighborhood around the diagonal. In this place, the same coding of ϵ-synchronized subnetworks defined for the Laplacian flow in Section 2.1.1 can be used, due to the order of the coordinates is preserved by the Kuramoto flow, and therefore the increasing functions in Φ_N are suitable for the coding. Indeed, according to Equation (1.25), where is the Kuramoto model applied on a network with a coupling strength σ, then for a couple

of index $1 \leq n, m \leq N$:

$$\begin{aligned} \frac{d(x_n - x_m)}{dt} &= \sigma \left(\sum_{j=1}^{N} \sin\big(x_j - x_n\big) - \sin\big(x_j - x_m\big) \right), \\ &= \sigma\, r\, (\sin(\Theta - x_n) - \sin(\Theta - x_m)), \end{aligned}$$

where $r\, e^{i\Theta} = \left(\sum_{j=1}^{N} \cos\big(x_j\big)\right) + i \left(\sum_{j=1}^{N} \sin\big(x_j\big)\right)$, by expanding the Equation (1.22). Hence, whenever $x_n = x_m$,

$$\frac{d}{dt}(x_n - x_m) = 0,$$

which implies that the order in the coordinates is preserved under the flow since no crossing of coordinates is possible.

Assume that:

$$\max\{|x_n - \bar{x}| : 1 \leq n \leq N\} < \frac{\pi}{4},$$

where $\bar{x} = \sum_{n=1}^{N} x_n(0)$.

In this case:

$$|\Theta - \bar{x}| \leq \frac{\pi}{4} \quad \text{and} \quad \frac{d}{dt}(x_n - x_m) = 0,$$

if and only if $x_m = x_n$.

Furthermore, in this case, the sign of $(\sin(\Theta - x_n) - \sin(\Theta - x_m))$ is the same as the sign of $(x_m - x_n)$, and therefore $|x_n - x_m|$ decreases monotonously for all initial conditions $x \in \mathbb{R}^N$.

Some numerical calculations verify that the transition diagram defined for the Laplacian system applied in the complete graph K_N, is respected by the Kuramoto flow if one considers $\epsilon > 0$ sufficiently small with respect to $\pi/4$ and initial conditions $x \in (S^1)^{|V|}$ such that $|x_n - \bar{x}| < \pi/4$ for all $1 \leq n \leq N$.

The Table is a summary about the applicability of the Laplacian system to the Kuramoto model in K_N.

On the other hand, for the case of the complete bipartite graph $K_{N,N}$, the order of the coordinates at each of the two parts is preserved by the Kuramoto flow. For this, it can be proceed as in an analogous way, which was exposed before, that is, to explore

Laplacian system	**Kuramoto model**
Monotonical behavior	
All space $\mathbb{R}^N$	$\max\|x_n - \Theta\| < \pi/2$
ϵ dependency	
No	Yes
Number of possible states	
Catalan number	Catalan number
Number of paths towards synchronization	
Golomb$^*(N)$	$\geq$ Golomb$^*(N)$
Longest path towards synchronization	
$\binom{N}{2}$	$\geq \binom{N}{2}$

Table 2.6 – Applicability to the Kuramoto model in K_N.

the behavior between each couple $1 \leq n, m \leq N$ of coordinates, and obtain:

$$\begin{aligned} \frac{d(x_n - x_m)}{dt} &= \sigma\, r_2 \left(\sin(\Theta_2 - x_n) - \sin(\Theta_2 - x_m)\right), \\ \frac{d(x_{N+n} - x_{N+m})}{dt} &= \sigma\, r_1 \left(\sin(\Theta_1 - x_n) - \sin(\Theta_1 - x_m)\right), \end{aligned}$$

in this case, there is: $r_1\, e^{i\Theta_1} = \left(\sum_{j=1}^N \cos(x_j)\right) + i\left(\sum_{j=1}^N \sin(x_j)\right)$ and similarity, $r_2\, e^{i\Theta_2} = \left(\sum_{j=1}^N \cos(x_j)\right) + i\left(\sum_{j=1}^N \sin(x_j)\right)$.

From this it follows that if $x_n = x_m$ then:

$$\frac{d}{dt}(x_n - x_m) = 0,$$

and similarly for $x_{N+n} - x_{N+m}$,

$$\frac{d}{dt}(x_{N+n} - x_{N+m}) = 0.$$

Therefore the order in the coordinates at each part is preserved under the flow, this fact allows to use the coding of ϵ-synchronized subnetworks defined for the Laplacian flow applied on the complete bipartite graph $K_{N,N}$, that are defined before.

As there is mentioned Section 2.2, the transition diagram defined for the Laplacian

flow over the complete bipartite graph $K_{N,N}$, describes only the paths towards synchronization corresponding to balanced initial conditions. In Figure 2.19 there are marked in red the ϵ-synchronized subnetworks incompatible with balanced initial conditions. The complete transition diagram, which contains those subnetworks, admits non-monotonous paths. Furthermore, for unbalanced initial conditions $x \in \mathbb{R}^{2N}$, the order in the differences between coordinates is not preserved by the flow.

As a conclusion of this section, it is possible to use the two codes that were used in the case of the Laplacian system to apply them in the study of the transitory dynamics of the Kuramoto model, when certain conditions are considered. In the case of the complete graph, when initial conditions close to the diagonal are considered. In the case of the complete bipartite graph, when the initial conditions are balanced (that is, the same conditions that are considered for the linear case). The fact that the codes can be reused allows to think of more general conditions to use them, for example, for the complete graph it would be enough that the system that synchronizes is monotonic, and its differences are monotonic. This generalization is expected to be made formally in future works.

3 Exploratory study of the transient state of systems that synchronize

Contents

3.1 Exploring the Laplacian system

This section shows the exploratory studies that were carried out from computational simulations for a set of 10^6 random initial conditions on $(0, N^2)^N$, in the Laplacian system over: the cycle graph and the family of ring lattices. The aim is to find the patterns that meet the initial conditions on their way towards synchronization. In the two graph types that are analysed, the same initial condition is evaluated to observe the different behavior it has when the topology of the graph changes. In addition, for each of them, the number of feasible subgraphs, the length of the longest path, the number of paths and the distribution of path lengths are explored, all in a set of random initial conditions.

3.1.1 The Laplacian system of M_{C_N}

In this section the quantitative properties of the Laplacian system on the cycle graph of dimension N are seen, which were calculated computationally. Specifically, the behavior of this system is investigated when the dimension grows. These calculations were made for a set of 10^6 random initial conditions in $(0, N^2)^N$ as was said in Section **??**. To begin with, the trajectory under the Laplacian flow, starting with a fixed initial condition, will be evaluated, that will be used throughout Section 3.1 in order to observe the differences when the topology of the graph is changed. Then, a comparison of the longest path to synchronization found from computational calculations

and the number of subgraphs that C_N has is presented. Next, a formula of the number of feasible subgraphs of C_N is presented. In addition, a case in dimension 6 in which a subgraph does not belong to any path starting from the totally disconnected graph despite being feasible. Also, the transition diagram of the Laplacian system applied to the cycle graph of dimension 6 is shown. Then, the behavior of the number of different paths to synchronization that were found is presented. Finally, two path lengths normalized distributions each separated by parity of path lengths, for a set of random initial conditions are shown, with the purpose of observing the length of typical paths.

Just as it was presented in the two previous sections, the behavior of the initial condition

$$x = (2.64958, 1.9171, 1.86587, -0.861234, -0.41248, 0.5232),$$

in the cycle graph C_6 is shown in Figure 3.1. It can be seen that all of its coordinates approaches monotonically (increasingly or decreasingly) to $\bar{x} = 0.947006$, which is the average of the coordinates of x. Furthermore, in this case, it is observed that the convergence time is longer than for when x is considered over the complete graph and the complete bipartite graph (it can be seen that the convergence time is more than double than in the other cases).

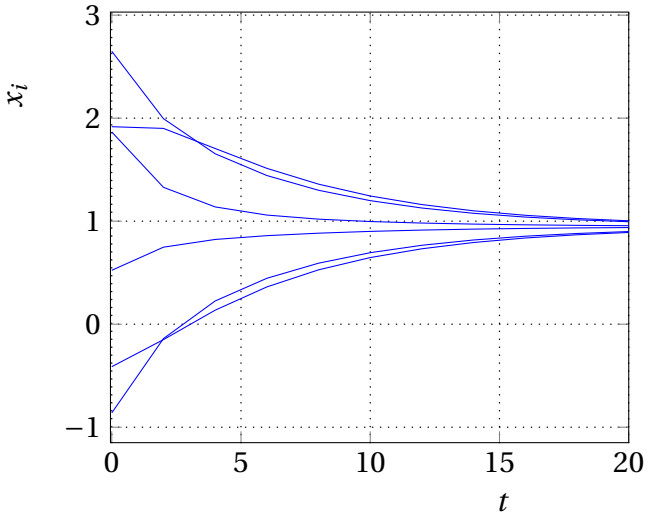

Figure 3.1 – The Laplacian flow in the cycle graph of dimension 6 C_6 applied on a fixed initial condition $x \in \mathbb{R}^6$. Each one of the six lines represents the projection of each one of the coordinates x_i of x. It is observed that all of them reach the same value asymptotically monotonically, and they cross each other.

Besides, as in the case presented in Section **??**, due to the crossings that occur in the

flow of the coordinates that we observe in Figure 3.1, it can be thought that the maximum number of steps to reach the synchronization exceed the number of edges of the cycle graph of dimension N (which is $N-1$). Thereby, computational calculations were performed to observe the behavior of the longest path in the Laplacian system applied to M_{C_N}, as is shown in Figure 3.2. The blue line represents the maximum number of steps towards synchronization in the Laplacian system in the cycle graph C_N. The red line represents the number of edges that C_N has. It is observed that the maximum number of steps to reach the synchronization, approximately triples the dimension in which it is found.

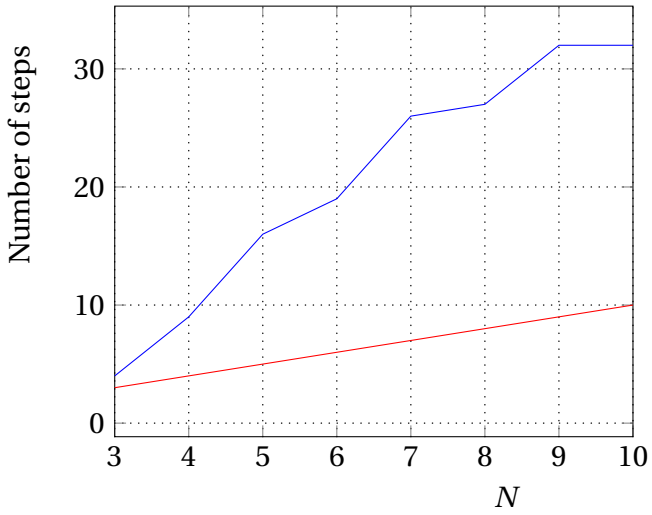

Figure 3.2 – Depth of $L(M_{C_N})$ transition diagram. The blue line represents the maximum number of steps towards synchronization in the Laplacian system of the cycle graph of dimension N. The red line represents the number of edges that the cycle graph of dimension N has.

On the side of the feasible subgraphs of the cycle graph of dimension N, according to the simulations carried out, it was found that all of them are feasible. Here, the number of possible states in the transition diagram of de Laplacian system applied to M_{C_N} was exactly found. In Section 2.3 there is a way to construct an initial condition for each subgraph of C_N. Below is the formula with which the number of possible states in the transition diagram of the Laplacian system applied to the cycle graph is obtained.

$$\text{Number of vertices of } L(M_{C_N}) \text{ transition diagram} = 2^N.$$

As an observation, the corresponding cases of C_2 and C_3, coincides with the complete graphs K_2 and K_3 respectively. The behaviors that are strictly corresponding to the cycle graph can be observed for dimensions larger than 4. That's why, evaluating

initial conditions in a 4-dimensional hypercube of sides $(0,23)$, the trajectory that an initial condition takes, only a maximum of two turns remain in the directed cycles (that is, there are no periodic points in this dynamics).

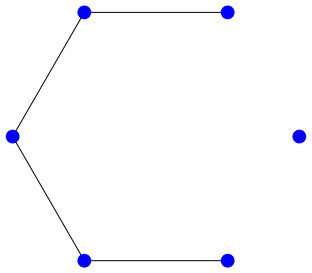

Figure 3.3 – Subgraph of C_6 that, despite being feasible due to an initial condition, cannot be reached from the totally disconnected graph, due to the symmetries presented by the Laplacian spectrum applied to the cycle of dimension 6.

Focusing on the behavior of the path step by step, that is, when at each step it is only added one edge to a subgraph, in the specific case of dimension 6, the transition diagram is shown in Figure 3.4. Vertex 1 represents the totally disconnected graph with 6 vertices and vertex number 64 represents C_6. When the initial conditions start at vertex 1, it is possible that they oscillate at the first and second levels, but eventually they reach vertex 1 and follow a path to vertex 64. Specifically, the subgraphs that do not pass from vertex 1 to some vertices in level 5 in the transition diagram of $M(L_{C_6})$ are all the symmetries of Figure 3.3. This is because the behavior of the flow coordinates inherits the symmetry of the cycle graph, so this configuration cannot be reached from vertex 1.

Next, in the Figure 3.5, some computational calculations for random initial conditions in $(0,N^2)^N \subset \mathbb{R}^N$ of the number of different paths towards synchronization in the Laplacian of the cycle graph are shown. It is observed that although the number of possible states in the transition diagram of M_{C_N} is small, the number of paths they generate grows considerably faster.

The path length distribution of the Laplacian system of the cycle graph was also analyzed for a set of random initial conditions. It was noted that there was a different behavior, depending on whether the dimension N considered is even or odd. Furthermore, it came to light that there is also a difference in paths having even or odd lengths.

On the one hand, in Figure 3.6, an example for the behavior of path length distributions when the dimension is odd is depicted, particularly when $N = 9$. Represented with a blue line, the behavior of paths with odd length is shown, and represented with a red line, the behavior of paths with even length. It is observed that there is a not so biased tendency of the paths to prefer even lengths, because the area associated

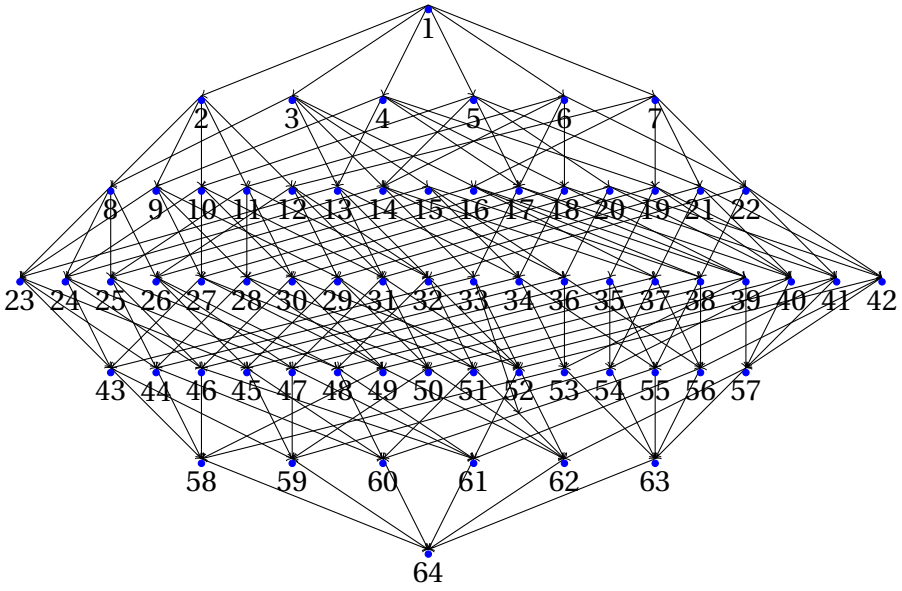

Figure 3.4 – Transition diagram of $L(M_{C_6})$ with labels assigned by the number of the subgraph that lexicographically corresponds to it, is shown. This is composed of 64 vertices and 192 edges. At the top, the vertex 1 corresponds to the totally disconnected graph of dimension 6, and at the bottom, the vertex 64 corresponds to the cycle graph of dimension 6, C_6.

with this curve is notably larger than that associated with the blue curve. On the other hand, in Figure 3.7, an example of the behavior of these path length distributions is presented when the dimension is even, in particular when $N = 10$. In the figure, the blue line represents the behavior paths with odd length and the red line the paths with even length. In this case, it is observed that it is more likely that the paths have odd length, because the associated curve has a larger area.

To end, as a conclusion of this section, due to the non-monotonicity of differences in the Laplacian flow applied to the cycle graph of dimension N, there is a lower bound for the maximum length of the paths to synchronization in its transition diagram, which is the number of edges that C_N has, and computer simulations suggest that the longest path triples it. On the other hand, due to the non-diversity of subgraphs, it is possible for all of them to be feasible by initial conditions, which means that the number of states in the transition diagram is equal to the number of subgraphs of C_N. Despite this, it is not possible to get from the fully disconnected graph to all other subgraphs by a realizable path, and an example is presented. On the other hand, it was observed that the growth of the number of different paths that can be found in this transition diagram grows by means of a rule that seems greater than exponential. Finally, the path length distributions provide an idea of what to expect from the behavior of a random initial condition, which should be treated carefully when ϵ is varied,

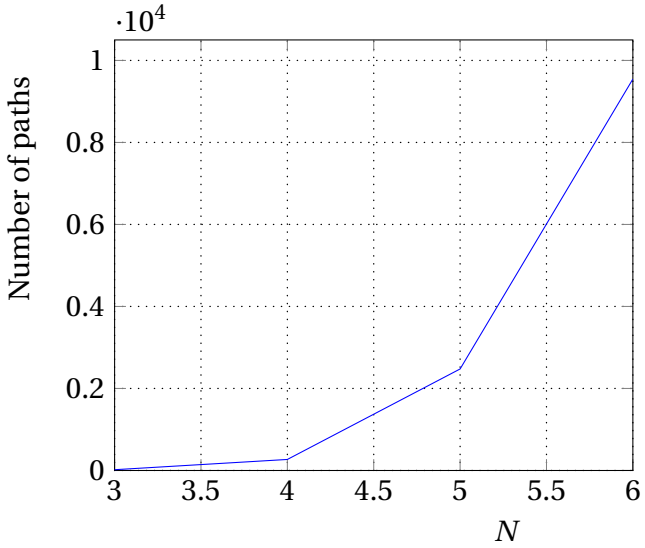

Figure 3.5 – Number of paths towards synchronization in $L(M_{C_N})$. The blue line represents the number of paths towards synchronization in the Laplacian system of the cycle graph of dimension N.

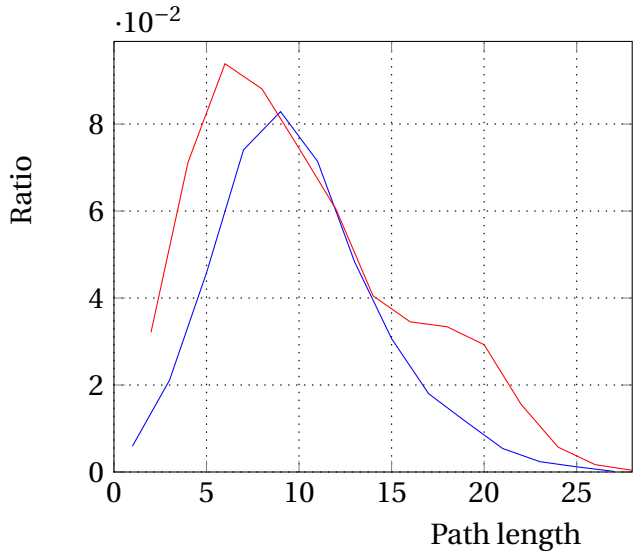

Figure 3.6 – Path length distribution of $L(M_{C_N})$, odd dimension. The blue line represents the normalized path odd length distribution of Laplacian system of the cycle graph of dimension $N = 9$ and red line the normalized path even length distribution in the same dimension, for a set of random initial conditions.

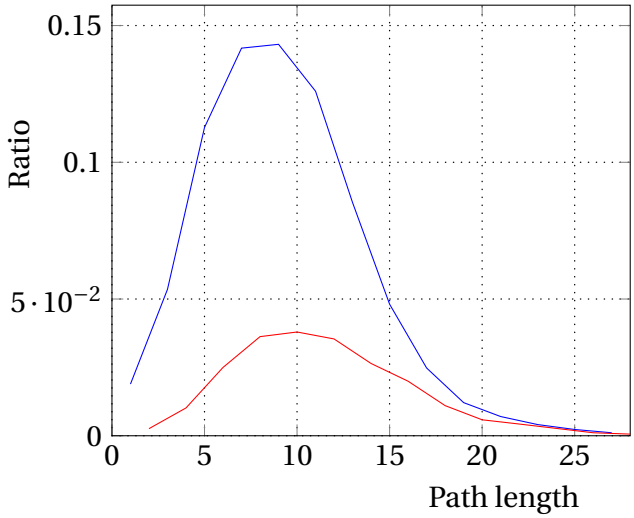

Figure 3.7 – Path length distribution of $L(M_{C_N})$, even dimension. The blue line represents the normalized path odd length distribution of Laplacian system of the cycle graph of dimension $N = 10$ and red line the normalized path even length distribution in the same dimension, for a set of random initial conditions.

because by making this threshold smaller, then the average of the typical length grows. In this case, it was found that there is a difference in the distributions depending on the parity of the dimension and the parity of the length of the paths. The observations made in this section are the basis for the future formalization of the results presented in Section 2.3 with respect to the transient state behavior of the Laplacian system over the cycle graph of dimension N.

3.1.2 The Laplacian system of $M_{C(N,k)}$

In this section the quantitative properties of the Laplacian system on the ring lattice family $C(N,k)$ are seen, which were calculated computationally. Specifically, the behavior of this system is investigated when the dimension grows. These calculations were made for a set of 10^6 random initial conditions in $(0,N^2)^N$ as was said in Section **??**. To begin with, the trajectory under the Laplacian flow, starting with a fixed initial condition, will be evaluated, to observe the differences when the topology of the graph is changed. An estimate of the number of unfeasible subgraphs when $k = 2$ is then presented and a comparison with the subgraphs of $C(N,2)$. Then, a comparison of the longest path to synchronization found from computational calculations when $k = 2$ and $k = 3$ is presented. Finally, four path lengths normalized distributions, separated by path lengths parity and dimensions parity when $k = 2$, and four path lengths normalized distributions when $k = 3$ are shown, for a set of random initial

conditions, with the purpose of observing the length of typical paths.

Now, the behavior of the initial condition

$$x = (2.64958, 1.9171, 1.86587, -0.861234, -0.41248, 0.5232),$$

that has been analyzed throughout this chapter is observed in the ring lattice $C(6,2)$. In Figure 3.8, it can be seen that all of its coordinates approach monotonically (increasingly or decreasingly) to $\bar{x} = 0.947006$, which is the average of the coordinates of x. Furthermore, no crossings in the trajectories towards the asymptotic are observed. It seems that the more connected the principal graph is, the fewer crossings are found in the flow of coordinates and also, its convergence is faster.

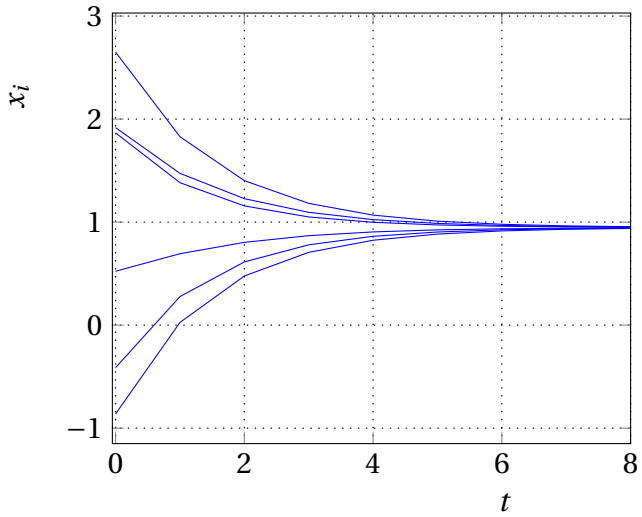

Figure 3.8 – The Laplacian flow in the ring lattice of dimension 6 $C(6,2)$ applied on a fixed initial condition $x \in \mathbb{R}^6$. Each one of the six lines represents the projection of each one of the coordinates x_i of x. It is observed that all of them reach the same value asymptotically monotonically, and they do not cross each other.

This case is interesting because it said how the family of ring lattices behaves and what happens when the connectivity between the vertices increases, that is, how is the transition from being in a graph with a very low density of edges (as is C_N) to be in a graph with the maximum edge density (that is, K_N).

Below is an estimate of the number of unfeasible subgraphs of the ring lattice when $k = 2$, based on the presence of fork graphs. Note that for each vertex of the ring lattice $C(N,2)$, there are 4 different ways to make forks. Enlisting the edges of the outer cycle

of the ring from 1 to N, clockwise, and the inner ones of $N+1$ to $2N$, clockwise forming the triangle $1 \rightarrow 2 \rightarrow N+1$, for $N > 6$, the 4 forks that are formed in each vertex are:

$$i, i+N, Mod[i-1,N,1], \quad Mod[i+1,N,1], Mod[i-1,N,1]+N$$

$$i, Mod[i+N-2,N,1]+N, Mod[i-1,N,1], \quad Mod[i+N-2,N,1], Mod[i-1,N,1]+N$$

$$i, i+N, Mod[i+N-2,N,1]+N, \quad Mod[i+1,N,1]$$

$$i+N, Mod[i+N-2,N,1]+N, Mod[i-1,N,1], \quad Mod[i+N-2,N,1]$$

for $1 \leq i \leq N$. Where on the left side, the edges that make up the fork are written, and on the right side, the edges that should not appear in the subgraph are written. The $Mod[m,n,d]$ gives the remainder on division of m by n uses an offset d. As already stated, when a subgraph does not contain a fork (or a hole), then it is feasible by an initial condition, then, calculating this number allows to give an upper bound on the number of unfeasible graphs. In Figure 3.9, a representation of the number of unfeasible subgraphs of $C(N,2)$ is presented with a blue line, which was estimated using fork containment, and in a red line, the total number of subgraphs of $C(N,2)$, the difference between these two lines would be the total of feasible subgraphs.

Regarding the length of the longest path found in the ring lattice family $C(N,k)$, computational calculations were made for $k = 2$ and $k = 3$, which are presented in Figure 3.10. The blue line represents the maximum number of steps towards synchronization when $k = 2$, and the red line when $k = 3$. Since $C(N,3)$ has more edges than $C(N,2)$, then it is natural to think that its paths towards synchronization will be longer. But, when $N = 7$, it can be observed which is less. Note that $C(7,3) = K_7$, then, its longest path is exactly 21, and $C(7,2)$ is a sufficiently disconnected graph that there are internal cycles in its transition diagram. Then, at that $N = 7$ a difference is observed.

Then, the path length distribution of the transition diagram over the Laplacian system of the ring lattice $C(N,2)$ and $C(N,3)$ were also analyzed for a set of random initial conditions. It was noted that there was a different behavior, depending on whether the dimension N considered is even or odd. For the first case, for the dimensions N that were analyzed, as the behavior in C_N, there is a difference when the paths have even and odd lengths. In the second case, for the analyzed dimensions N, no difference that depends on the path length parity is seen. This behavior is associated with the fact that the density of edges in $C(N,3)$ (for the analyzed dimensions), is large enough to resemble the behavior of K_N or $K_{N,N}$. Contrary to $C(N,2)$, whose behavior (for the analyzed dimensions), is more similar to C_N.

On the one hand, in Figure 3.11, two examples for the behavior of path length distri-

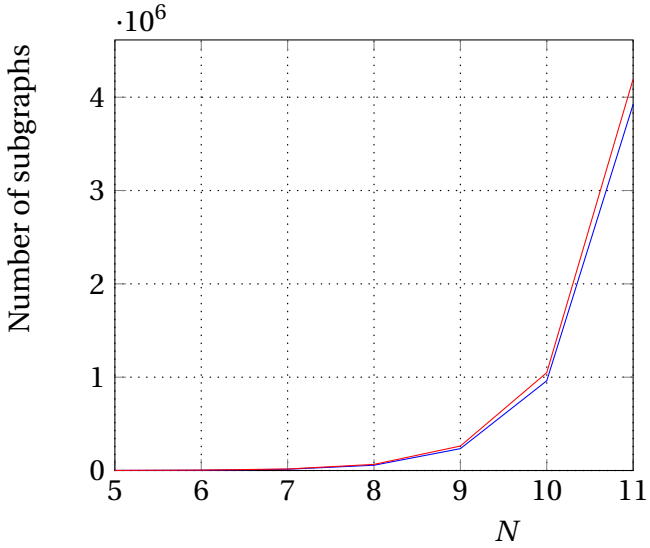

Figure 3.9 – Number of unfeasible subgraphs by initial conditions in $C(N,2)$ and number of subgraphs of $C(N,2)$. The blue line represents the number of unfeasible subgraphs of $C(N,2)$ and the red line represents the number of subgraphs of $C(N,2)$, the difference between them is the number of feasible subgraphs.

butions when the dimension is odd are depicted. Particularly when $N = 9$, they are represented with blue lines. When $N = 11$, they represented with red lines. In both cases, one line represents the paths that have an even length, and the other the paths that have an odd length. In addition, the curves with the most area in each case are those associated with odd lengths of the paths.

On the other hand, in Figure 3.12, two examples of the behavior of path length distributions when the dimension is even are depicted. When $N = 10$, they are represented with blue lines. When $N = 12$, they are represented with red lines. In both cases, one line represents the paths that have an even length and the other the paths that have an odd length. In addition, the curves with the most area in each case are those associated with even lengths of the paths.

In contrast, the distributions presented for odd dimensions in Figure 3.11 are more symmetric than those presented for even dimensions in Figure 3.12, which has a bias to the left. That is why they were presented in different figures.

Now, for the case of the ring lattice $C(N,3)$, its path length distributions were obtained for a set of random initial conditions, with the aim of give an idea of the behavior of the conditions initials when they are evaluated in the Laplacian system on this type of graph. Specifically, they are shown in Figure 3.13 for $N = 8,9,10,11$. The blue line

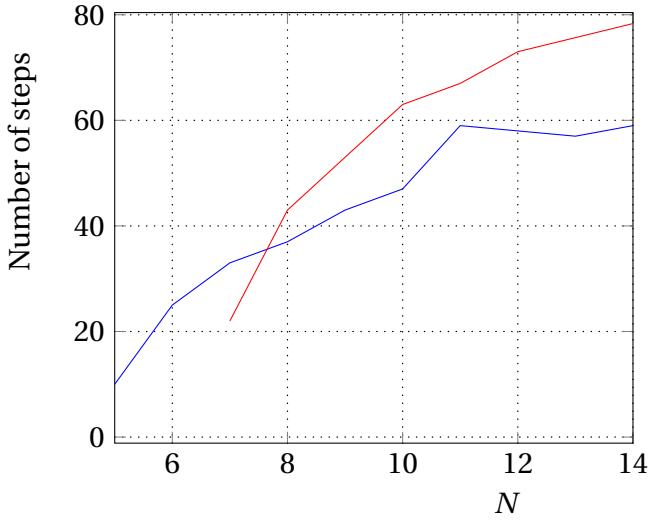

Figure 3.10 – Depth of $L(M_{C(N,k)})$ transition diagram. The blue line represents the maximum number of steps towards synchronization in the transition diagram over the Laplacian system of the ring lattice $C(N,2)$ and the red line represents the maximum number of steps towards synchronization in the transition diagram over the Laplacian system of the ring lattice $C(N,3)$.

represents the normalized path length distribution of Laplacian system of the ring lattice $C(8,3)$, red line is for $C(9,3)$, green line is for $C(10,3)$ and yellow line is for $C(11,3)$. In the four cases, no change in the distributions is observed depending on the parity of the length of the paths, that is why for each distribution, only a single line is assigned. For the dimensions analyzed in this case, the density of the edges for each of the four ring lattices is very high, then, a radically different behavior is not observed depending on the dimension parity, then they are shown in the same figure. This behavior is more similar to that of the complete graph K_N, or that of the bipartite complete graph $K_{N,N}$.

Then, to conclude, the computational calculations that were made to study the behavior of the family of ring lattices $C(N,k)$, allows to relate and understand the behavior of the different types of graphs studied in this thesis, which range from the complete graph K_N that has all its vertices connected (so the edge density is 1), to the behavior of the cycle graph C_N (whose edge density is small $\frac{2}{N-1}$ for $N \geq 3$), when the dimension N grows. This is because $K_N = C(N, \lfloor N/2 \rfloor)$, when N is odd and when N is even it is only necessary to remove the duplicate edge. Besides, the other extreme case, is when $k = 1$, that means $C_N = C(N,1)$. The observations made from the analyzes presented in this section suggest that when the density of edges is small, the behavior will be like that of the cycle graph C_N, and when the density is large, it will resemble

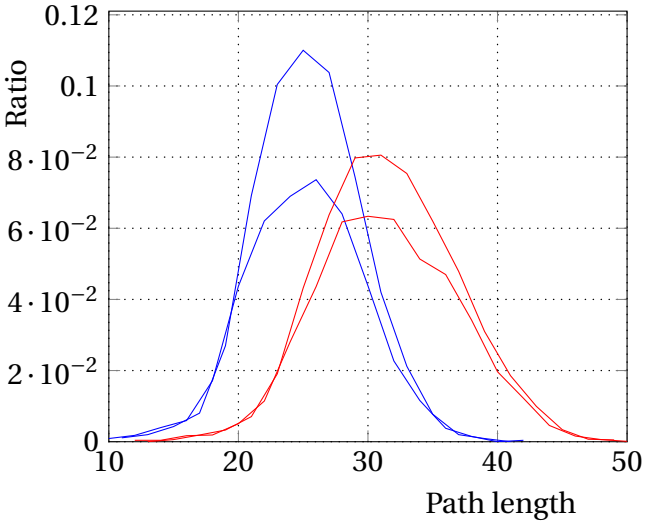

Figure 3.11 – Path length distribution of $L(M_{C(N,2)})$, odd dimensions. The blue line represents the normalized path odd and even length distribution of Laplacian system of the ring lattice $C(9,2)$ and red line is for $C(11,2)$, for a set of random initial conditions.

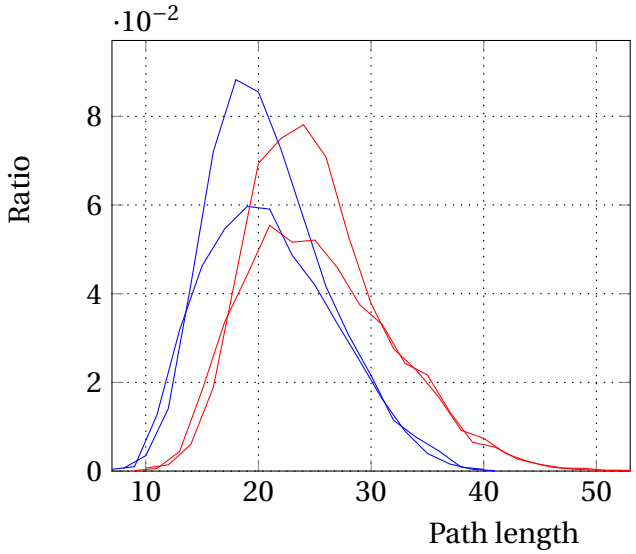

Figure 3.12 – Path length distribution of $L(M_{C(N,2)})$, even dimensions. The blue line represents the normalized path odd and even length distribution of Laplacian system of the ring lattice $C(10,2)$, and red line is for $C(12,2)$, for a set of random initial conditions.

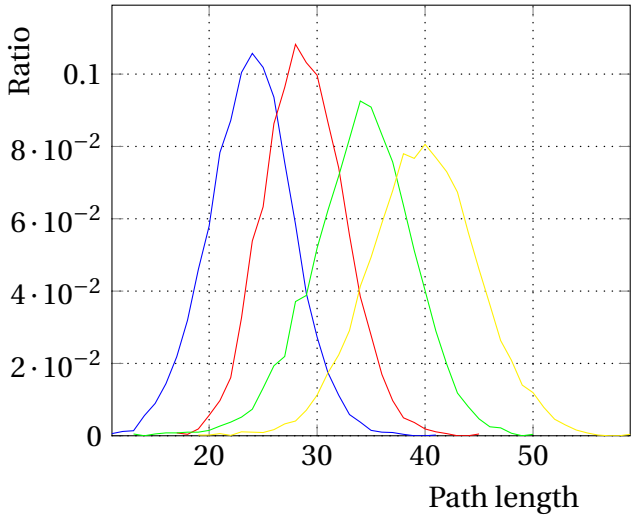

Figure 3.13 – Path length distribution of $L(M_{C(N,3)})$. The blue line represents the normalized path length distribution of Laplacian system of the ring lattice $C(8,3)$, red line is for $C(9,3)$, green line is for $C(10,3)$ and yellow line is for $C(11,3)$, for a set of random initial conditions.

the complete graph K_N. The formal results of these observations will be presented as perspectives of this thesis.

3.1.3 Discussion

In this section, an exploratory study of the transitory state of the Laplacian system was carried out. The system was applied to the the cycle graph, and the ring lattice family, to show the behavior of the system before reaching the synchronization. To begin, a random and fixed initial condition was applied in the four types of graphs in order to observe the similarities and differences between the systems. The number of vertices contained in each of the transition diagrams was estimated. The length of the longest path in each diagram was calculated. In addition, the number of realizable paths towards synchronization was calculated, and the section is concluded with the presentation of the normalized distributions of path lengths for each case.

Analyzing the same initial condition in the two types of graphs, allow to see the differences between the dynamics when the Laplacian flow is applied. It is recalled that the cases analyzed were in dimension six. It was observed in both cases that the way to approach the asymptotic value is monotonically, either with increasing or decreasing values. Also, the differences between the coordinates are monotonically reduced in the case of the ring lattice, in contrast to the cases of the the cycle graph. In addition, the time in which synchronization is reached for the ring lattice is smaller

than 8-time units. In the case of the cycle graph, the convergence time appears to be $t > 20$, which may be due to poor connectivity of the graph.

The number of realizable states for each of the graph was analyzed, this refers to the number of subgraphs of the cycle graph, and the ring lattice family that are feasible for some initial condition. Only for the case of the cycle graph, each of its subgraphs are feasible, then, from computational calculations, it was possible to give an exact formula for the number of states in their respective transition diagram. For the other case, the types of unfeasible subgraphs were found, and an estimate was made of how many subgraphs there are of each of them.

Regarding the length of the longest path found in the transition diagram of the Laplacian system, the following results were obtained. In the case of the the families of ring lattices when $k = 2$ and $k = 3$, due to the monotony it presents, the longest length found corresponds to the number of edges that K_N has, because there is a coincidence between these and the complete graph, but when the dimension increases, then the presence of directed cycles in the transition diagrams is observed, therefore, its depth increases, until it triples the number of edges they have. This behavior is observed in the cycle graph, and in the families of ring lattices when $k = 2$ and $k = 3$ when the dimension is relatively large, then, the edge density decreases and is comparable to the density of the cycle graph.

About the number of different paths towards synchronization in the different types of transition diagrams, it was observed that although the number of realizable states is much less than the number of possible states (referring to the number of subgraphs that the ring lattice family has), the number of paths towards synchronization in these case seems to grow at least exponentially. Therefore, it can be concluded that with little information (that is, when considering low-dimensional initial conditions), the number of possibilities to build new information is large enough (that is, the number of paths to synchronization that can be generated with these initial conditions grows significantly). This fact can be exploited in the future, making use of applications, for example, in information storage and classification, because several initial conditions have the same path to synchronization associated with them, so, this path construction process can be viewed as a vector classifier.

To end this discussion section, the behavior of a set of 10^6 random initial conditions in $(0, N^2)^N$ was analyzed, and whose sequence of ϵ-synchronized subnetworks was calculated, the length of each of them was measured and the normalized distribution of the length of these paths was constructed. For cases with a high density of edges, such as the ring lattice when $k = 3$, unimodal distributions like the Gaussian distribution were observed, which the average increases when the dimension increases. In the case where the density of edges is small, as in the cases of the cycle graph and the ring lattice when $k = 2$, then a case-by-case behavior is observed, which separates the parity of the dimension and the parity of the path's length, these distributions

are also unimodal, and appear to be slightly skewed to the left. Knowing how these distributions behave for a set of random initial conditions, gives an idea of what to expect about the length of a path to synchronization for a random initial condition. In all cases, it is observed that there is very little possibility of choosing randomly an initial condition that has a path that reaches synchronization in a few or many steps, rather the behavior would be intermediate. In addition, this behavior depends on the threshold ϵ that is chosen to make the computational calculations, when the threshold is lower, the average length of the paths will increase.

3.2 Exploring the Kuramoto model

This section shows the exploratory studies that were carried out from computational simulations for a set of 10^6 random initial conditions on $(0,2\pi)^N$ in the Kuramoto model the cycle graph and the family of ring lattices, with the aim of finding the patterns that meet the initial conditions on their way to finding the synchronization. In the two types of subgraphs that are analysed, the same initial condition is evaluated to observe the different behavior it has when the topology of the graph changes. In addition, for each of them, the number of feasible subgraphs, the length of the longest path, the number of paths and the distribution of path lengths are explored, for a set of random initial conditions.

3.2.1 The Kuramoto model of M_{C_N} and $M_{C(N,k)}$

In this section the quantitative properties of the Kuramoto model on the cycle graph of dimension N and the ring lattice family $C(N,k)$ are seen, which were calculated computationally. Specifically, the behavior of this model when the dimension grows is investigated. The trajectory under the Kuramoto flow, starting with a fixed initial condition, will be evaluated, this will be used throughout Section 3.2, to observe the differences when the topology of the graph is changed. The objective of this section is to observe the transient behavior of the Kuramoto model in the space $\mathbb{R}^N$, before reaching synchronization, that is, all its coordinates have the same value after a certain period. Sections 3.1 and 3.2 have focused on the behavior when the dimension of spaces N increases, and the problem presented in these cases is exposed.

Just as it was presented in the two previous sections, the behavior of the initial condition

$$x = (3.69253, 1.95285, 2.48317, 0.984696, 3.39029, 4.82533),$$

in the cycle graph C_6 is presented. In Figure 3.14 it can be seen that all of its coordinates approaches monotonically (increasingly or decreasingly) to $\bar{x} = 0.947006$, which is the average of the coordinates of x. Furthermore, in this case, it is observed that the

convergence time is longer than for when this initial condition is considered over the complete graph and the complete bipartite graph (the convergence time is more than double than in the other cases). In addition, this behavior occurs when the Laplacian system is considered.

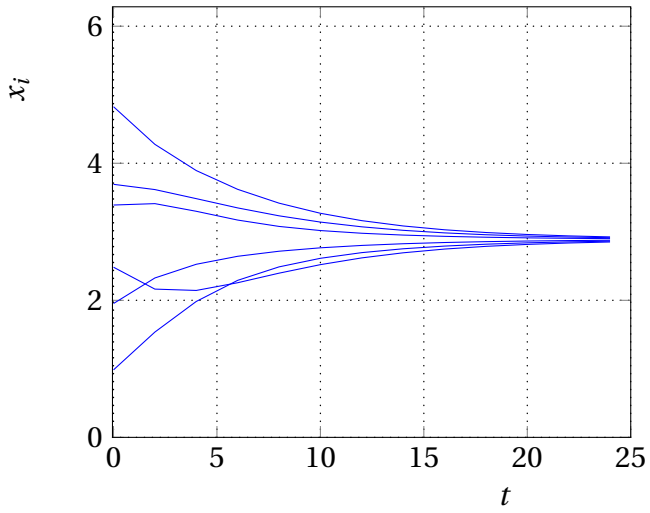

Figure 3.14 – The Kuramoto flow in the cycle graph of dimension 6, C_6, applied on a fixed initial condition $x \in \mathbb{R}^6$. Each one of the six lines represents the projection of each one of the coordinates x_i of x. It is observed that all of them reach the same value asymptotically monotonically, and they cross each other.

Once again, as was said for the case of the Laplacian system applied to these graphs, C_N and $C(N,k)$, the same subgraphs are feasible in the case of the Kuramoto model.

In Figure 3.15, a comparison of the proportion of initial conditions that synchronize in the Kuramoto system in the cycle graph C_N, and in three types of ring lattices ($C(N,2)$, $C(N,3)$ and $C(N,4)$), which depends on the dimension are shown. They are represented with a blue, red, green, and yellow line respectively. As can be seen, as the dimension increases, the probability of finding synchronizing initial conditions decreases, therefore, it is not possible to provide an analysis like that of the other cases presented, in which what is of interest is to know the behavior of the transient state when the dimension N increases.

To end, as a conclusion of this section, regarding the number of possible states in the transition diagrams associated with these graphs, it is observed that they are the same quantity as in the Laplacian system, because it is a property that depends on the topology of the graph and not on the system that is applied. On the other hand, it is not possible to give an analysis of the behavior of the transition diagram when

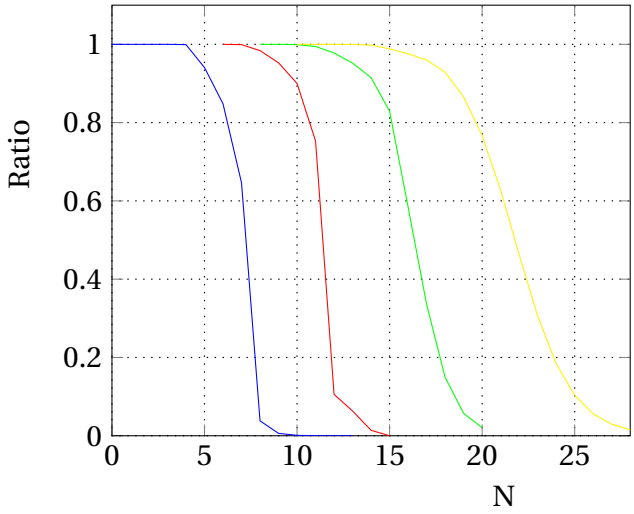

Figure 3.15 – Proportion of initial conditions that synchronize in the Kuramoto model in the ring lattice family $C(N,k)$ for $k = 1,2,3$ and 4.

N grows, because the probability of finding synchronizing initial conditions tends to zero from very small dimensions. Despite this, the asymptotic state reached by the initial conditions corresponds to phase locking, that is, to a state where the angles of each of the initial conditions are equally distributed in the interval $(0,2\pi)$. The analysis of this state will remain as a perspective of the thesis.

Conclusions

In this thesis, I have studied the transient behavior of fully synchronizing systems. To this aim, I have proposed a new approach to describe the paths towards synchronization, focusing on two types of systems on networks: the Laplacian flow and the Kuramoto model. I have considered three families of graphs: the completely connected network, the complete bipartite graph and the cycle graph.

From my perspective, the main contribution of this thesis is the complete description of the transition diagram of the paths towards synchronization for the Laplacian flow on the fully connected network, and on the complete bipartite graph when only balanced initial conditions are considered. I was able to analyze those transition diagrams, thanks to an equivalence between these structures and some classical combinatorial objects, an equivalence that I was able to demonstrate. The main ingredient allowing this description for the complete graph is the monotonicity of the Laplacian flow, which allows a codification of the synchronized subnetworks by increasing functions above the diagonal. These functions have been extensively studied in combinatorial theory and I was able to adapt some of those classical results to obtain relevant information about the transition diagram of the paths towards synchronization. In the case of the complete bipartite graph, a similar codification appears, but it is limited to synchronizing paths that started at balanced initial conditions, those initial conditions are precisely for which the monotonous behavior is preserved.

In all cases I obtained an explicit formula for the number of synchronized subnetworks. Adversely, the closed formula for the number of paths towards synchronization of the Laplacian systems, which can be seen as a complexity function, remains as an open problem in all cases. Nevertheless, I was able to obtain explicit bounds and I performed computational calculations in order to determine the growth order of the number of paths towards synchronization. It is remarkable the fact that these numbers grow at least as a factorial with respect to the dimension of the system. That is, a systems converging to a fully synchronized state in finite time, and the number of ways it does, grows super-exponentially fast with respect to the dimension.This combinatorial explosion opens the possibility to use synchronizing systems to devise systems for information storing.

The equivalence between synchronized subgraphs and certain combinatorial objects that I obtained, allows to establish a dictionary between characteristics of these combinatorial objects and characteristics of the transition diagram of paths towards synchronization. Below I present this dictionary.

Combinatorial concept	**Transition diagram property**
Complete graph	
Catalan number	Number of synchronized subnetworks
Combinatorially different Golomb rulers	Number of paths towards synchronization
Number of Dyck paths of order N and area $N^2 - \ell$	Number of paths of length ℓ
N-th line of Narayana	Degree distribution
Complete bipartite graph	
Narayana number	Number of synchronized subnetworks
Combinatorially different Golomb rulers	Number of paths towards synchronization
Number of parallelo-polyminoe with area $(N+1)^2 - \ell$	Number of paths of length ℓ

The probability density functions of the asymptotic distribution of the normalized length of a path towards synchronization are continuous, unimodal, and negatively skewed. The typical length with respect to the longest path is larger in the case of the complete bipartite graph $K_{N,N}$ than for the complete graph K_N.

The transient behavior of the Kuramoto model on the complete graph can be described by using the same methodology, if the initial conditions in a neighborhood around the diagonal are considered. Similarly, the description of a transition diagram for the Kuramoto model over $K_{N,N}$, can be made by means of the codification used to study the linear case. This, however, will exclude the paths towards synchronization defined by some initial conditions, as in the linear case where only balanced initial conditions are considered. The description of the complete transition diagram of this system would be the subject of future work.

Finally, I would like to emphasize that the ϵ-synchronizing sequences presented in this thesis, can be seen as partitioning the basin of attraction of a given attractor (here the fully synchronized state). Since for a given finite $\epsilon > 0$, the final ϵ-synchronized subnetwork will be reached in a finite time $\tau(\epsilon, N)$, if the space of initial conditions has a finite volume, the full space-time will be as well bounded, and these sequences are partitioning that full space around the diagonal. Moreover, by associating to a given sequence an ensemble of initial conditions realizing that sequence, I should be able to measure that ensemble and add corresponding weights (measures) to each sequence and characterize even further the space-time complexity. This probabilistic characterization of the paths towards synchronization would be the subject of future work as well.

Most of the above mentioned results are published in (España, Leoncini, and Ugalde 2022), and in a second article now in preparation.

3.3 Perspectives

Below I present some perspectives and future work regarding the analysis of the transient dynamics of synchronizing systems.

3.3.1 Extension to other kind of synchronized states

Besides the full synchronization, when all the nodes of the system coalesce, one may consider other organized asymptotic states as generalized synchronized states. For example, in the Kuramoto model a phase locking state can be observed. In this state, the phases of the N oscillators are equidistributed on the circle, and this state may also define an invariant attracting manifold. In my definition of the ϵ-synchronized subnetwork, the condition $|x_u - x_v| \leq \epsilon$, needed to declare synchronized the link $\{u, v\}$, can be replaced by requiring the couple (x_u, x_v) to be ϵ-close to the corresponding two-dimensional projection of the synchronized manifold. This alternative point of view is susceptible to be generalized to other kind of synchronization manifolds, as for instance the one corresponding to the phase locking in the Kuramoto model.

3.3.2 Analysis of the family of ring lattices

Regarding the formal and rigorous study of the cycle graph C_N, it is still necessary to find a convenient codification and to bound correctly the number and type of oscillations observed in the corresponding paths towards synchronization. These oscillations in the synchronized subnetworks are due to the lack of monotony in the dynamics, but they can be bounded and this information can be included in the transition diagram. On the other hand, It is possible to find classes of initial conditions for which the convergence towards the synchronized manifold is monotonous. This can be done by taking into account the symmetries of the eigenvectors of the Laplacian. Those initial conditions would be described by families of increasing functions. For the family of the ring lattices $C(N, k)$, since by increasing the connectivity parameter k we can approach the fully connected network, it is natural to investigate in depth the transition of the corresponding transition diagrams, from those corresponding to the cycle graph to the one defined by the Laplacian flow on K_N.

In a preliminary study I performed computational simulations for the Laplacian system and the Kuramoto model in C_N and $C(N, k)$. For this, I considered randomly generated initial conditions in $(0, N^2)^N$ in the case of the Laplacian system and $(0, 2\pi)^N \subset \mathbb{R}^N$ in the case of the Kuramoto model, taking $N = 1, 2, \ldots, 10$. I analysed the dynamics of the initial conditions, in the two systems (the linear system and the non-linear

system), and studied the corresponding paths towards synchronization in the sake to make a formal characterization. The following features were considered:

— Feasible and unfeasible synchronized subnetworks.
— Depth of the transition diagram.
— Number of observed paths towards synchronization.
— Distribution of the path length.

The objective of this numerical exploration was to formulate conjectures regarding the rigorous description of the transition diagram of the paths towards synchronization for the Laplacian flow in C_N and $C(N,k)$. The observations made will allow us to continue with a general and rigorous study in the future.

The computational calculations made for these cases are shown in the Chapter 3.

It is important to remark the difference between the exploratory study, in which randomly generated initial conditions were considered, and the rigorous study, in which typical initial conditions were considered. In the rigorous study, it has been said that randomly generating a non-typical initial condition has probability zero, and therefore the paths to synchronization for the typical initial conditions would be the longest possible. On the other hand, in the experimental study, when the initial conditions are randomly generated, the results indicate that the generated paths are not the longest, as expected. This discrepancy is due to the fact that in the numerical study I consider a fixed finite threshold $\epsilon > 0$. Hence, when this threshold decreases, the behavior tends to the one expected for a typical initial condition. This kind of discrepancies between the theoretically expected behavior and the experimentally observed one, have to be precisely formalized and taken into account in the future works.

Bibliography

[Ace+05] Juan A. Acebrón, L. L. Bonilla, Conrad J. Pérez Vicente, et al. “The Kuramoto model: A simple paradigm for synchronization phenomena”. In: *Rev. Mod. Phys.* 77 (1 Apr. 2005), pp. 137–185. DOI: 10.1103/RevModPhys.77.137 (cit. on p. 26).

[ACC01] V. Afraimovich, J.-R. Chazottes, and A. Cordonet. “Synchronization in directionally coupled systems: Some rigorous results”. In: *Discrete and Continuous Dynamical Systems - B* 1.4 (2001), pp. 421–442. ISSN: 1531-3492. DOI: 10.3934/dcdsb.2001.1.421. URL: /article/id/cdf6163a-d540-4f0f-b345-199662f6d037 (cit. on p. 25).

[AZ03] V. Afraimovich and G. M. Zaslavsky. “Space-Time Complexity in Hamiltonian Dynamics”. en. In: *arXiv* 2003.0 (2003) (cit. on p. 27).

[Are+08] Alex Arenas, Albert Diaz-Guilera, Jurgen Kurths, et al. “Synchronization in complex networks”. English. In: *Physics Reports* 469.3 (Dec. 2008), pp. 93–153. ISSN: 0370-1573. DOI: 10.1016/j.physrep.2008.09.002 (cit. on p. 26).

[ADP06] Alex Arenas, Albert Díaz-Guilera, and Conrad J. Pérez-Vicente. “Synchronization Reveals Topological Scales in Complex Networks”. In: *Phys. Rev. Lett.* 96 (11 Mar. 2006), p. 114102. DOI: 10.1103/PhysRevLett.96.114102 (cit. on p. 27).

[BYL18] Dianbin Bao, Kisung You, and Lizhen Lin. *Network Distance Based on Laplacian Flows on Graphs*. 2018. DOI: 10.48550/ARXIV.1810.02906. URL: https://arxiv.org/abs/1810.02906 (cit. on p. 54).

[BFR05] Elena Barcucci, Andrea Frosini, and Simone Rinaldi. “On directed-convex polyominoes in a rectangle”. In: *Discrete Mathematics* 298.1 (2005). Formal Power Series and Algebraic Combinatorics 2002 (FPSAC’02), pp. 62–78. ISSN: 0012-365X. DOI: https://doi.org/10.1016/j.disc.2005.01.006 (cit. on p. 94).

[BBP11] Matthias Beck, Tristram Bogart, and Tu Pham. “Enumeration of Golomb Rulers and Acyclic Orientations of Mixed Graphs”. In: (2011). DOI: 10.48550/ARXIV.1110.6154. URL: https://arxiv.org/abs/1110.6154 (cit. on p. 52).

[BHM00] F Blanchard, B Host, and A Maass. “Topological complexity”. In: *Ergodic Theory and Dynamical Systems* 20.3 (2000), pp. 641–662. DOI: 10.1017/S0143385700000341 (cit. on p. 79).

[BP12] Saúl A. Blanco and T. Kyle Petersen. “Counting Dyck Paths by Area and Rank”. In: *Annals of Combinatorics* 18 (2012), pp. 171–197 (cit. on pp. 50, 83).

[CR64] L. Carlitz and John Riordan. “Two element lattice permutation numbers and their q-generalization”. In: *Duke Mathematical Journal* 31 (1964), pp. 371–388 (cit. on p. 83).

[CE06] Pierre Collet and Jean-Pierre Eckmann. “Concepts and Results in Chaotic Dynamics: A Short Course”. In: *Concepts and Results in Chaotic Dynamics: A Short Course, by P. Collet and J.P. Eckmann. Berlin: Springer, 2006* (Jan. 2006) (cit. on p. 25).

[CDS95] Dragos M. Cvetkovic, Michael Doob, and Horst Sachs. “Spectra of graphs : theory and application”. In: 1995 (cit. on pp. 35, 44).

[Das04a] K.Ch. Das. “The Laplacian spectrum of a graph”. In: *Computers and mathematics with Applications* 48.5 (2004), pp. 715–724. ISSN: 0898-1221. DOI: https://doi.org/10.1016/j.camwa.2004.05.005. URL: https://www.sciencedirect.com/science/article/pii/S0898122104003074 (cit. on p. 36).

[Das04b] Kinkar Ch. Das. “Sharp lower bounds on the Laplacian eigenvalues of trees”. In: *Linear Algebra and its Applications* 384 (2004), pp. 155–169 (cit. on p. 36).

[DJD19] Robin Delabays, Philippe Jacquod, and Florian Dörfler. “The Kuramoto Model on Oriented and Signed Graphs”. In: *SIAM Journal on Applied Dynamical Systems* 18.1 (2019), pp. 458–480. DOI: 10.1137/18M1203055. eprint: https://doi.org/10.1137/18M1203055. URL: https://doi.org/10.1137/18M1203055 (cit. on pp. 26, 48).

[DFM22] Andreas Deutsch, Nazim Fatès, and Danuta Makowiec. “Discrete models of complex systems: Recent trends and analytical challenges”. In: *Physica D: Nonlinear Phenomena* 436 (2022), p. 133328. ISSN: 0167-2789. DOI: https://doi.org/10.1016/j.physd.2022.133328. URL: https://www.sciencedirect.com/science/article/pii/S016727892200104X (cit. on p. 24).

[DE16] Lee DeVille and Bard Ermentrout. “Phase-locked patterns of the Kuramoto model on 3-regular graphs.” In: *Chaos* 26 9 (2016), p. 094820 (cit. on pp. 26, 48).

[Dim02] Apostolos Dimitromanolakis. *Analysis Of The Golomb Ruler And The Sidon Set Problems And Determination Of Large Near-Optimal Golomb Rulers*. Tech. rep. 2002 (cit. on p. 52).

[ELU22] A España, X Leoncini, and E Ugalde. *Combinatorics of the paths towards synchronization*. 2022. DOI: 10.48550/ARXIV.2205.05948. URL: https://arxiv.org/abs/2205.05948 (cit. on p. 134).

[Far03] Michael Farber. "Topological Complexity of Motion Planning". In: *Discrete & Computational Geometry* 29 (2003), pp. 211–221 (cit. on p. 14).

[Fer12] Bastien Fernandez. "Discontinuous generalized synchronization of chaos". In: *Dynamical Systems* 27.1 (2012), pp. 105–116. DOI: 10.1080/14689367.2011.594787. eprint: https://doi.org/10.1080/14689367.2011.594787. URL: https://doi.org/10.1080/14689367.2011.594787 (cit. on p. 25).

[FA18] J. D. da Fonseca and Celso Vieira Abud. "The Kuramoto model revisited". In: *Journal of Statistical Mechanics: Theory and Experiment* (2018) (cit. on pp. 26, 46).

[GMA07] Jesús Gómez-Gardeñes, Yamir Moreno, and Alex Arenas. "Paths to synchronization on complex networks." In: *Physical review letters* 983 (2007), p. 034101 (cit. on pp. 26, 27, 48).

[GC04] Guillaume Grégoire and Hugues Chaté. "Onset of Collective and Cohesive Motion". In: *Phys. Rev. Lett.* 92 (2 Jan. 2004), p. 025702. DOI: 10.1103/PhysRevLett.92.025702. URL: https://link.aps.org/doi/10.1103/PhysRevLett.92.025702 (cit. on p. 25).

[Gro59] D. M. Grobman. "Homeomorphisms of systems of differential equations". In: *Doklady Akademii Nauk SSSR* (1959), pp. 880–881 (cit. on p. 49).

[Har60] Philip Hartman. "A lemma in the theory of structural stability of differential equations". In: *Proceedings of the American Mathematical Society* 11 (1960), pp. 610–620 (cit. on p. 49).

[Hil07] Roland Hildebrand. "Positive partial transpose from spectra". In: *Physical Review A* 76.5 (Nov. 2007), 052325:1–052325:5 (cit. on p. 80).

[Joh14a] Nathaniel Johnston. *A237749*. https://oeis.org/A237749. "[Online; accessed 04-May-2022]". 2014 (cit. on pp. 52, 80).

[Joh14b] Nathaniel Johnston. *Counting the Possible Orderings of Pairwise Multiplication*. http://www.njohnston.ca/2014/02/counting-the-possible-orderings-of-pairwise-multiplication/. "[Online; accessed 04-May-2022]". 2014 (cit. on p. 79).

[Kur75] Yoshiki Kuramoto. "Self-entrainment of a population of coupled non-linear oscillators". In: *International Symposium on Mathematical Problems in Theoretical Physics*. Ed. by Huzihiro Araki. Berlin, Heidelberg: Springer Berlin Heidelberg, 1975, pp. 420–422. ISBN: 978-3-540-37509-8 (cit. on p. 25).

[LZ02] X. Leoncini and G. M. Zaslavsky. "Jets, Stickiness and Anomalous Transport". In: *Physical Review E : Statistical, Nonlinear, and Soft Matter Physics* 65 (2002). 17 pages, 17 figures, p. 046216 (cit. on p. 27).

[Liu+15] Hongxiao Liu, Maxim Dolgushev, Yi Qi, et al. “Laplacian spectra of a class of small-world networks and their applications”. In: *Scientific Reports* 5 (Mar. 2015), p. 9024. DOI: 10.1038/srep09024 (cit. on p. 36).

[MT17] Georgi S. Medvedev and Xuezhi Tang. “The Kuramoto model on power law graphs”. In: *arXiv: Adaptation and Self-Organizing Systems* (2017) (cit. on pp. 26, 48).

[Mer94] Russell Merris. “Laplacian matrices of graphs: a survey”. In: *Linear Algebra and its Applications* 197-198 (1994), pp. 143–176. ISSN: 0024-3795. DOI: https://doi.org/10.1016/0024-3795(94)90486-3. URL: https://www.sciencedirect.com/science/article/pii/0024379594904863 (cit. on p. 36).

[MP04] Yamir Moreno and Amalio F. Pacheco. “Synchronization of Kuramoto oscillators in scale-free networks”. In: *EPL* 68 (2004), pp. 603–609 (cit. on pp. 26, 48).

[Nar79] T. V. Narayana. “Lattice Path Combinatorics With Statistical Applications”. In: 1979 (cit. on p. 50).

[PC90] Louis M. Pecora and Thomas L. Carroll. “Synchronization in chaotic systems”. In: *Phys. Rev. Lett.* 64 (8 Feb. 1990), pp. 821–824. DOI: 10.1103/PhysRevLett.64.821. URL: https://link.aps.org/doi/10.1103/PhysRevLett.64.821 (cit. on p. 25).

[PRK01] Arkady Pikovsky, Michael Rosenblum, and Jürgen Kurths. “Synchronization - A Universal Concept in Nonlinear Sciences”. In: *Cambridge Nonlinear Science Series*. 2001 (cit. on p. 24).

[Rob08] David C. Roberts. “Linear reformulation of the Kuramoto model of self-synchronizing coupled oscillators”. In: *Phys. Rev. E* 77 (3 Mar. 2008), p. 031114. DOI: 10.1103/PhysRevE.77.031114. URL: https://link.aps.org/doi/10.1103/PhysRevE.77.031114 (cit. on p. 26).

[Slo21] N. J. A. Sloane. *A001263*. https://oeis.org/A001263. “[Online; accessed 12-May-2022]". 2021 (cit. on p. 50).

[Slo22] N. J. A. Sloane. *A000712*. https://oeis.org/A000712. “[Online; accessed 04-May-2022]". 2022 (cit. on p. 103).

[Slo] N. J. A. Sloane. *A000108*. https://oeis.org/A000108. “[Online; accessed 12-May-2022]" (cit. on p. 51).

[SE19] Yury Sokolov and G. Bard Ermentrout. “When is sync globally stable in sparse networks of identical Kuramoto oscillators?” In: *Physica A: Statistical Mechanics and its Applications* (2019) (cit. on p. 26).

[SF99] Richard P. Stanley and Sergey Fomin. *Enumerative Combinatorics*. Vol. 2. Cambridge Studies in Advanced Mathematics. Cambridge University Press, 1999. DOI: 10.1017/CBO9780511609589 (cit. on pp. 50, 68).

[Str00] Steven H. Strogatz. “From Kuramoto to Crawford: exploring the onset of synchronization in populations of coupled oscillators”. In: *Physica D: Nonlinear Phenomena* 143.1 (2000), pp. 1–20. ISSN: 0167-2789. DOI: https://doi.org/10.1016/S0167-2789(00)00094-4. URL: https://www.sciencedirect.com/science/article/pii/S0167278900000944 (cit. on p. 26).

[Thr52] R. M. Thrall. “A combinatorial problem.” In: *Michigan Mathematical Journal* 1.1 (1952), pp. 81–88. DOI: 10.1307/mmj/1028989731. URL: https://doi.org/10.1307/mmj/1028989731 (cit. on p. 80).

[vW93] J. L. van Hemmen and W. F. Wreszinski. “Lyapunov function for the Kuramoto model of nonlinearly coupled oscillators”. In: *Journal of Statistical Physics* 72.1-2 (July 1993), pp. 145–166. DOI: 10.1007/BF01048044 (cit. on p. 26).

[Vic+95] Tamás Vicsek, András Czirók, Eshel Ben-Jacob, et al. “Novel Type of Phase Transition in a System of Self-Driven Particles”. In: *Phys. Rev. Lett.* 75 (6 Aug. 1995), pp. 1226–1229. DOI: 10.1103/PhysRevLett.75.1226. URL: https://link.aps.org/doi/10.1103/PhysRevLett.75.1226 (cit. on p. 24).

[Yod05] Joella G. Yoder. “Chapter 3 - Christiaan Huygens, book on the pendulum clock (1673)”. In: *Landmark Writings in Western Mathematics 1640-1940*. Ed. by I. Grattan-Guinness, Roger Cooke, Leo Corry, et al. Amsterdam: Elsevier Science, 2005, pp. 33–45. ISBN: 978-0-444-50871-3. DOI: https://doi.org/10.1016/B978-044450871-3/50084-X. URL: https://www.sciencedirect.com/science/article/pii/B978044450871350084X (cit. on p. 24).

[ZA05] G. M. Zaslavsky and V. Afraimovich. “Working with Complexity Functions”. In: *Chaotic Dynamics and Transport in Classical and Quantum Systems*. Ed. by P. Collet, M. Courbage, S. Métens, et al. Dordrecht: Springer Netherlands, 2005, pp. 73–85. ISBN: 978-1-4020-2947-9 (cit. on p. 27).